The Geology and Geochemistry of the Millennium Uranium Deposit, Athabasca Basin, Saskatchewan, Canada

By

Charles J. Beshears

A Thesis submitted to the Faculty of Graduate Studies of

The University of Manitoba

In partial fulfilment of the requirements of the degree of

MASTER OF SCIENCE

Department of Geological Science

University of Manitoba

Winnipeg

Abstract:

Renewed interest in the development and expansion of nuclear energy has lead to increased uranium exploration, in order to meet the demand for new uranium resources. The Athabasca Basin in northern Saskatchewan, Canada, hosts the world's largest and highest grade unconformity-associated uranium deposits. Uranium mineralization is hosted at the Athabasca Group unconformity or within the crystalline basement rocks. The unconformity hosted deposits have been studied extensively for more than 30 years and multiple models have been developed. In comparison to the unconformity hosted deposits, the basement-hosted deposits have not been well documented. The basement hosted Millennium deposit was discovered in 2000, and is located 35 km north of the Key Lake mine. The orebody is situated between a deformed graphitic pelite known as the "Marker Unit" (a reverse fault) and the "Mother" fault located foot-wall to the main orebody. Movement along these two sub-parallel reverse faults resulted in the development of a dilational structure that increased the permeability of the basement rocks within the hanging-wall block.

Within, the Millennium deposit uranium mineralization occurs in four distinct mineralization styles which include: style 1- massive replacement, style 2- fracture filling veins, style 3-"mini" roll-fronts, and style 4- disseminated mineralization. Massive replacement uraninite is associated with chlorite whereas fracture filled uraninite is associated with euhedral quartz-carbonate veins. The disseminated grains are altered uraninite with galena, are associated with hematite and clay minerals, and are assumed to be primary grains that were altered by a sulfur rich fluid. In drill core, massive replacement and fracture filling veins are the most prevalent mineralization styles. While, "mini" roll-fronts, and disseminated mineralization are only minor constituent of the uranium mineralization. Mineralization consists mainly of pitchblende and uraninite with lesser amounts of coffinite. Fluid inclusion studies on euhedral quartz- uraninite veins identified two fluids. The first fluid is moderately saline with 10-15wt% NaCl. The second fluid is highly saline with 22-24wt% NaCl which is within the range of fluid salinities for basinal brines within the Athabasca Basin. Heating results were unsuccessful due to decrepitation of the fluid inclusions. Uraninites have low $\delta^{18}O$ values -35‰ to -15‰, and similar to those measured for unconformity hosted uranium deposits in the Athabasca Basin. Metamorphic and secondary euhedral quartz grains associated with vein-type uraninite have $\delta^{18}O$ values of 11.1‰ to 15.1‰ and 16.2‰ to 19.1‰ respectively. The low $\delta^{18}O$ values for uraninite and the high $\delta^{18}O$ values for quartz suggest that the original isotopic composition of both minerals have been overprinted by recent low temperature meteoric waters.

The chemical Pb and isotopic $^{207}Pb/^{206}Pb$ ages of the massive (style 1), vein-type (style 2), and fine-aggregate (style 3) uraninite cluster at 1400-1200 and 1100-900 Ma. The ~1400 Ma ages coincide with the primary mineralization event for many of the uranium deposits (1550-1400 Ma) within the Athabasca Basin. The younger age groups reflect lead loss associated with post depositional fluid events. However, unlike other uranium deposits from the Athabasca basin, disseminated uraninite (style 4) have $^{207}Pb/^{206}Pb$ ages from 1770-1650 Ma. These ages are older than the depositional age for the Athabasca sediments (~1710 Ma) and similar to U-Pb dates obtained from the Beaverlodge vein-type uranium deposits. This suggests the basement rocks, in addition to the overlying Athabasca Group rocks, are a possible source of uranium mineralization at the Millennium deposit. The $^{207}Pb/^{206}Pb$ ages obtained for galena associated with style 4 uraninite is ~1400 Ma and reflects the time when the disseminated uraninite was reset during the primary mineralization event.

Acknowledgements:

I would like to convey my sincere thanks to the many individuals who have provided me with their time and shared their invaluable expertise in the completion of this research. I wish to thank the Cameco Corporation for their invitation and support to work on this project. I want to thank Dan Jiricka, Charles Roy, John Halaburda, Dave Thomas and Vlad Sopuck of the Cameco Corporation who have provided me with their time and expertise on the geology of the Millennium deposit. I wish to thank my advisors, Dr. Mostafa Fayek and Dr. Alfredo Camacho, who have shared many hours of discussion and support during the last three years. I would like to thank Dr. Panseok Yang for his assistance in the operation of the EMPA, Dr. Rong Liu for the help in the operation of the SIMS, Sergio Mejia for his help and operation of the SEM, and Dr. Yassir Abdu for help and assistance running the Mössbauer spectrometer. I would also like to give my sincere thanks Dr. Frank Hawthorne for providing the use of the Mössbauer spectrometer. I would like to express my sincere thanks to my family and friends who have given me their love and support over the years. Funding for this research was provided by the Natural Science and Engineering Research Council of Canada (NSERC) - CRD Program and Cameco Corporation.

Table of Contents:

List of Figures:

Chapter 1: Introduction

1.1 Overview

Concerns over increased air pollution, global warming, as well as uncertainties over the supply and price of traditional fuel resources, has lead to renewed interest in the development and expansion of nuclear energy. There are currently 441 nuclear reactors operating in 31 countries, with 27 nuclear reactors under construction and an additional 38 either planned or on order (EIA, 2007; Cuney and Kyser, 2008). Approximately 60% of the global uranium fuel supply comes from the mining of uranium deposits. The remaining 40% is currently filled by existing uranium stockpiles and the dismantling of nuclear weapons (IAEA, 2001). The International Atomic Energy Agency (IAEA) projects that there will be short-fall in the global supply of uranium as new nuclear power stations are constructed and current stockpiles are consumed, to meet the future demand new uranium resources need to be located.

Uranium deposits world-wide have been grouped into 14 major types based on their geological setting. Unconformity associated uranium deposits account for approximately 33% of the current global uranium production (Cuney and Kyser, 2008), and occur within large Paleoproterozoic basins in Canada and Australia. In these deposits, uranium mineralization is spatially related to the unconformity between Archean-Paleoproterozoic crystalline basement and overlying Paleo-Mesoproterozoic clastic sediments. The Athabasca Basin in northern Saskatchewan and Alberta, Canada, hosts the world's largest and highest grade uranium deposits which include McArthur River and Cigar Lake. In the Athabasca Basin, basement-hosted uranium deposits are considered to be derivatives of the unconformity associated uranium deposit model

(Thomas, *et. al*, 1998, Alexandre, *et. al*, 2005). These deposits include the Rabbit Lake, Eagle Point, Sue C, Dominique-Peter, and Millennium uranium deposits (Roy, *et. al*, 2005).

In contrast to the more typical deposits hosted at or near the Athabasca Group unconformity, the basement-hosted deposits have not been well studied. As a result, the origin and characteristics of basement-hosted uranium deposits are not well understood (Alexandre, *et. al*, 2005). The Millennium deposit is the most recent discovery (2000 by Cameco) of basement-hosted uranium deposits within the Athabasca Basin (Roy, *et. al*, 2005; Thomas, 2002). This deposit has uranium reserves of 13,292 tonnes U at an average grade of 2.43% and an additional 6,065 tonnes U at 2.07% is inferred (Roy, *et. al*, 2005). On the basis of these reserves the Millennium deposit is the second largest deposit of its kind and the sixth largest in the Athabasca area (Roy, *et. al*, 2005). The Millennium deposit shows the potential of the basement rocks to contain large economic uranium resources. The present study, on the Millennium deposit, provides an opportunity to increase our understanding of the mechanisms responsible for the formation of basement-hosted uranium deposits.

1.2 Previous Work

The geological setting of the Millennium deposit is based on regional magnetic geophysical surveys and observations from drill core (Thomas, 2002; Roy, *et. al,* 2005). Preliminary drill core logging identified a series intercalated graphitic and non-graphitic pelitic to psammopelitic gneisses/schists, with minor calc-silicate, and amphibolite that have been intruded by anatectic pegmatites within the basement of the Millennium area (Thomas, 2002). A basement alteration pattern that reflects a zonation from distal

saussuritization and sericitization, through a more proximal zone of chloritization into a central zone of increasing argillic alteration, bleaching and dravitization within proximity of a major reverse fault located footwall to the main ore zone (Roy, *et. al*, 2005). The main area of uranium mineralization broadly straddles the zone of chloritization and argillic alteration. A relative temporal relationship between mineral assemblages was developed based on crosscutting relationships of alteration visible in drill core, and supported by limited geochemistry and petrography.

1.3 Purpose and Scope of Study

Recent studies of the basement-hosted Millennium deposit are largely based on macroscopic drill core observations, with limited geochemistry and petrography. The objective of this research is to expand our current understanding of the fluid history and emplacement of uranium mineralization on the basement rocks within the Millennium deposit. A total of ten drill holes were relogged for this study (Appendix B). Two drill holes (DDH CX-44-1, and CX-56-1) that intersect the "main zone" of uranium mineralization within the Millennium deposit and one barren drill hole (DDH CX-58) were selected for detailed study. This work included thin-section petrography using reflected and transmitted light microscopy and scanning electron microscopy (SEM), fluid inclusion analysis, stable and radiogenic isotopic and geochemical analyses.

Petrography and mineral chemistry was used to determine the paragenetic relationship between host rock alteration and uranium mineralization at the microscopic scale. Fluid inclusions and stable isotopes are useful in characterizing the fluids associated with multiple generations of minerals (i.e. fluid reservoir and chemistry).

Chemical Pb and $^{207}Pb/^{206}Pb$ isotope ages were used constrain the emplacement and alteration history of uranium mineralization within the Millennium deposit.

Chapter 2: Geological Setting

2.1 Regional geology

2.1.1 Basement

The Athabasca Basin covers an area of approximately 100,000 km^2 and overlies the Hearn and Rae sub-provinces of the Western Churchill Province in northern Saskatchewan and Alberta, Canada (Fig.2.1) (Jefferson, *et. al*, 2007). The Millennium deposit occurs in the Hearn Province which has been sub-divided into three domains based on the differences in geology (i.e. lithology, structure and metamorphic grade) (Sibbald, 1985; Bruneton, 1993). These domains are the Virgin River Domain in the west, the central Mudjatik Domain, and the eastern Wollaston Domain (Roy, *et. al,* 2005) (Fig.2.1). The Millennium deposit lies at the transition zone between the Mudjatik and Wollaston Domains.

The Mudjatik Domain is composed of a series of felsic granitoid gneisses, which are thought to be Archean in age, interlayered with supracrustal sequence which includes metapelites, amphibolites, and local iron formations (Gilboy, 1985; Bruneton, 1993). Three major Hudsonian age deformation events have been recognized within the Mudjatik Domain. The earliest event (D_1) produced a regional gneissic and schistose fabric. The second deformation (D_2) produced large west-northwest trending folds. Upright northeast-trending folds with sub-horizontal axes resulted in the formation of domes and basins during the third (D_3) deformation event (Lewry and Sibbald, 1977; Gilboy, 1985; Sibbald, 1985; Bruneton, 1993). Metamorphism within the Mudjatik Domain is characterized by upper amphibolite to granulite facies metamorphism, which

peaked at approximately 4.5 kb and 725°C during the Trans-Hudson orogeny (Gilboy, 1985).

The Wollaston Domain is composed primarily of an Aphebian age supracrustal succession known as the Wollaston Group, with a total thickness of ~3-4 km. The metasedimentary gneisses of the Wollaston Group lie directly on the Archean basement over a majority of the Wollaston Domain (Hoeve and Sibbald, 1978; Bruneton, 1993). Within the Wollaston Group four major litological units have been recognized: 1) a basal unit composed of mature arkosic metasediments, quartz meta-conglomerate, and semi-pelitic to pelitic muscovite and biotite gneisses/schists. Locally, the basal unit is thought to unconformably overlie a sequence of immature meta-arkoses, arkosic metasediments and interbedded basic meta-volcanics known as the lower arkosic unit; 2) the basal unit is overlain by a unit which is dominated by graphitic pelites, with interlayers of quartz rich metapsammites, calc-silicates, and minor marbles; 3) the graphitic pelites are overlain by a thick sequence of calcareous and non-calcareous meta-arkoses, interlayered with minor calc-silicate, carbonate, and pelitic to psammopelitic metasediments; and 4) the uppermost stratigraphic unit within the Wollaston Group is dominated by amphibolite-quartzite unit with minor interlayers of calcareous metasediments and graphitic metapelites. This unit is synonymous with the Hidden Bay assemblage and is visible in outcrops in the Wollaston Lake area, along the eastern margin of the Wollaston Domain (Sibbald, 1985; Bruneton, 1993). The rocks within the Wollaston Domain have undergone four major deformational events (D_1-D_4) and two episodes of metamorphism (M_1 and M_2) (Yeo, 1998; Tran and Yeo, 1997; Tran, *et. al*, 1998). M_1 is associated with D_1. Based on metamorphic mineral assemblages P-T conditions during M_1 were at 4-5 kb

and <750°C. M_2 occurred at peak metamorphism during the Trans-Hudson orogeny and is associated with D_2. P-T conditions during M_2 were at 5 kb and 750-780°C and fall within the upper amphibolite- granulite facies (Yeo, 1998).

2.1.2 Athabasca Group

The Athabasca Basin is filled with a sequence of red-bed sandstones, conglomerates, minor shales, and dolomites which were deposited approximately 1700 Ma (Armstrong and Ramaekers, 1985; Kotzer and Kyser, 1990). This sequence is known as the Athabasca Group and has a thickness of approximately 1500 meters (Ramaekers, 1990). Fluid inclusion data and clay mineral studies suggest the original thickness of the sedimentary sequence was much greater (~4-5 km) (Bruneton, 1993; Hoeve and Quirt, 1987). Ramaekers (1979, 1980, 1981, and 1990) has proposed that the Athabasca Group was deposited in a tectonically active sedimentary basin located on a continental margin, the development of which was initiated by the formation of three northeast-southwest oriented sub-basins (Fig.2.2) which were controlled by major Hudsonian faults rooted in the metamorphic basement. The sub-basins were then filled by detrital sediments and subsequently merged to form the larger Athabasca Basin. Peak diagenesis within the Athabasca Basin occurred from 1650-900 Ma (Kotzer and Kyser, 1990, 1992).

On the eastern edge of the Athabasca basin, the Manitou Falls Formation forms the basal unit of the Athabasca Group (Fig.2.3), and unconformably overlies a deeply weathered lateritic surface developed on the Aphebian metasediments and Archean gneisses (Ramaekers, P., 1990). The Manitou Falls Formation is sub-divided into four members: the lower two members are comprised of coarse conglomerates and pebbly sandstones of fluvial origin, the overlying members are interpreted as sandy, braided-

stream deposits. Outcrop and drill core measurements of sedimentary structures suggest the Athabasca Group sediments were primarily sourced from the east (Ramaekers, 1979, 1980, 1981, 1990; Bruneton, 1993).

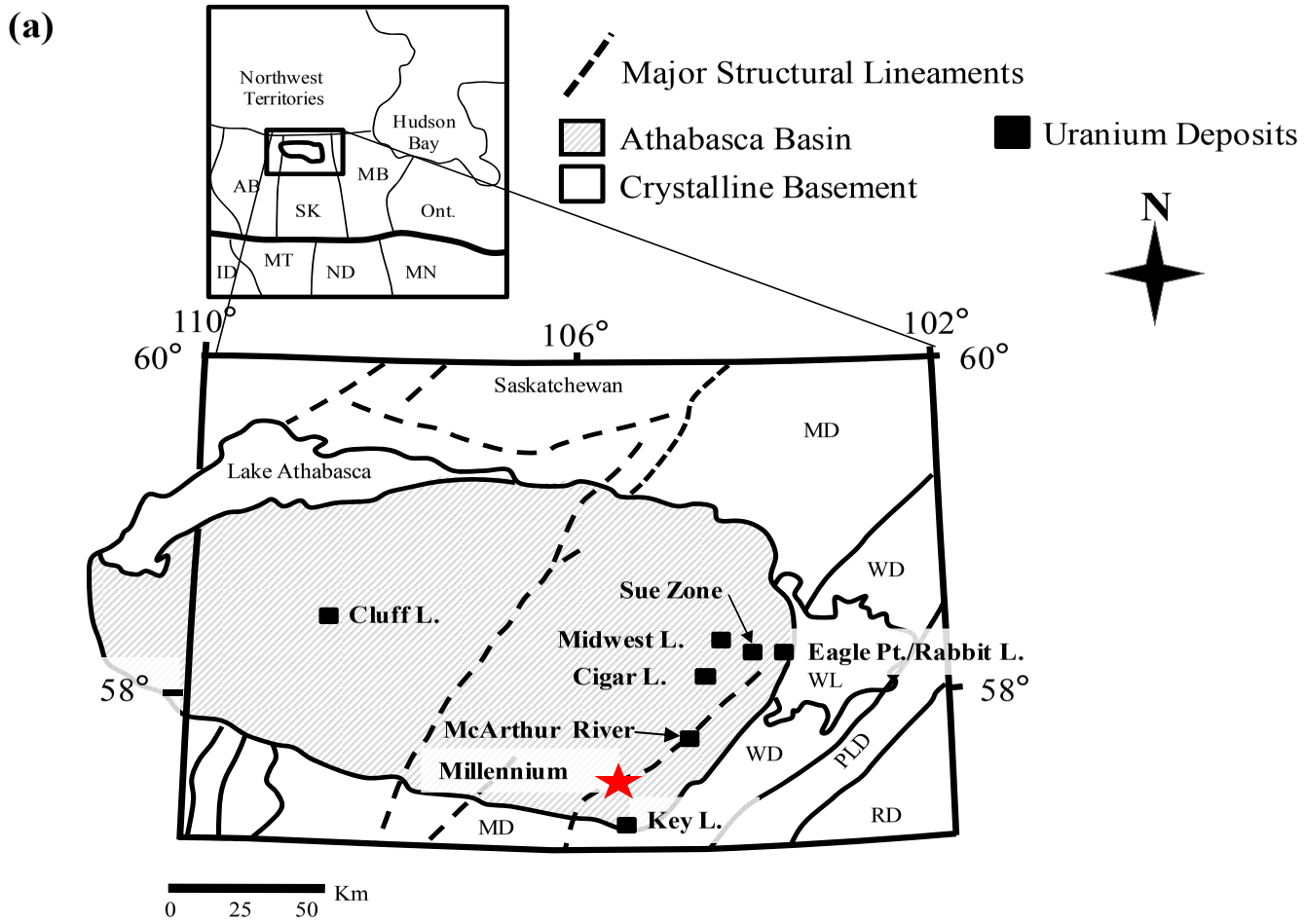

Figure 2.1: A map of the Athabasca Basin showing the location of uranium deposits and major lithostructural domains in the crystalline basement of northern Saskatchewan, Canada. Abbreviations: MD= Mudjatik Domain; WD= Wollaston Domain; PLD= Peter Lake Domain; RD= Rottenstone Domain; WL= Wollaston Lake; R= River; L= Lake (Modified from Fayek, *et.al*, 1997, *reference modified from Hoeve and Sibbald, 1978*.).

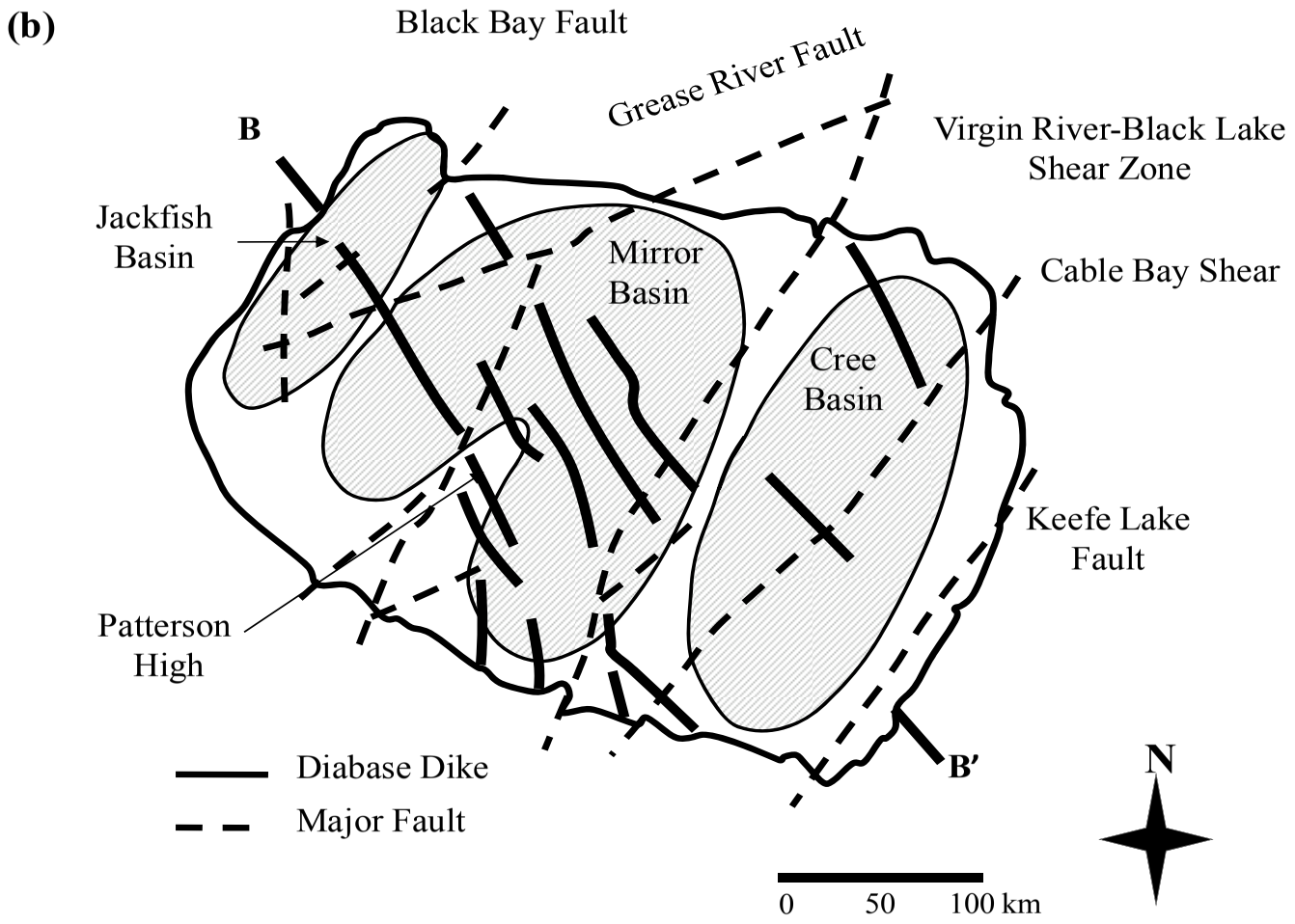

Figure 2.2: Location of sub-basins, major faults and diabase dikes in the Athabasca Basin (Modified from Fayek, *et. al*, 1997, *reference modified from Kotzer and Kyser, 1995.*).

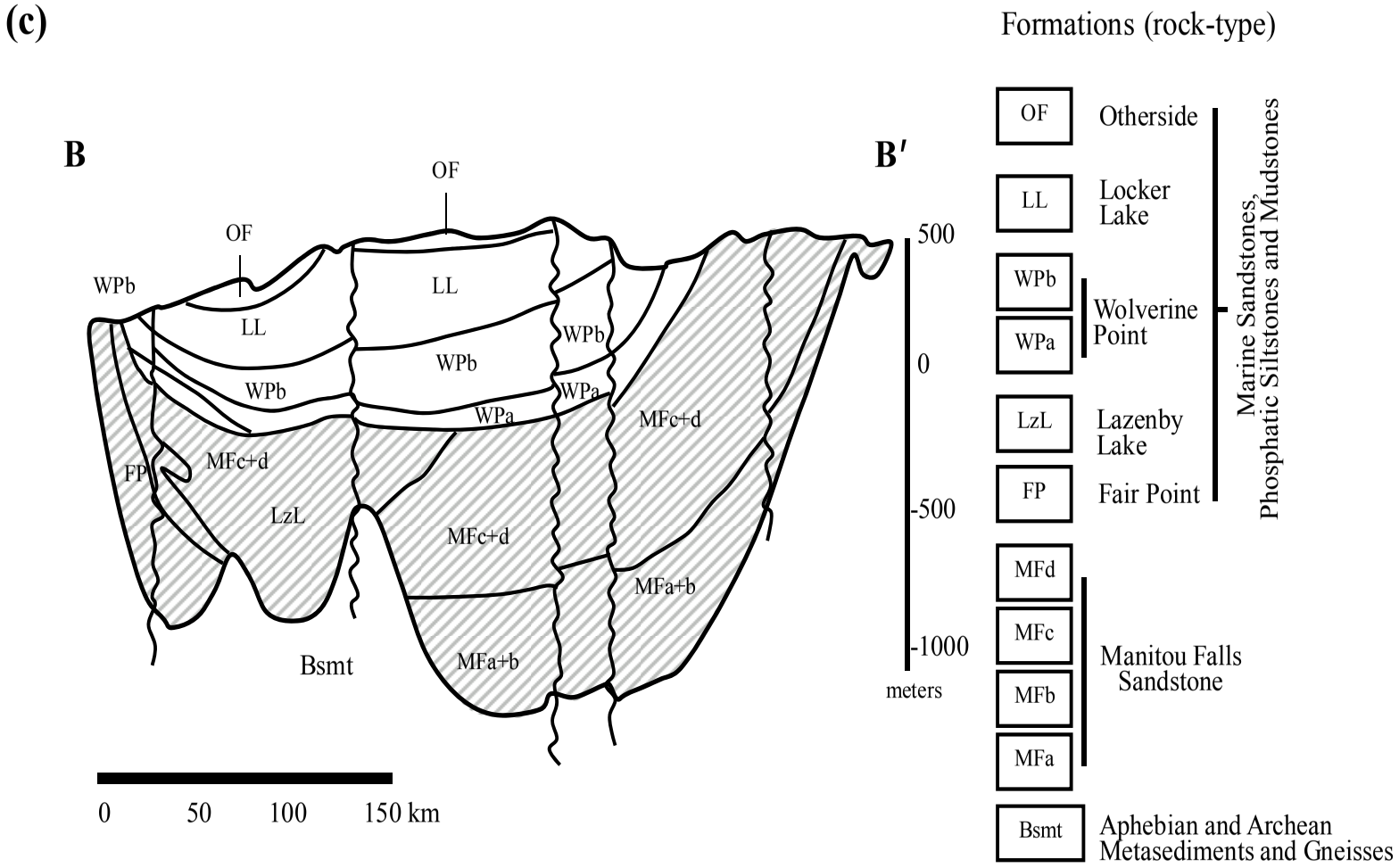

Figure 2.3: Generalized cross-section of the Athabasca Basin along B-B' (Fig.2.2) ~ showing the general stratigraphy of the Athabasca Basin (Modified from Fayek, *et. al*, 1997, *reference modified from Kotzer and Kyser, 1995*.).

2.2 Millennium deposit geology

2.2.1 Deposit Location and Exploration

The Millennium deposit is located within the Cree Extension project approximately 45 kilometers from the southeastern edge of the Athabasca Basin, and 35 kilometers to the north of the Key Lake mine, near the contact between the Wollaston and Mudjatik Domains (Fig.2.1). The Cree Extension project is a joint venture between Cameco Corporation, JCU (Canada) Exploration Ltd., and Areva Resources (Canada) Inc. (Roy, *et. al,* 2005; Thomas, 2002). The Cree Extension project covers an area of 12,777 hectares and is the remnant of a much larger property that once totaled nearly 200,000 hectares (Roy, *et. al,* 2005) (Fig.2.4).

Four north-northeast trending conductive packages (identified as B_1-B_4) were located beneath the Cree Extension property in the mid 1980s (See B_1 corridor Fig.2.5) using airborne and ground based geophysical electromagnetic surveys (Roy, *et. al,* 2005; Thomas, 2002). The electromagnetic conductors correlate with graphitic metasedimentary rocks within the basement beneath the Athabasca Group cover rocks on the Cree Extension project (Roy, *et. al,* 2005). The electromagnetic conductors were designated as priority exploration targets; since previous exploration experience (i.e. the 1976 discovery at Key Lake) showed graphitic metasediments in the basement rocks have a control on the location of unconformity-associated uranium deposits (Sibbald, 1985). More focus was applied along the B_1 conductor, when evidence of post-Athabasca faulting and abnormal sandstone geochemistry was identified along the southern end of the conductor (Roy, *et. al,* 2005).

When the Cameco Corporation took over as exploration operator on the Cree Extension project in 1998; they took particular interest in diamond drill hole (DDH) CX-38, drilled by the previous operator Uranerz Exploration and Mining (Fig.2.6). The lower 200 meters of altered sandstone within CX-38 averaged 0.9 ppm U and the basement rocks displayed strong hydrothermal alteration that extended >80 meters beneath the unconformity. The sandstone and basement rocks also displayed abnormal lead and boron values in DDH CX-38 (Roy, *et. al,* 2005). Continued exploratory drilling of the B1 conductor lead to the discovery of the Millennium deposit in March 2000. The discovery drill hole, DDH CX-40, contained mineralization extending for over 153 meters. The best segment of continuous mineralization within this intersection was 29 meters at approximately 1% U (Fig.2.5, 2.6) (Roy, *et. al,* 2005, Thomas, 2002).

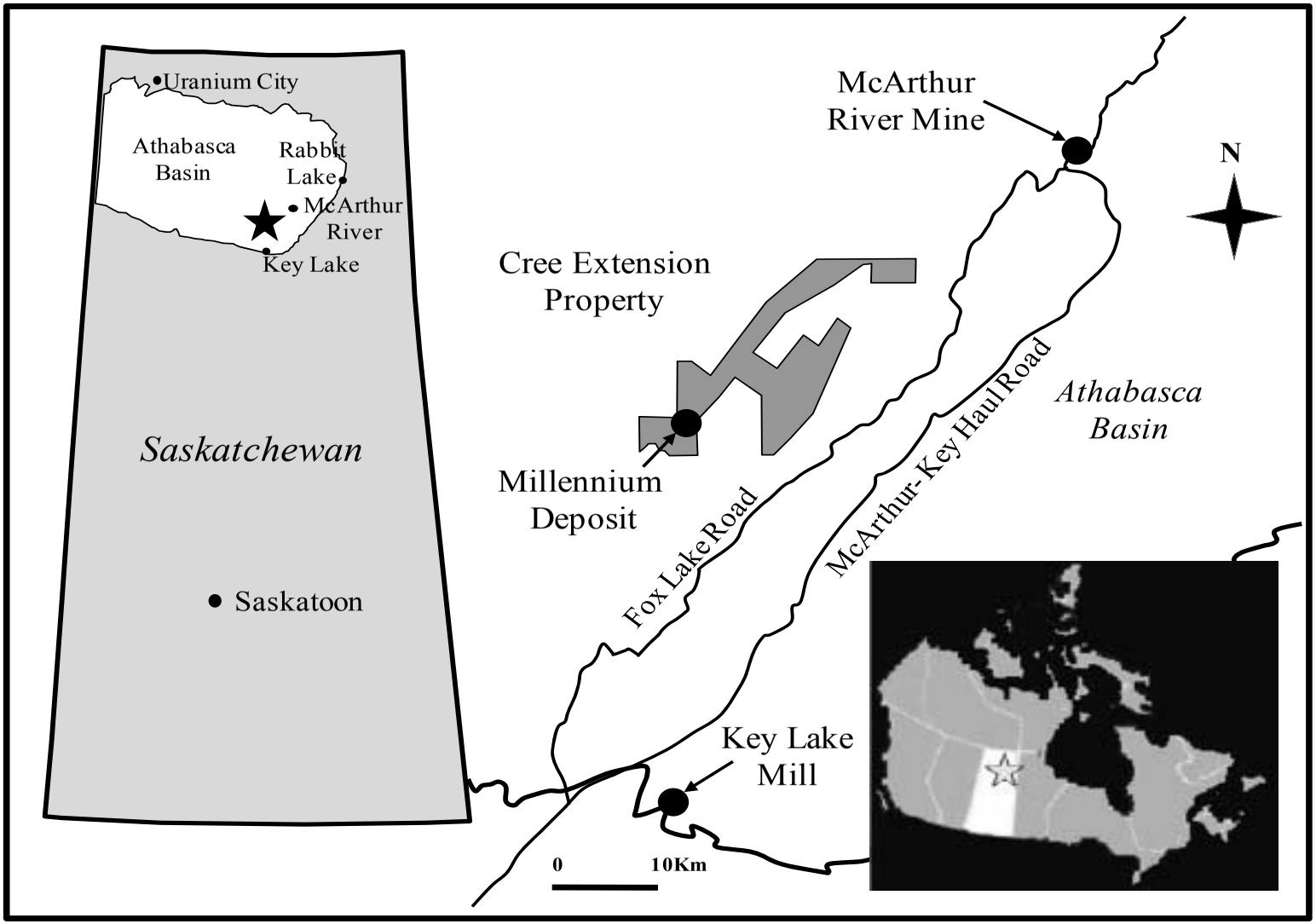

Figure 2.4: Location map of Cree Extension Property Athabasca Basin, Saskatchewan, Canada (Modified from Roy, *et. al*, 2005).

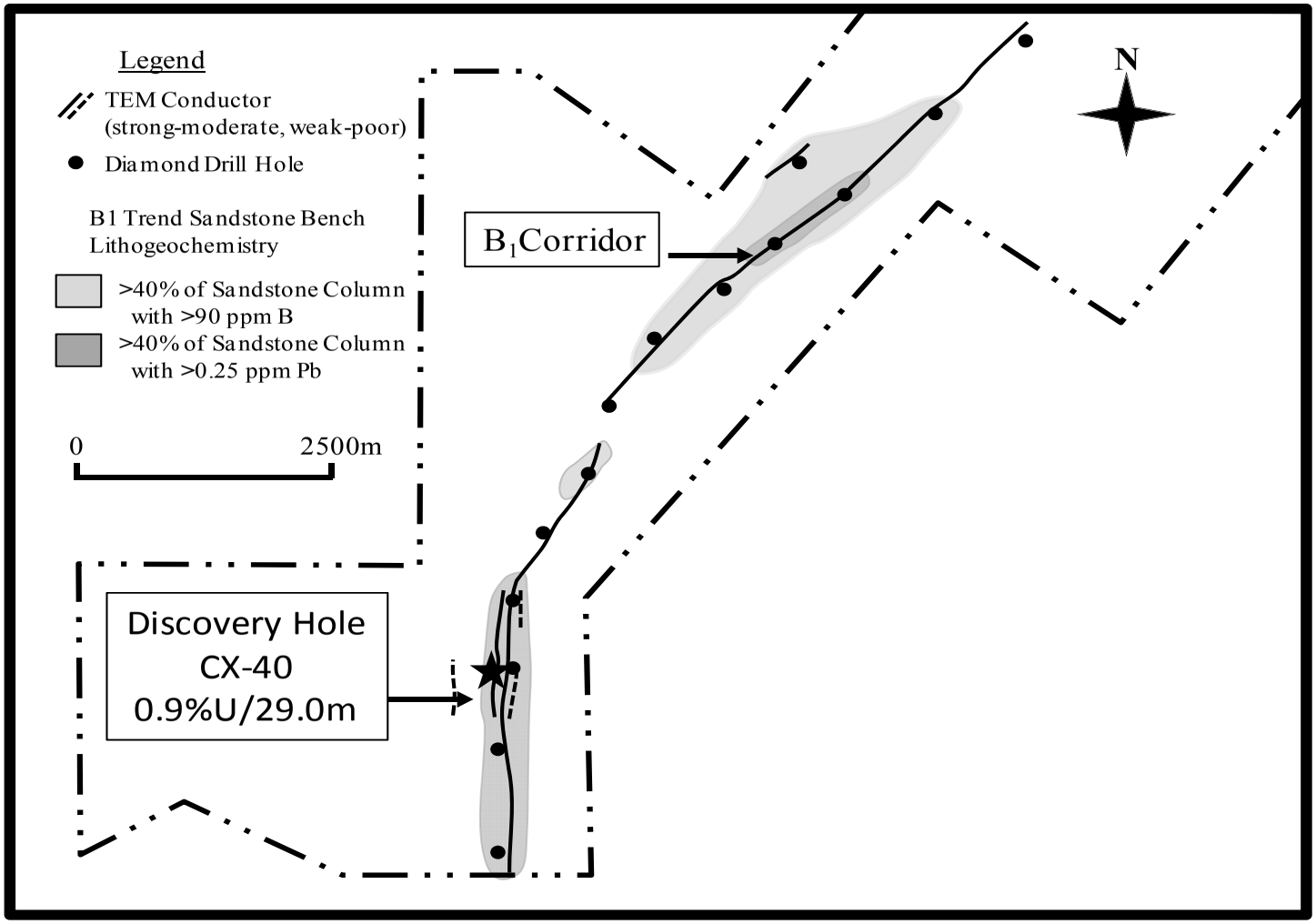

Figure 2.5: Map of the Cree Extension property showing B1 graphitic conductor and location of diamond drill holes (DDH), Millennium discovery DDH CX-40, and sandstone geochemistry anomalies. Abbreviations: CX= Cree Extension Project (Modified from Roy, *et. al*, 2005).

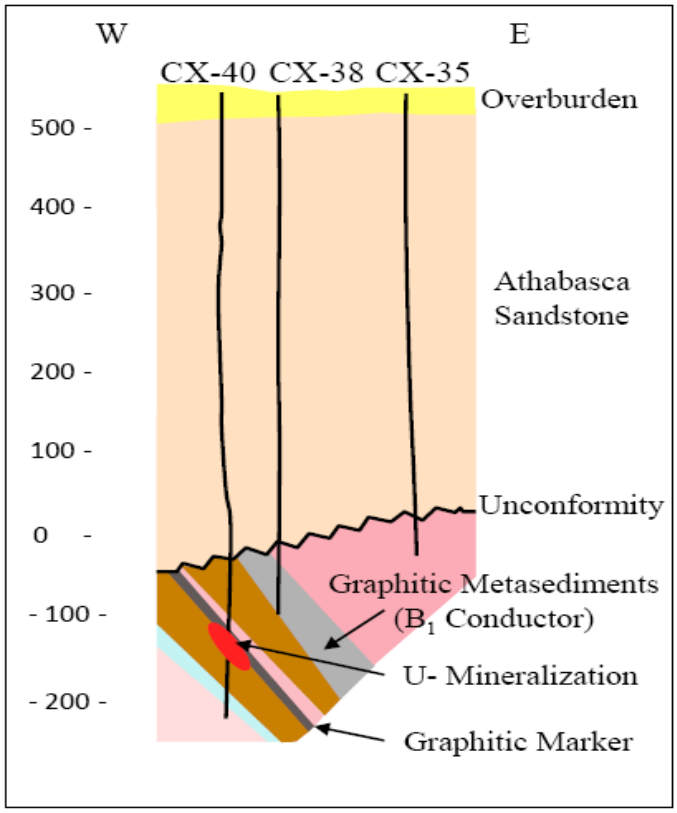

Figure 2.6: Generalized W-E cross-section through the Millennium deposit showing the location of DDH CX-38 and the Millennium discovery hole CX-40.
Abbreviations: CX= Cree Extension Project (Roy, *et. al*, 2005).

2.2.2 Basement geology

The basement rocks that host the Millennium deposit are composed of graphitic and non-graphitic pelitic to psammopelitic gneisses/schists, with minor intercalated calc-silicate and amphibolites that have been locally intruded by anatectic pegmatites (Thomas, 2002). The basement sequences have been defined by Roy, *et. al*, (2005), and divided into ten lithological units (here termed assemblages) (Fig.2.7):

I. *Granitic Assemblage* – The granitic assemblage is dominated by pegmatite-leucogranite units intercalated with minor units of semipelitic gneiss/schists and typically underlies the unconformity to the east of the Millennium deposit.

II. *Graphitic Metasediments* – The graphitic metasediments consist of graphitic and non-graphitic pelitic to semipelitic gneisses/schists. The graphitic pelitic gneisses/schists are believed to be the cause of the B_1 conductor. These units are typically intercalated with leucogranite. The thickness of the graphitic metasediments varies from 40 to 55 metres.

III. *Heterogeneous Metasediments* - The heterogeneous metasedimentary assemblage is dominated by texturally and compositionally varied, non-graphitic pelitic to semipelitic gneisses/schists and minor calc-silicates. This unit also contains anatectic pegmatite intrusions which vary from a few centimeters to several metres in thickness. The contacts between these pegmatites and the pelitic-semipelitic gneisses/schists are locally the sites of weak uranium mineralization. The apparent thickness of this unit varies from 20 to 40 metres.

IV. *Hanging Wall Pegmatite* - A pegmatite dike unit which is referred to as the 'hanging wall pegmatite' generally overlies the main uranium mineralization within the Millennium deposit. The thickness of the hanging wall pegmatite varies between 3 and 20 metres.

V. *Graphitic Marker Unit* – The graphitic marker unit is a moderately to strongly graphitic, pelitic schist that contains cordierite porphyroblasts. The marker unit, ranges between 0.5 and 10 metres in thickness, and is locally the site of uranium mineralization. This unit commonly exhibits semi-brittle shear fabrics and locally it has been observed in fault contact with the underlying pelitic-semipelitic gneisses/schists.

VI. *Host Assemblage* - The host assemblage is composed of a series of non-graphitic pelitic to semi-pelitic gneisses/schists that host the more significant uranium mineralization. The total thickness of the host assemblage is estimated at 25 to 55 metres, but the lower limit of the assemblage is not well defined due to intense hydrothermal alteration.

VII. *Upper Calc-Silicate Assemblage* - This unit is dominated by calc-semipelitic gneisses/schists and is commonly interbedded with semipelitic schists. Minor occurrences of weak uranium mineralization have been observed within this assemblage and are preferentially distributed within the semipelitic schists. The thickness of this interval ranges from 9 to 15 metres.

VIII. *Bracketed Assemblage* – The bracketed assemblage is composed of a series of pelitic to semipelitic gneisses/schists The unit commonly displays weakly disseminated uranium mineralization and/or elevated background radioactivity over its entire length. The bracketed unit ranges in thickness from 15 to 25 metres.

IX. *Lower Calc-Silicate Assemblage* - This interval is largely comprised of interbedded calc-semipelitic and calc-pelitic gneisses/schists with lesser amphibolite gneiss. The assemblage commonly displays intense clay alteration, dravite ± quartz healed hydraulic brecciation and little to no uranium mineralization. The thickness of the assemblage ranges from 25 to 40 metres and this unit forms the immediate hanging wall margin of a major reverse fault within the Millennium area.

X. *Footwall Assemblage* – The footwall assemblage is composed of a series of non-graphitic semipelitic gneisses interbedded with massive well foliated granitic

gneisses. The frequency of the semipelitic gneisses within the footwall assemblage decreases with depth and separation from the overlying fault zone, where the granitic gneisses become the dominant lithological units. The thickness of this unit has not been defined.

2.2.3 Structure

The structural setting of the Millennium area is based on airborne and ground based magnetic surveys and oriented drill core measurements. Thomas (2002) suggests that the Millennium area is located within a regional north-northeast trending structural corridor that is the result of a complex fold interference pattern. This is based on interpretation of regional magnetic data. Two principal axial surfaces traces (F_1 and F_2) have been recognized within the Millennium area (Roy, *et. al*, 2005). Early deformation (D_1) produced shallow dipping recumbent structures (F_1) that verge to the northwest. The early F_1 folds were subsequently refolded by a later deformational event (D_2) into more upright northeast trending F_2 folds that are inclined towards the northwest. The Millennium Zone is interpreted to lie within a north-trending F_2 synform (Thomas, 2002; Roy, *et. al*, 2005).

The most significant structural feature within the Millennium area is a reverse fault, known as the "Mother Fault" located at the base of the Lower Calc-Silicate Assemblage (Fig.2.7). This fault zone is characterized by angular wall rock clasts in a clay/dravite matrix and locally by fine-grained resilicified fault breccia. According to Thomas (2002) the fracturing of basement units in proximity of the fault zones makes the determination of their orientations difficult. Roy et. al, (2005) suggest that the Mother fault has an approximate thickness of 10 meters, strikes to the north and has a moderate

easterly dip. In drill-core, the graphitic "marker unit" displays, semi-brittle shear fabric and locally it has been observed in fault contact with the underlying pelitic-psammopelitic gneisses and schists. The "marker unit" is interpreted as a potential reverse fault that has offset the unconformity by approximately 25 meters (Fig.2.7) (J. Halaburda, pers. comm.). The basement units situated between the "marker fault" and the Mother fault display increased brecciation, argillic alteration, and multiple generations of fracture filled veins. Based on these observations it is inferred that a dilational zone was developed between the two sub-parallel reverse faults which increased the permeability of the basement rocks within the hanging-wall block.

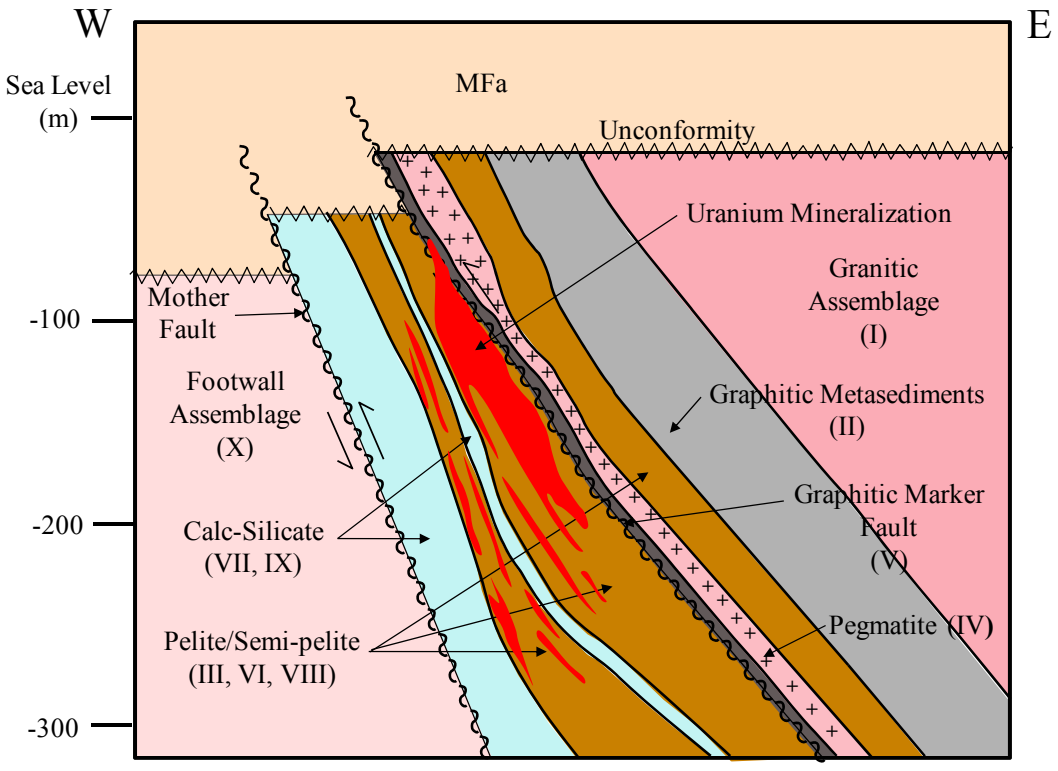

Figure 2.7: Generalized west-east cross-section through the basement-hosted Millennium Deposit, Athabasca Basin, Saskatchewan, Canada. Showing unconformity offset along the Mother fault and the reverse fault at the graphitic "marker unit". See text for description of basement units (Modified from Roy, *et. al*, 2005).

Chapter 3: Methodology

3.1 Overview

The basement units in ten drill holes from the Millennium Deposit were reviewed in the summer of 2006 (Appendix B) to develop an understanding of the hydrothermal alteration and emplacement of uranium mineralization on the host rocks. From these ten drill holes, three were selected for detailed study. Two of these drill holes DDH's CX-44-1 and CX-56-1 intersect uranium mineralization and display strong hydrothermal alteration. The third DDH CX-58 does not intersect uranium mineralization or the Mother fault and is weakly altered.

3.2 Sampling procedures

A total of 49 drill-core samples were collected from the basement units (25 samples from mineralized DDH's CX-44-1 and CX-56-1 and 24 samples from unmineralized DDH CX-58) for petrography, fluid inclusion analysis, stable and radiogenic isotopic and geochemical analyses. In DDH's CX-44-1 and CX-56-1, samples were selected from areas of high-grade uranium mineralization, alteration halos associated with uranium mineralization, and unmineralized basement units proximal to uranium mineralization. Samples were also collected from an unmineralized and weakly altered DDH CX-58 and compared to the highly altered and mineralized basement units in DDH's CX-44-1 and CX-56-1.

Polished thin-sections of samples collected from drill core were prepared to determine the paragenetic relationship between primary and secondary uranium minerals and the alteration minerals. The mineralogical characteristics of the uranium minerals were examined using reflected and transmitted light microscopy, as well as scanning

electron microscopy (SEM) and back-scattered electron imaging (BSE). The chemical composition of clay and silicate minerals, and uranium oxides were determined by electron microprobe (EMP).

3.2 Analytical techniques

3.2.1 Scanning Electron Microscopy

Polished thin-sections were analyzed using a Cambridge Stereoscan 120 scanning electron microscope (SEM) at the University of Manitoba. The samples were cleaned and carbon coated to ensure sample surface would be conductive. The samples were then mounted and placed under vacuum and analyzed with a 15 keV electron beam. Backscattered electron images were collected and electron dispersive spectroscopy (EDS) was used to characterize the samples.

3.2.2 Electron Microprobe

The compositions of clay and silicate minerals in mineralized and unmineralized drill core were measured using an automated CAMECA SX-100 X-ray microanalyzer by wavelength-dispersive spectroscopy. Analyses were performed using the following analytical conditions: 15 keV, a beam diameter of 10 μm, with counting times of 40 seconds per element with the exception of fluorine with a counting time of 120 seconds. The following elements were analyzed: sodium (Na), aluminum (Al), silicon (Si), fluorine (F), magnesium (Mg), potassium (K), calcium (Ca), iron (Fe), titanium (Ti), chromium (Cr), chlorine (Cl) and manganese (Mn). Albite was used as a standard for the calibration of Na, andalusite for Al, diopside for Si and Ca, topaz for F, olivine for Mg, orthoclase for K, fayalite for Fe, sphene for Ti, chromite for Cr, tugtuphite for Cl and spessartine for Mn.

Uranium minerals were also measured using the same analytical conditions with the exception of a smaller beam diameter of 1 μm. The following elements were analyzed: silicon (Si), uranium (U), titanium (Ti), iron (Fe), lead (Pb), calcium (Ca), aluminum (Al), thorium (Th), and sulfur (S). Diopside was used as a standard for the calibration of Si and Ca, UO_2 for U, sphene for Ti, fayalite for Fe, Pb-Te for Pb, andalusite for Al, ThO_2 for Th and pyrite for S. Detection limits for elements in both uranium and silicate minerals is on the order of 0.1 wt%. The program ZAF was used to reduce the data. Oxygen content of uraninite and silicate minerals was calculated by stoichiometry using an ideal chemical composition.

3.2.3 Mössbauer spectroscopy

Mössbauer spectroscopy measurements on whole-rock samples were obtained using transmission geometry at room temperature with a ^{57}Co (Rh) point source. The spectrometer was calibrated relative to the room-temperature spectrum of α-Fe. For preparing the Mössbauer absorber, ~ 2-5 mg of powdered sample was mixed with sugar and finely ground under acetone to avoid excessive oxidation. The mixture was then loaded into a Pb ring (2 mm inner diameter) and covered by tape on both sides. The spectra were analyzed by a Voigt-function-based quadrupole splitting distribution method using the RECOIL software (Rancourt and Ping, 1991).

3.2.4 Fluid Inclusions

Fluid inclusion measurements were made on a Fluid Inc. adapted U.S.G.S. Gas-Flow Heating/Freezing System at the University of Manitoba. The system is equipped with a Doric Trendicator that is used to measure temperatures from -190 °C – 700 °C. The Trendicator is used in conjunction with a thermocouple to measure the temperature

within the sample chamber. In order for the Trendicator to know that a given voltage potential occurring at the welded joint of the thermocouple corresponds to a specific real temperature, the Trendicator was calibrated at three points: a zero point, a point to set the negative slope of the voltage-temperature curve, and a point to set the positive slope of the voltage-temperature curve. For this study, the Trendicator was calibrated at -56.6 °C, 0.0 °C, and 374.1 °C using fluid inclusion standards of pure H_2O and CO_2 enclosed in synthetic quartz. After initial calibration, a standard was measured each day to ensure the stage remained calibrated before measuring fluid inclusions of unknown composition.

3.2.5 Secondary Ion Mass Spectrometry (SIMS)

3.2.5.1 Stable Isotopes

The oxygen isotopic composition of uraninites, metamorphic and secondary euhedral quartz associated with vein-type uranium mineralization from the Millennium deposit were measured by secondary ion mass spectrometry (SIMS) using a CAMECA IMS 7F ion microprobe. Operating conditions for oxygen isotopic analysis of uraninites were 1.0-nA, +10 kV primary beam of Cs^+ ions, and a 5-nA primary beam was used for quartz. These operating conditions produced sputter craters ~10 μm and 15 μm in diameter, respectively. The secondary accelerating voltage was set at -5 kV and a 300 V offset was used to eliminate molecular ion interferences (Riciputi, *et.al*, 1998; Fayek, *et.al*, 2002). Ions were detected with an ETP electron multiplier coupled with and ion-counting system and an overall dead time of 27 nanoseconds. $^{16}O^-$ and $^{18}O^-$ were detected sequentially by switching the magnetic field. A typical analysis lasted 10 minutes, comprising 90 cycles of analysis. All oxygen isotopic data are presented in the standard δ-notation relative to the appropriate standard. The $\delta^{18}O$ values of uraninite and quartz

are reported in units of per mil (‰) relative to Vienna Standard Mean Ocean Water (V-SMOW). The equation for calculating δ values in of per mil (‰) is

$$\delta^{18}O = [[(^{18}O/^{16}O)_{sample} / (^{18}O/^{16}O)_{V\text{-}SMOW})] - 1] \times 10^3 \qquad [1]$$

Isotopes measured by SIMS were compared to the accepted ratios (calculated from δ values determined by isotope bulk analysis) for each mineral using equation [2]:

$$(^{18}O/^{16}O)_{sample} = [(\delta^{18}O_{sample}/1000) + 1] \times (^{18}O/^{16}O)_{V\text{-}SMOW} \qquad [2]$$

where the $^{18}O/^{16}O$ ratio of V-SMOW is defined as 2.0052×10^{-3}. These data can be used to calculate the isotope mass fractionation that occurs during SIMS analysis using equation [3]:

$$\beta_{bias} = (^{18}O/^{16}O)_{SIMS} / (^{18}O/^{16}O)_{CONV.} \qquad [3]$$

where the $(^{18}O/^{16}O)_{SIMS}$ is the ratio measured by SIMS and the $(^{18}O/^{16}O)_{CONV.}$ the accepted ratio measured by conventional bulk gas source isotope mass spectrometry. The isotope mass fractionation that occurs during SIMS analysis (β_{bias}) can be converted into δ notation by using equation [4]:

$$\delta^{18}O_{bias} = [(^{18}O/^{16}O)_{SIMS/} (^{18}O/^{16}O)_{CONV.} - 1] \times 1000 = (\beta_{bias} - 1) \times 1000 \qquad [4]$$

3.2.5.2 Radiogenic Isotopes

The isotopes of lead and uranium in Millennium uraninite samples were measured by secondary ion mass spectrometry (SIMS) using a CAMECA IMS 7F ion microprobe. Operating conditions for U and Pb analysis were ~2.0-nA primary ion beam of O^- accelerated at 12.5 keV. The secondary accelerating voltage was set to +5 kV. A voltage offset of -50 V in conjunction with a mass resolving power of 1300 was used to eliminate isobaric interferences. Ions were detected with an ETP electron multiplier coupled with an ion-counting system. The following species were detected sequentially by switching

the magnetic field: $^{204}Pb^{+}$, $^{206}Pb^{+}$, $^{207}Pb^{+}$, $^{208}Pb^{+}$, $^{208}Pb^{+} + {}^{1}H^{+}$, $^{235}U^{+}$, $^{238}U^{+}$, $^{238}U^{+} + {}^{1}H^{+}$, $^{235}UO^{+}$, and $^{238}UO^{+}$. A typical analysis lasted ~10 minutes, comprising 20 cycles of analysis. Negligible amounts of common Pb ($^{204}Pb^{+}$) were detected. The following isotopic ratios were calculated: $^{206}Pb^{+}/^{204}Pb^{+}$, $^{207}Pb^{+}/^{204}Pb^{+}$, $^{207}Pb^{+}/^{206}Pb^{+}$, $^{208}Pb^{+}/^{204}Pb^{+}$, $^{235}U^{+}/^{238}U^{+}$, $^{206}Pb^{+}/^{238}U^{+}$, $^{207}Pb^{+}/^{235}U^{+}$, $^{238}UO^{+}/^{238}U^{+}$ and $^{238}U^{+}/\ ^{238}U^{+} + {}^{1}H^{+}$, and reported in %.

The isotopic data was reduced using the program Isoplot (Ludwig, 1993). U-Pb data was discordant and fractionation factors were applied. Due to, an age discrepancy between the internal UO_2 standard and unknowns, the matrix effects and instrumental mass fractionation (IMF) for U and Pb could not be appropriately corrected. Therefore, the isotopic ratios of Pb were used to calculate ages for the uranium minerals because IMF for Pb isotope ratios in uraninite is negligible (<1 %; Fayek et al. 2002). Once the $^{207}Pb/^{206}Pb$ ratios for uraninite were obtained and since there was very little common Pb (i.e., a common Pb correction was not necessary), ages can be directly calculated using equation [1].

$$(^{207}Pb/^{206}Pb)^{*} = 1/137.88\ (e^{\lambda 2t} - 1/e^{\lambda 1t} - 1) \qquad [1]$$

where $(^{207}Pb/^{206}Pb)^{*}$ is the ratio of radiogenic ^{207}Pb to ^{206}Pb; t is time; $\lambda_1(^{238}U) = 1.55125 \times 10^{-10}\ y^{-1}$; and $\lambda_2(^{235}U) = 9.8485 \times 10^{-10}\ y^{-1}$ are the decay constants for ^{238}U and ^{235}U respectively; and 1/137.88 is a constant ratio for all uranium of normal isotopic composition in the Earth, Moon and meteorites at the present day.

Chapter 4: Results

4.1 Core description: mineralized vs. unmineralized samples

A total of 4 weeks in the summer of 2006 were spent at the Cree Extension project describing the major alteration phases, structural features (i.e. faults, breccias, and veins), and uranium mineralization styles visible in mineralized and unmineralized drill core in the basement rocks from the Millennium deposit. The objective of this work was to develop a broader understanding of the spatial relationship between uranium mineralization and host rock alteration. Alteration within the basement rocks is variable but generally increases with depth and proximity to fault structures (See drill core logs in Appendix B). Alteration types visible in mineralized and unmineralized drill core include:

1) Saussuritization and sericitization occurs as mineral controlled replacement in granites and granitic pegmatites as a result of retrograde breakdown of plagioclase and k-feldspars, respectively (Fig.4.1). Sericitization of micaceous minerals (i.e. muscovite) is also visible in pelitic and psammopelitic gneisses/schists primarily along foliation planes. Saussuritization and sericitization occurs in both mineralized and unmineralized drill core, it is more prevalent above the "marker unit" where granites and granitic pegmatites are more abundant. Saussuritization and sericitization appears again beneath the main orebody in the footwall assemblage where the frequency of pelitic and psammopelitic gneisses/schists decrease with depth and massive well foliated granitic gneisses become the dominant lithological units. This alteration is not spatially related with the main orebody.

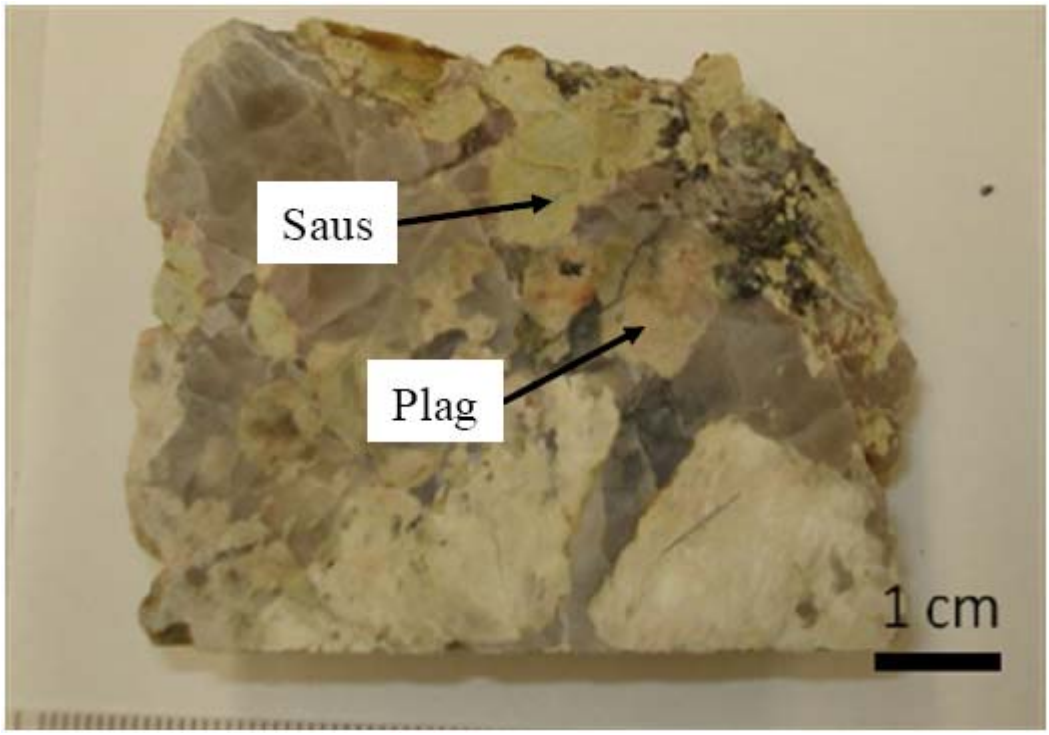

Figure 4.1: Drill core sample showing saussuritization of plagioclase in pegmatite CX-51 598.0 m. Abbreviations: Saus- saussuritization, Plag- plagioclase.

2) Chloritization occurs throughout the Millennium deposit. The first appearance of chlorite is visible within the paleoweathering profile just below the unconformity and typically occurs as a pale green coloration. Below the "marker unit" a zone of dark green-black chloritic alteration is spatially associated with the main orebody within mineralized drill core (Fig.4.2). Immediately above the Mother fault, intense argillic alteration and bleaching have effectively overprinted the chloritic alteration, with the result that these highly altered rocks display a pale green alteration (Fig.4.4). Locally chloritization occurs with and/or overprints an early hematization event which suggests the basement rocks have interacted with fluids under reducing and oxidizing conditions. In unmineralized drill hole CX-58, chlorite appears as dark green-black mineral that replaces iron rich minerals and feldspars (Fig.4.3).

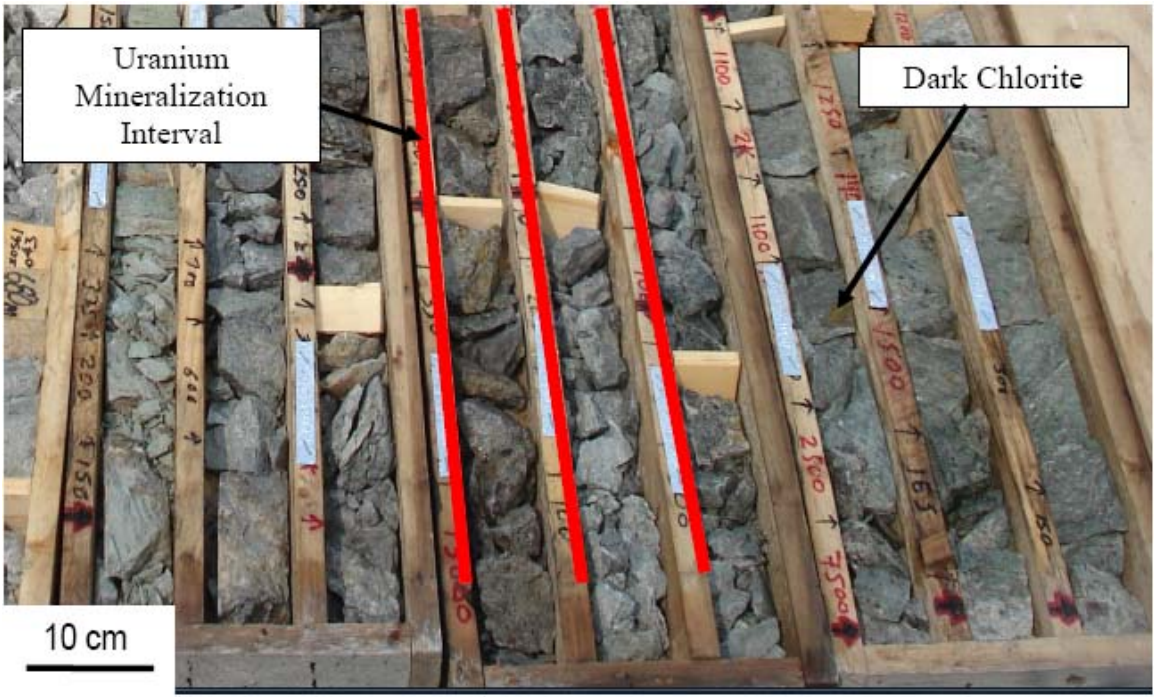

Figure 4.2: Drill core image showing uranium mineralization within chloritized pelite to semi-pelite DDH CX-56-1 665.3 – 678.5 m (Increasing depth from right to left).

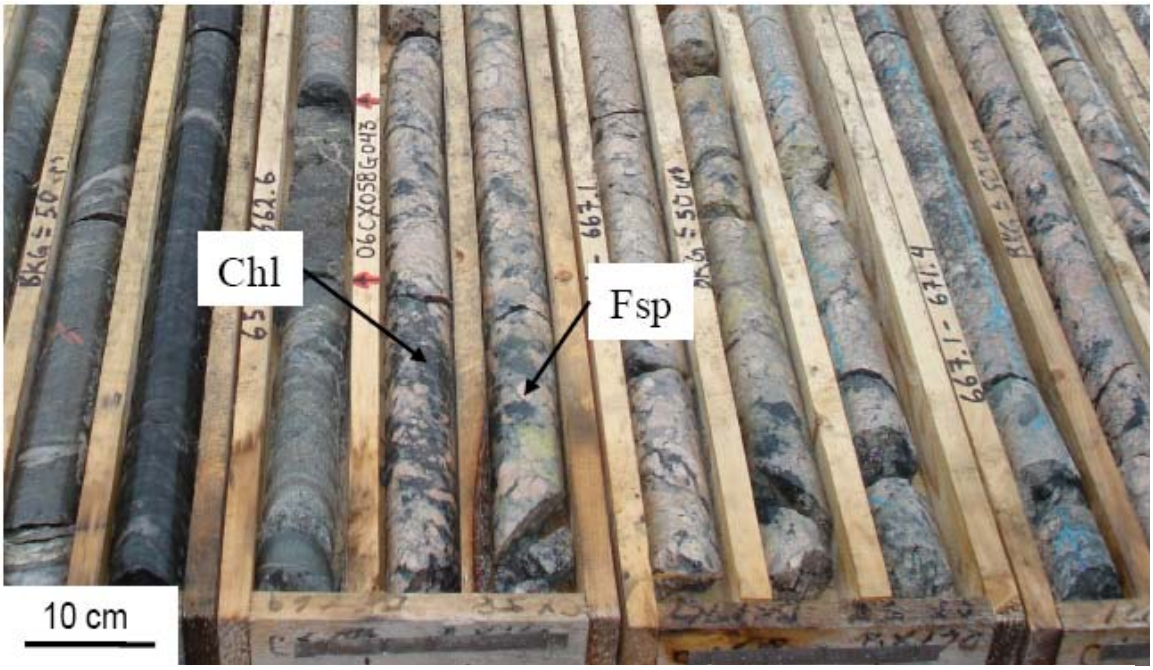

Figure 4.3: Drill core image showing dark green-black chlorite replacing feldspar in unmineralized pegmatite unit in DDH CX-58 653.6 - 671.4 m (Increasing depth from left to right). Abbreviations: Chl- chlorite, Fsp- feldspar.

3) Clay alteration and bleaching is variable in mineralized drill core but it increases in lower portions of the hanging wall beneath the “marker unit fault”. Clay alteration and bleaching increase with depth and is related to the reverse fault. Within the lower units, clay alteration and bleaching can completely mask the basement lithologies (Fig.4.4). A second clay alteration and bleaching event overprint hematite and uranium mineralization (Fig.4.5). In unmineralized DDH CX-58, bleaching is not well developed; with the exception of the paleoweathering profile at the unconformity

Figure 4.4: Drill core image showing strongly bleached and clay altered pelitic – psammopelitic gneisses and pegmatite units in proximity of reverse fault. Note pale green chloritization CX-44-1 799.5 - 815.5 m (Increasing depth from right to left).

Figure 4.5: Drill core image showing secondary hematite overprinted by late clay alteration and bleaching of psammopelitic schist DDH CX-51-1 737.5 m.

4) Several generations of hematization can be identified in the basement rocks within the Millennium area. Early hematite occurs as pale red-brown overprint marking the paleoweathering profile. Moderate red to brick-red intervals of secondary hematization typically occur beneath the main zone of uranium mineralization (Fig.4.6). Late remobilized hematite is associated with centimeter scale roll-front mineralization in bleached semi-pelitic schists (Fig.4.12b). Hematization appears frequently within mineralized drill core usually as a pervasive overprint of clay minerals and within pegmatitic units it is observed replacing clay altered feldspars (Fig.4.7). With the exception of hematization within the paleoweathering profile, the unmineralized drill hole displays no hematite overprint.

5) Quartz ± carbonate ± chlorite veins occur throughout the Millennium deposit in both mineralized and unmineralized drill core. Veins occur in a variety of styles including laminated quartz + carbonates (Fig.4.8), large drusy quartz veins (Fig.4.9), thin quartz veins cross-cutting earlier generations (Fig.4.10), and clay filled fractures/fault gouges

(Fig.4.11). These occur at different orientations and according to Thomas, (2002) these vein orientations are the result of several different fault structures and/or their reactivation during different deformation events.

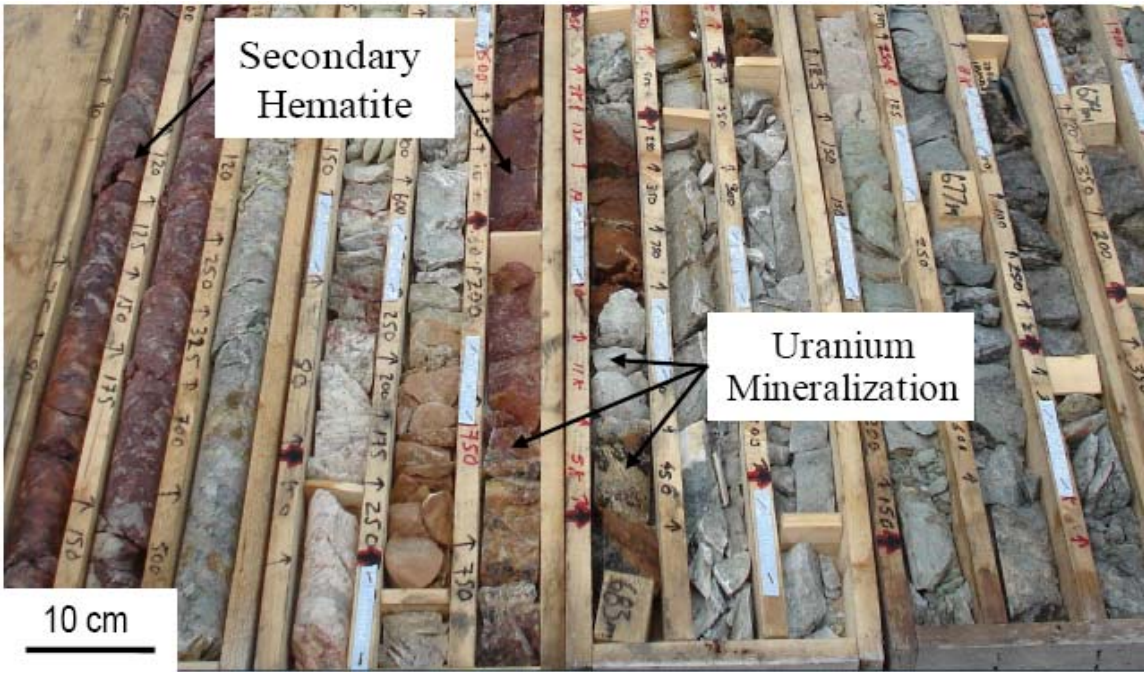

Figure 4.6: Drill core image showing secondary hematization interval located beneath high-grade uranium mineralization DDH CX-56-1 674.0 – 690.0 m (Increasing depth from right to left).

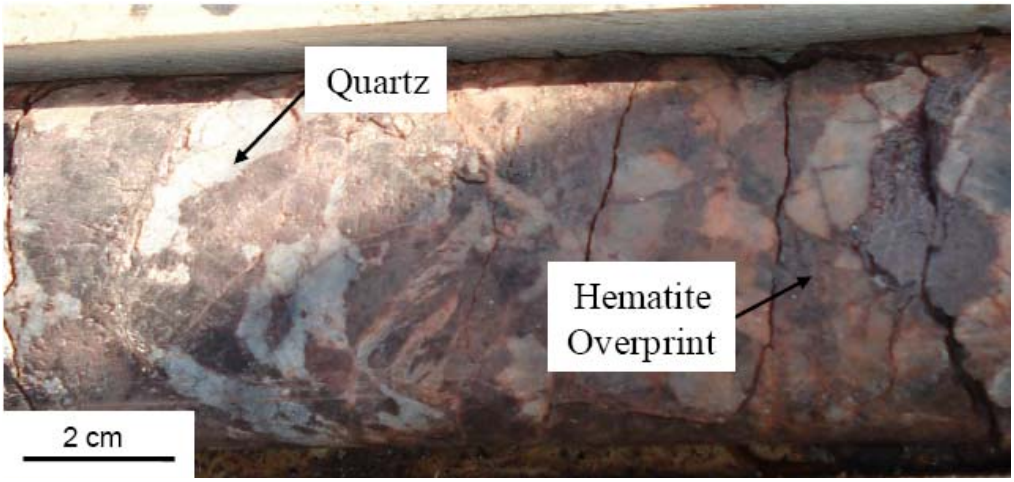

Figure 4.7: Drill core image showing hematite overprinting clay altered feldspars in pegmatite CX-56-1 670.2 m.

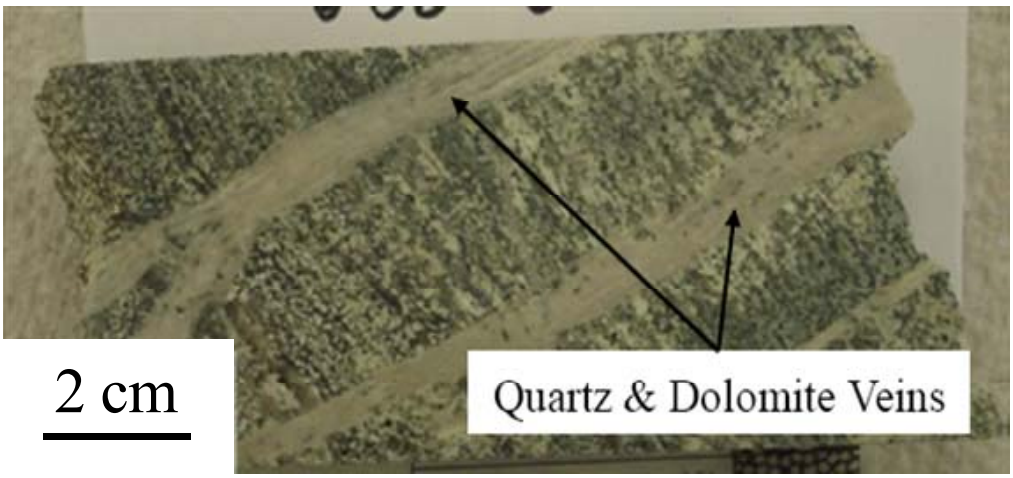

Figure 4.8: Drill core image of quartz and dolomite vein in chloritized psammopelitic schist DDH CX-58 652.0 m.

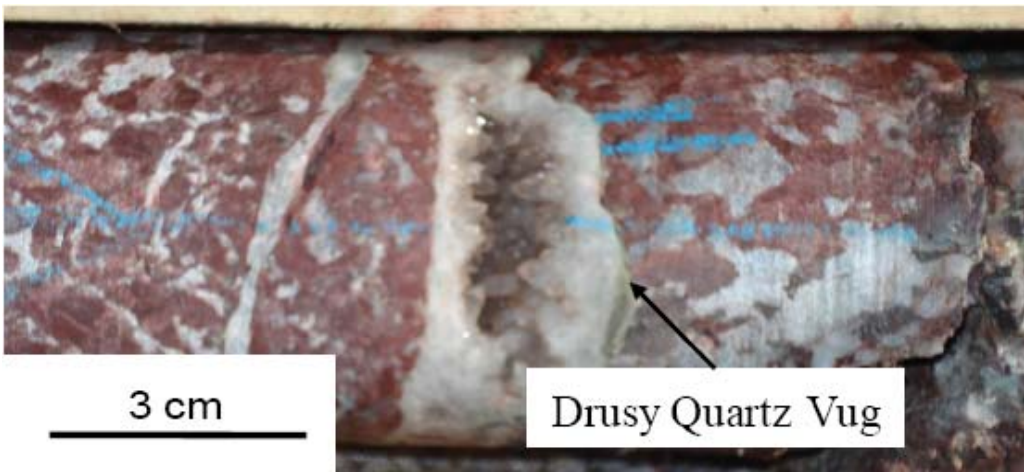

Figure 4.9: Drill core image of late quartz filled fracture with large drusy quartz vug in hematized pegmatite DDH CX-51 619.5 m.

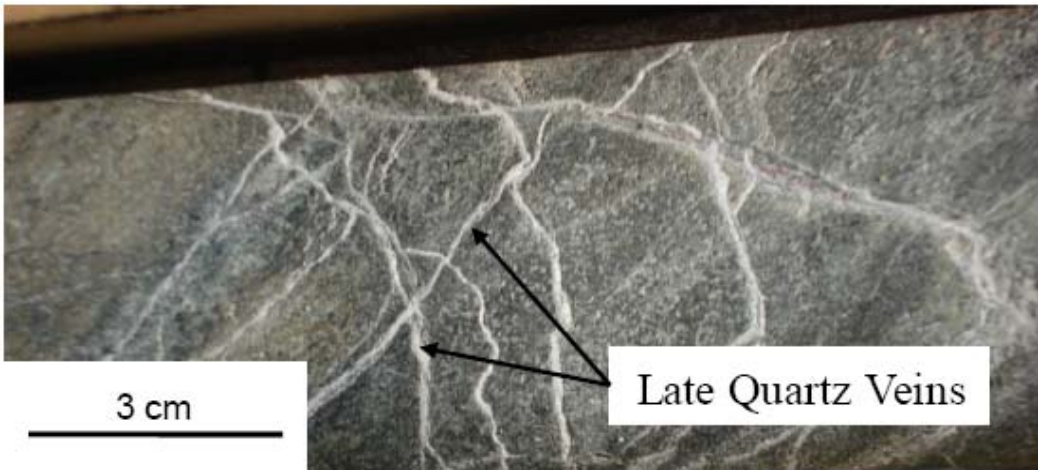

Figure 4.10: Drill core image showing late cross-cutting quartz veins in chloritized pelitic schist. DDH CX-51-1 618.5 m

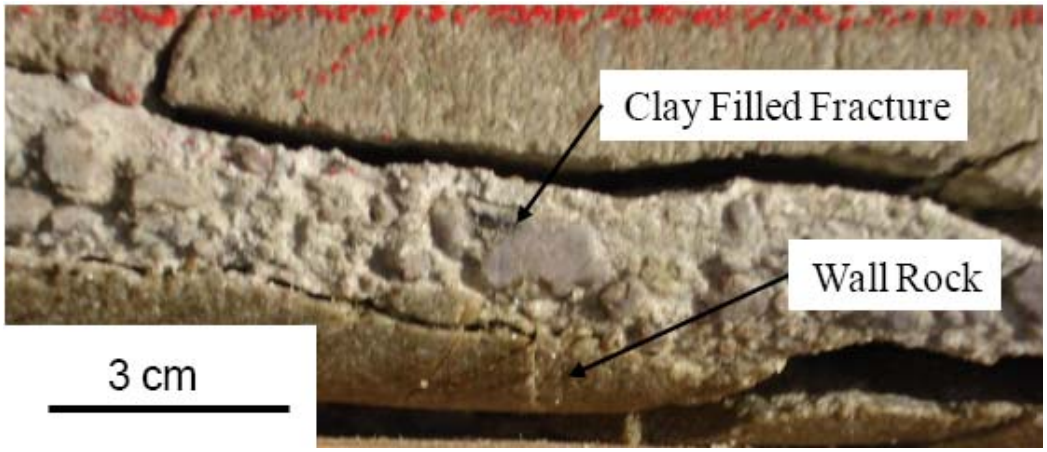

Figure 4.11: Drill core image showing clay filled fracture (fault gouge) with altered wall rock clasts in strongly-clay altered psammopelitic schist DDH CX-51-1 678.3 m.

6) Uranium mineralization within the Millennium deposit occurs in several distinct styles which include: massive replacement, fracture filling veins, "mini" roll-fronts and bleb-like grains (Fig.4.12). In drill core, massive replacement is the most prevalent mineralization style followed by vein type mineralization. The uranium mineralogy within the Millennium deposit consists mainly of pitchblende and uraninite with lesser amounts of coffinite.

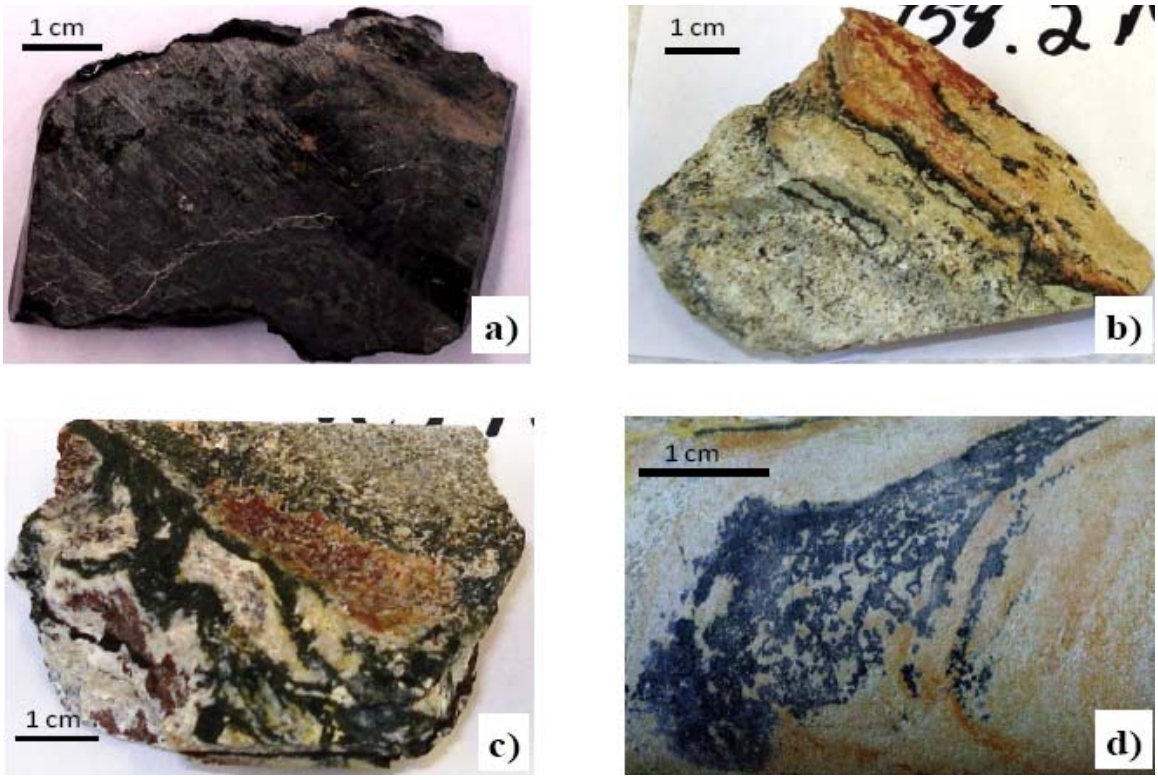

Figure 4.12: Uranium mineralization (black) in host pelitic-semipelitic gneisses/schists from the Millennium Deposit: a) massive replacement; b) mini roll-front, c) fracture filling vein; d) bleb-like replacement.

4.2 Petrography and Mineral Paragenesis

4.2.1 Clay and silicate minerals

The paragenetic relationship between host rock alteration and uranium mineralization cannot be clearly established from drill core observation alone. Polished thin sections have been prepared from the two mineralized drill holes (CX-44-1 and CX-56-1) and unmineralized drill hole (CX-58). Thin sections were examined by reflected and transmitted light microscopy and scanning electron microscopy (SEM). The chemical composition of clay and silicate minerals, and uranium oxides were measured by electron microprobe (EMP) and are used to support identification of fine-grained minerals in thin section. A summary of the paragenesis is shown in Figure 4.18.

Figure 4.13 contains transmitted light thin section images of mineralized and unmineralized basement rocks. A pegmatite unit (Fig. 4.13a) from unmineralized DDH CX-58 is composed of quartz, biotite, and k-feldspar. The sample displays weak argillic alteration (kaolinite) along grain boundaries, and weak chloritization of the biotite. Comparatively, pegmatites from mineralized drill core (Fig. 4.13b) display partial to complete breakdown of feldspars and micas to clay minerals (i.e. sericite, illite, and kaolinite). Figure 4.13c is a graphitic-cordierite pelite known as the "Marker Unit" in unmineralized DDH CX-58. This unit is composed of quartz, biotite, cordierite, and graphite and displays partial pinitization of cordierite porphyroblasts and chloritized biotite. The graphitic "marker unit" from mineralized drill core (Fig4.13d) is often altered and shows the breakdown of cordierite to pinite (chlorite + sericite), as well as chloritization and illitization of biotite.

Figure 4.13e an amphibolite from unmineralized DDH CX-58 is composed of hornblende and plagioclase and minor quartz, the unit displays weak alteration; mainly in the form of illite and chlorite along grain boundaries of plagioclase and hornblende. Figure 4.13f is a highly clay altered amphibolite collected in close proximity to the "mother fault" beneath the Millennium deposit in DDH CX-44-1. This unit displays few identifiable mineral phases due to an intense hydrothermal overprint. It has been identified as a calc-silicate in hand sample but in thin section remnant triple junctions are still visible and suggest that this unit is in fact a highly altered amphibolite.

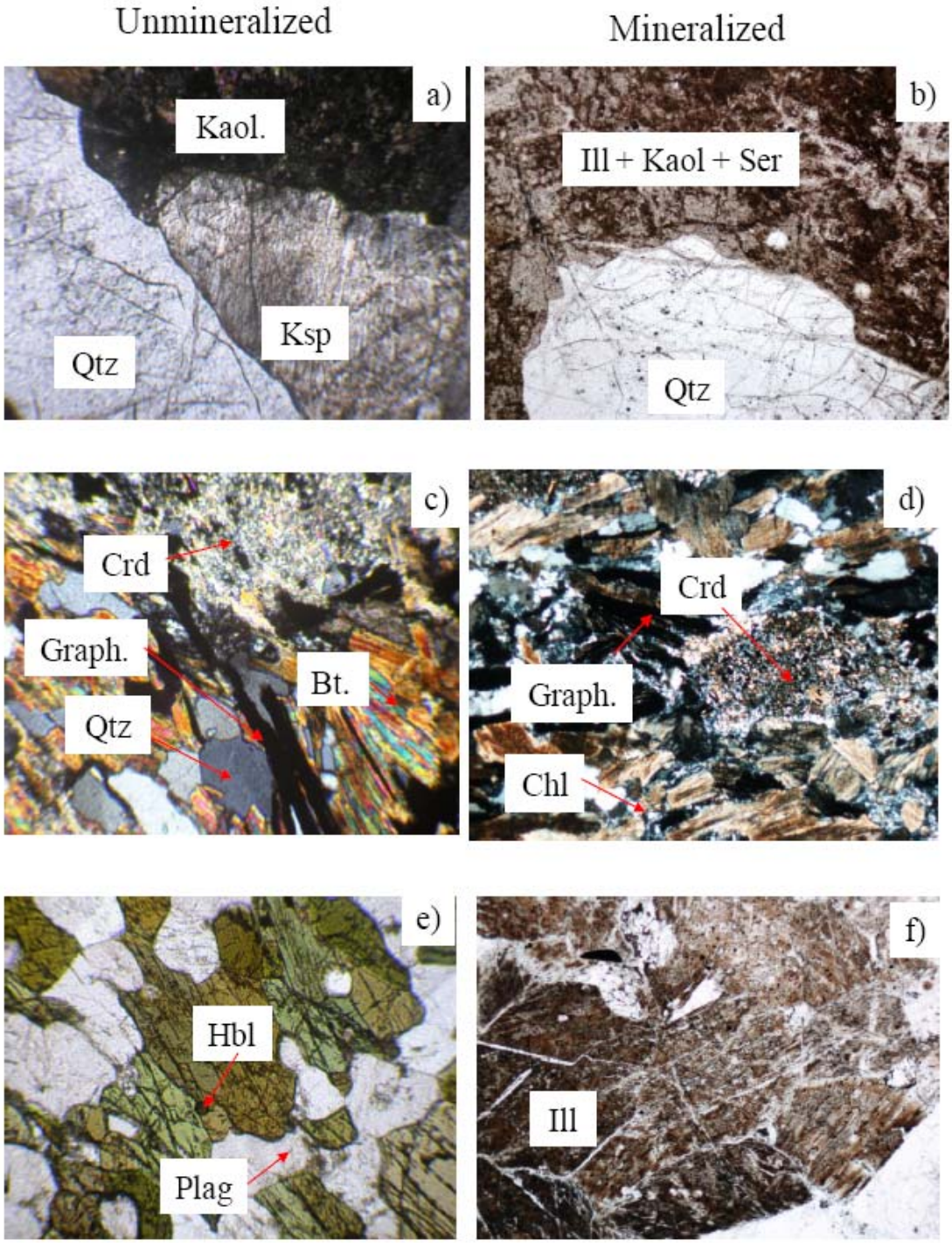

Figure 4.13: Transmitted Light images of unmineralized (CX-58) and mineralized (CX-56-1 and CX-44-1) drill core samples. a) Pegmatite CX-58 603.7 M, b) Pegmatite CX-56-1 602.0 M, c) Graphitic-Cordierite Pelite CX-58 625.6 M, d) Graphitic-Cordierite Pelite CX-44-1 651.0 M, , e) Amphibolite CX-58 724.0 M, f) Altered Amphibolite CX-44-1 722.9 M, Abbreviations: Qtz-quartz, Ksp-K-feldspar, Crd-cordierite, Graph-graphite, Bt-biotite, Plag-plagioclase, Hbl-hornblende, Ill-illite, Chl-chlorite, Kaol-kaolinite, Ser-sericite. Field of view is 2 mm.

4.2.1.1 Hydrothermal Alteration of Fe-rich Silicates

Electron microprobe analyses of Fe-rich silicate minerals (i.e. biotite and amphibole) show an approximate linear trend between FeO and MgO concentrations in biotite and amphibole (Fig. 4.14a) in unmineralized DDH CX-58. There is a significant decrease in the overall FeO and MgO concentrations in altered biotite from mineralized DDH CX-56-1 and they show a highly variable distribution (Fig. 4.14b). Compositionally biotite and amphibole in unmineralized DDH CX-58 contain ~10-30 wt% FeO and ~5-15 wt% MgO (See Table 2 Appendix A). Biotite compositions in mineralized drill core have ~2-10 wt% FeO and ~5-15 wt% MgO (See Table 3 Appendix A). The decrease in the FeO concentration in mineralized basement rock is attributed to chloritic alteration of biotite and amphiboles during fluid events, resulting in the release of Fe into the basement rocks.

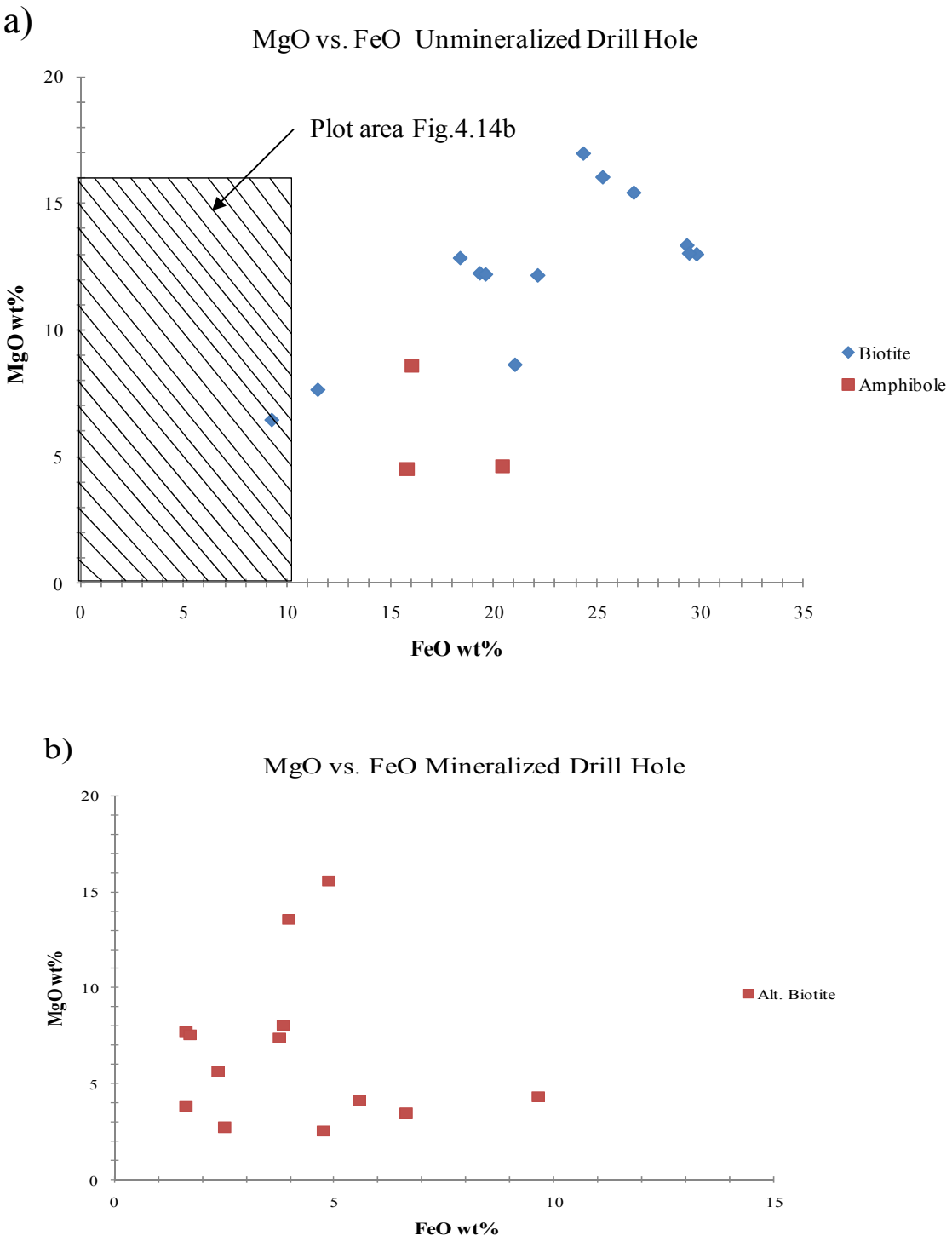

Figure 4.14: Plot of MgO *vs*. FeO concentrations in Fe-rich silicate minerals measured in a) unmineralized drill-hole CX-58, b) altered Fe-rich silicate minerals associated with uranium mineralization from drill-hole CX-56-1. (Data from Table 2 and 3 Appendix A)

4.2.2 Uranium Minerals

The mineralogical characteristics of the uranium minerals were examined using reflected and transmitted light microscopy, and scanning electron microscopy (SEM). In reflected light and BSE images, massive replacement mineralization is characterized by high reflectance uraninite that occurs as large anhedral colloform bands up to ≥ 500 μm in size (Fig.4.15a and b). Back scattered electron images show areas of lower reflectance associated with hydrothermal alteration along grain boundaries and fractures. Massive replacement mineralization is associated with chloritized biotite. Massive replacement uraninite is characterized by high Pb contents (10.13-16.23 wt% PbO), low Si and Ca contents (<3.00 wt% SiO_2, CaO) and very low Fe contents (<1.00 wt% FeO). The alteration of massive uraninite along fractures and grain boundaries are characterized by intermediate Pb contents (6.09- 8.57 wt% PbO), intermediate Si and Ca contents (4.02-6.17 wt% SiO_2, CaO) and low Fe contents (generally <1.00 wt% two points show 1.06 and 2.14 wt% Fe).

Fracture filling uranium mineralization is characterized by high reflectance uraninite which occurs as poorly formed cubic crystals and sub-rounded grains that display radial texture. Fracture filling veins are observed in association with secondary euhedral quartz-carbonate veins. Alteration of uraninite along grain boundaries and along the contact with the host rock is visible in BSE images (Fig.4.15c and d). Vein type mineralization is characterized by high Pb contents (10.32- 15.44 wt% PbO), low Si and Ca contents (<3.00 wt% SiO_2, CaO), and very low Fe content (<1.00 wt% FeO). The vein-type uraninite is altered to coffinite along fractures and grain boundaries. The altered vein uraninite is characterized by low to intermediate Pb contents (0.50- 9.70 wt%

PbO) intermediate Si and Ca contents (4.70- 6.40 wt% SiO_2, CaO) and low Fe content (<1.00 wt% FeO). The coffinite is characterized by very low Pb content (<0.05 wt% PbO), high Si and Ca contents (24.90-41.18 wt% SiO_2, 1.50-2.89 wt% CaO) and very low Fe contents (<1.00 wt % FeO).

Small "bleb-like" uraninite grains are typically associated with galena that formed from radiogenic lead mobilized by alteration of the uraninite. They are also associated with euhedral quartz (Fig.4.15e and f). The "bleb-like" aggregates of uraninite have been altered by multiple fluid events and display higher Si and Ca contents but, compositionally they do not have the high 25-40 wt% SiO_2 content of the coffinite in vein samples. Locally the "bleb-like" uraninites are altered to coffinite. The bleb-like uraninites are generally characterized by very low Pb contents (0.00-4.10 wt% PbO), intermediate Si and Ca content (4.14-6.84 wt% SiO_2, 3.29-4.00 wt% CaO), and very low Fe content (<0.09 wt% FeO), whereas the coffinite is characterized by low Pb content (0-4 wt% PbO), high Si and Ca content (11.25- 17.47 wt% SiO_2, 2.08- 3.84 wt% CaO), and very low Fe content (<1.00 wt% FeO) (Table 1, Appendix A).

4.2.3 Mineral Paragenesis

The paragenetic relationship between uranium mineralization and alteration of the basement rocks within the Millennium deposit was developed by examination of cross-cutting relationships visible in drill core and thin section petrography. Three stages of hydrothermal alteration have been identified within the Millennium deposit. These events are associated with pre-, syn, and post mineralization fluids and have extensively altered the basement rocks. See Fig. 4.18 for paragenesis.

Pre-ore alteration is characterized by sericite (ser1) produced by retrograde alteration of feldspars within pelite-semipelite gneisses/schists and pegmatites (Fig.4.1), hematite (H1) and chlorite (C1) (Fig.4.16i) preserved within the paleoweathering profile. Hydrothermal alteration of mica and feldspar also formed early illite (I1) and kaolinite (K1). Early movement along the "mother fault" produced fractures which were filled by quartz (Q1).

Syn-ore alteration is characterized by hydrothermal overprint of early alteration minerals (chlorite and hematite in paleoweathering profile). Further hydrothermal alteration of basement units associated with uranium mineralization is characterized by complete replacement of feldspars and micas by kaolinite (K2) and illite (I2) in pegmatites and psammopelitic schists (Fig.4.16f). Within the main zone of mineralization illite (I2) and chlorite (C2) are the dominant alteration minerals (main zone mineralization ~600- 750 m). A pervasive chloritization overprint (C2) of biotite and amphiboles is also visible in thin section and drill core (Fig.4.2, 4.3, Fig.4.16e). The chloritization (C2) is not well preserved due to late argillic alteration and bleaching (Fig.4.4, and 4.5). An interval of intense hematization (H2) (primary redox zone) associated with uranium deposition (U2) is located just below the main zone of mineralization (Fig.4.6).

Post-ore alteration is characterized by the further development of argillic alteration. For example, illite (I3) is visible in veins cross-cutting (I2) illite (Fig.4.16c). Brittle deformation has resulted in the formation of (Q2, Q3) microcrystalline quartz veins (Fig4.16a, b, c, d, f). Carbonates (Cal1, Dol1) are also observed intermixed with (Q2) microcrystalline quartz (Fig.4.8, Fig.4.16l). Pyrite (S2) also fills euhedral (Q2, Q3)

microcrystalline quartz veins (Fig.4.16a). Dravite (D1) occurs in veins and cements fault breccias in the lower portion of the hanging wall below the uranium orebody.

There are four styles of uranium mineralization: (1) massive replacement (Fig.4.15a and b); (2) fracture filling vein (Fig.4.15c and d); (3) mini “roll-front" (Fig.4.12b; 4.17a); (4) disseminated (“bleb-like” aggregate) (Fig.4.15e and f). Massive replacement and fracture filling veins constitute the majority of the ore, while, mini “roll-front” and disseminated uraninite are minor components of the ore. Three stages of uranium mineralization are recognized within the Millennium deposit. Early (U1) mineralization is characterized by small “bleb-like” uraninite associated with galena (S1), which is thought to form from an interaction between a sulfur rich fluid and remobilized radiogenic lead during a late stage fluid alteration event (Fig.4.15 e and f). Massive replacement and fracture filling veins (Fig.4.15a, b, c and d) formed during the primary mineralization event (U2). Mini “roll-front” mineralization (U3) (Fig.4.17) is associated with late hematite (H3) (Fig.4.12b).

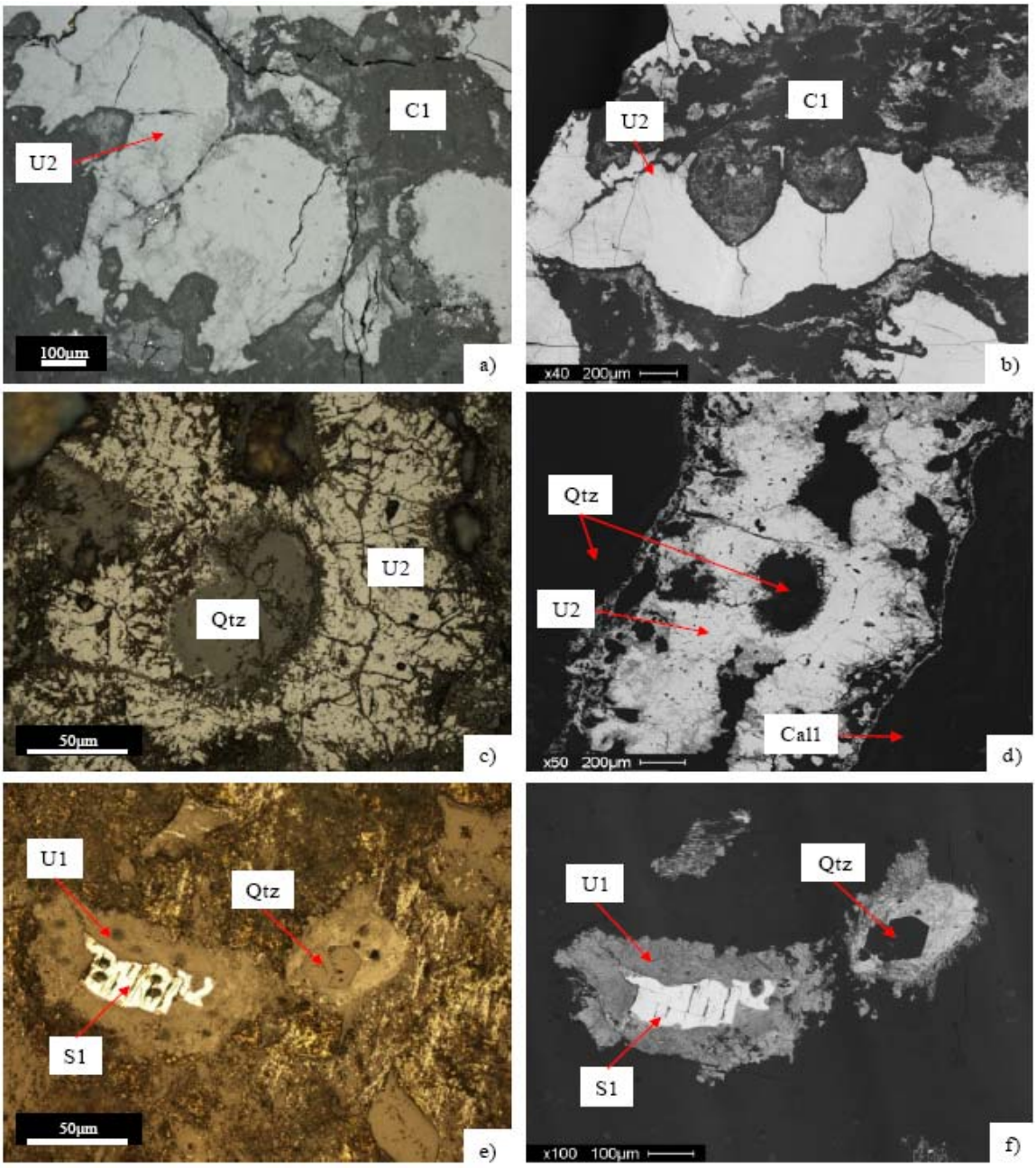

Figure 4.15: Reflected and back scattered electron (BSE) images of uranium mineralization styles within the Millennium deposit: a and b) massive replacement CX-56-1 663.4 M; c and d) euhedral quartz-carbonate-uraninite vein CX-56-1 644.5 M.; e and f) bleb-like aggregates CX-47-1 758.2 M. Abbreviations: letters correspond to specific generations of minerals described in paragenesis (Fig.4.18).

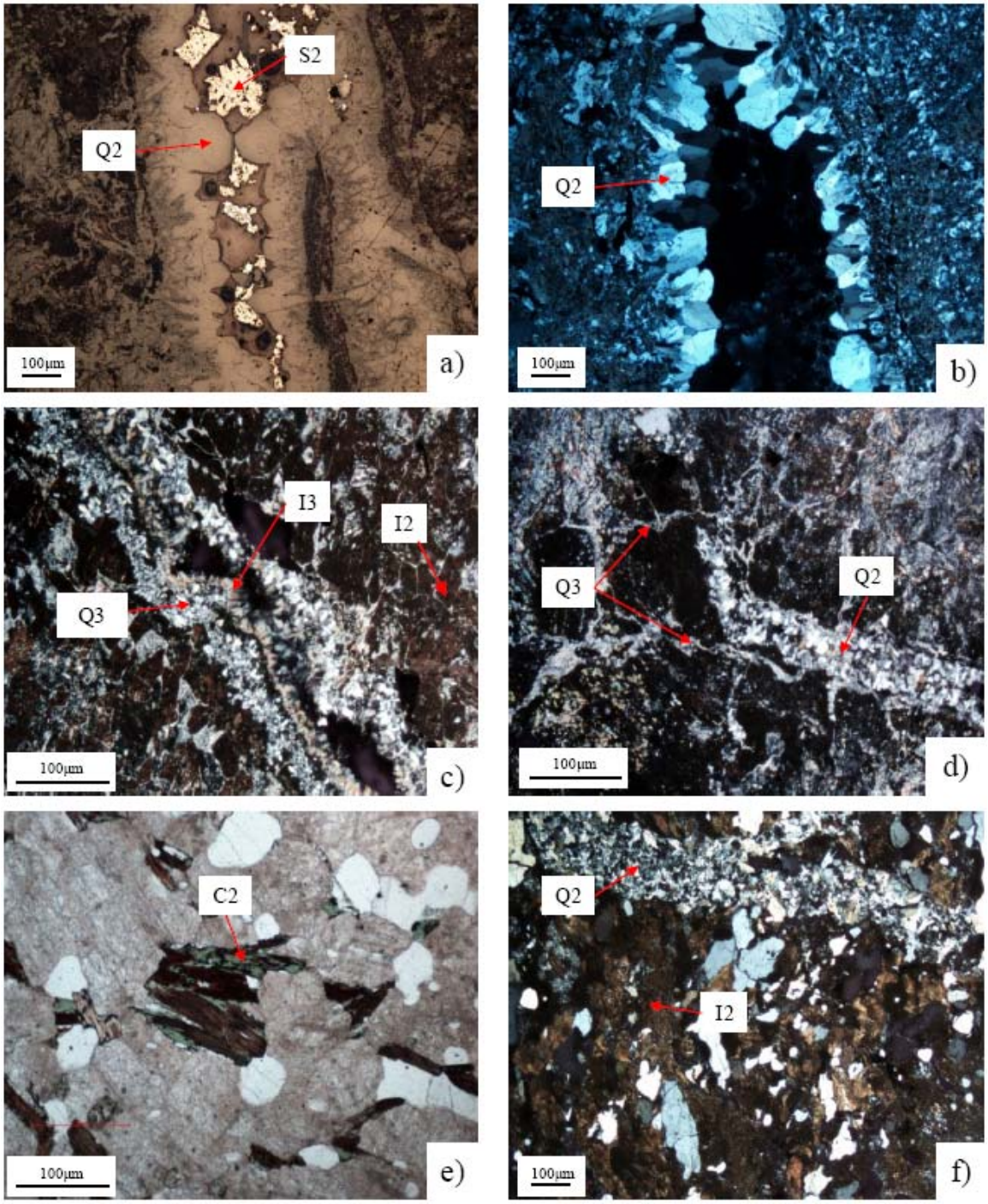

Figure 4.16: Transmitted light images: a) CX-47 715.0 m - Late S2 pyrite infilling Euhedral Q2 quartz vein; b) CX-47 715.0 m- Late euhedral Q2 quartz vein; c) CX-44-1 773.5 m- Q3 microcrystalline quartz vein filled with fibrous I3 illite crosscutting I2 altered amphibolite; d) CX-44-1 773.5 m- Q2 microcrystalline quartz vein cross-cut by small Q3 quartz vein in altered amphibolite; e) CX-51-1 681.4 m- plain polarized light image of chlorite altered biotite; f) CX-56-1 591.2 m Psammopelitic schist Q2 microcrystalline quartz vein cross-cutting illite (I2) altered mica.

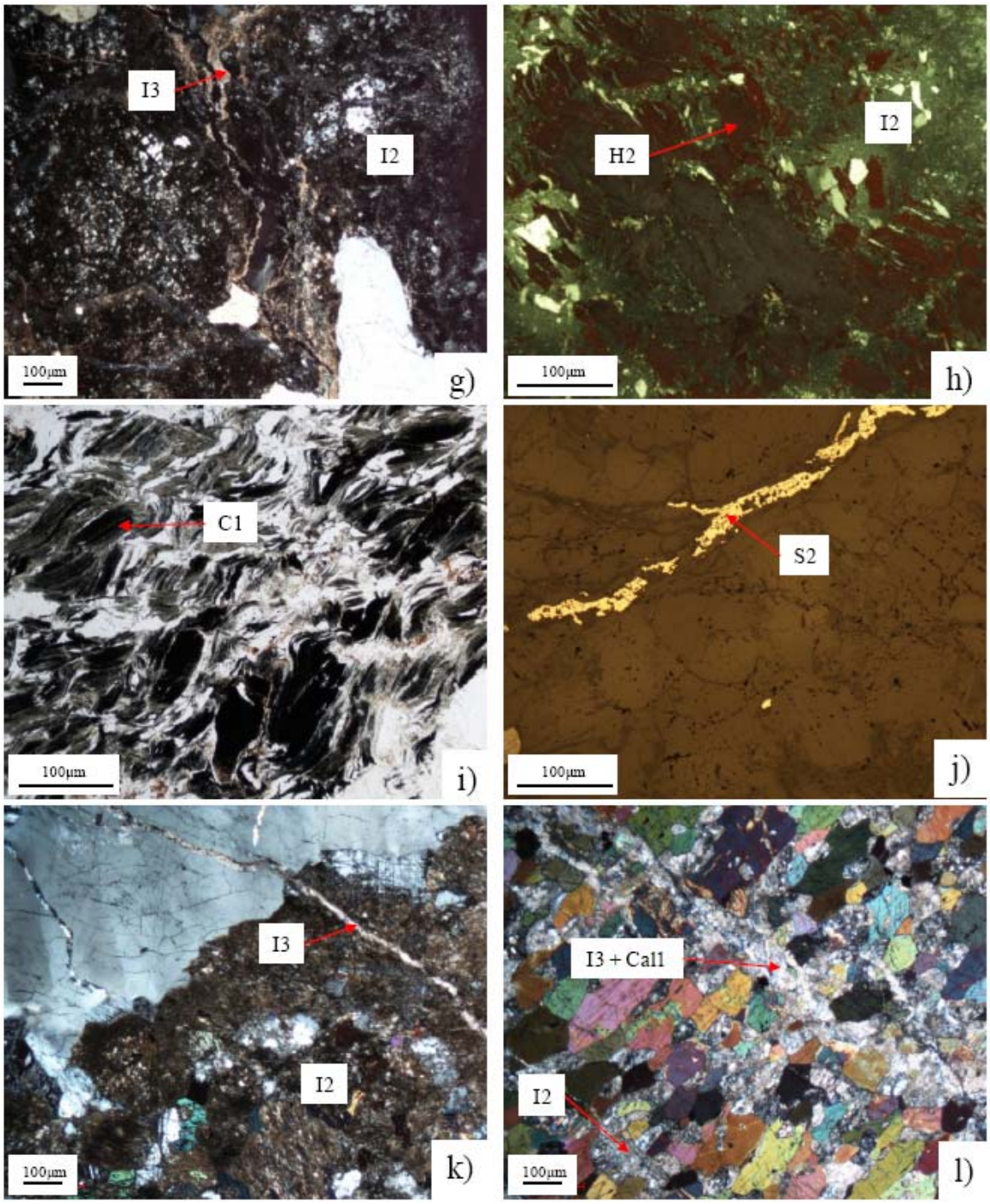

Figure 4.16 (cont.): g) CX-56-1 602.0 m pegmatite – illite (I3) filled fracture cross cutting (I2) altered plagioclase; h) CX-58 546.6 m- psammopelitic schist with illite (I2) altered biotite overprinted by hematite (H2). i) CX-58 552.0 m- psammopelitic schist displaying chlorite (C1) altered biotite in paleoweathering profile; j) CX-58 645.6 m- amphibolite –cross-cut by late S2 pyrite filling vein; k) CX-58 700.7 m- amphibolite- weak to moderate I2 altered plagioclase cross-cut by fracture filling illite (I3); l) CX-58 735.0 m- amphibolite- illite (I2) altered plagioclase, cross cut by illite (I3) + Calcite (Cal1) fracture filled vein. Letters correspond to specific generations of minerals described in the text.

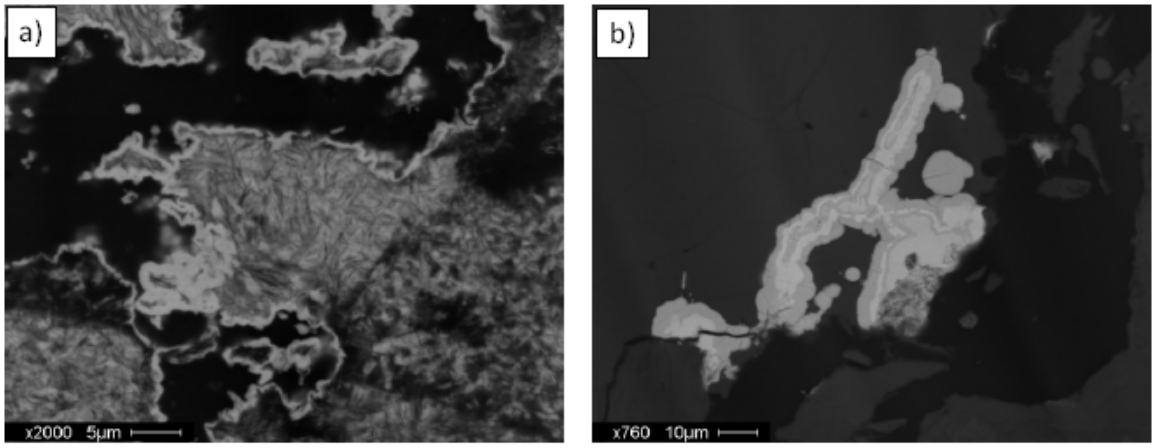

Figure 4.17: Back scattered electron (BSE) images uranium (U3) a) CX-47-1 758 m recrystallization growth on altered uranium mineral in small scale roll-front mineralization, b) CX-47-2 708 m small disseminated uranium mineral in quartz fracture displaying recrystallization.

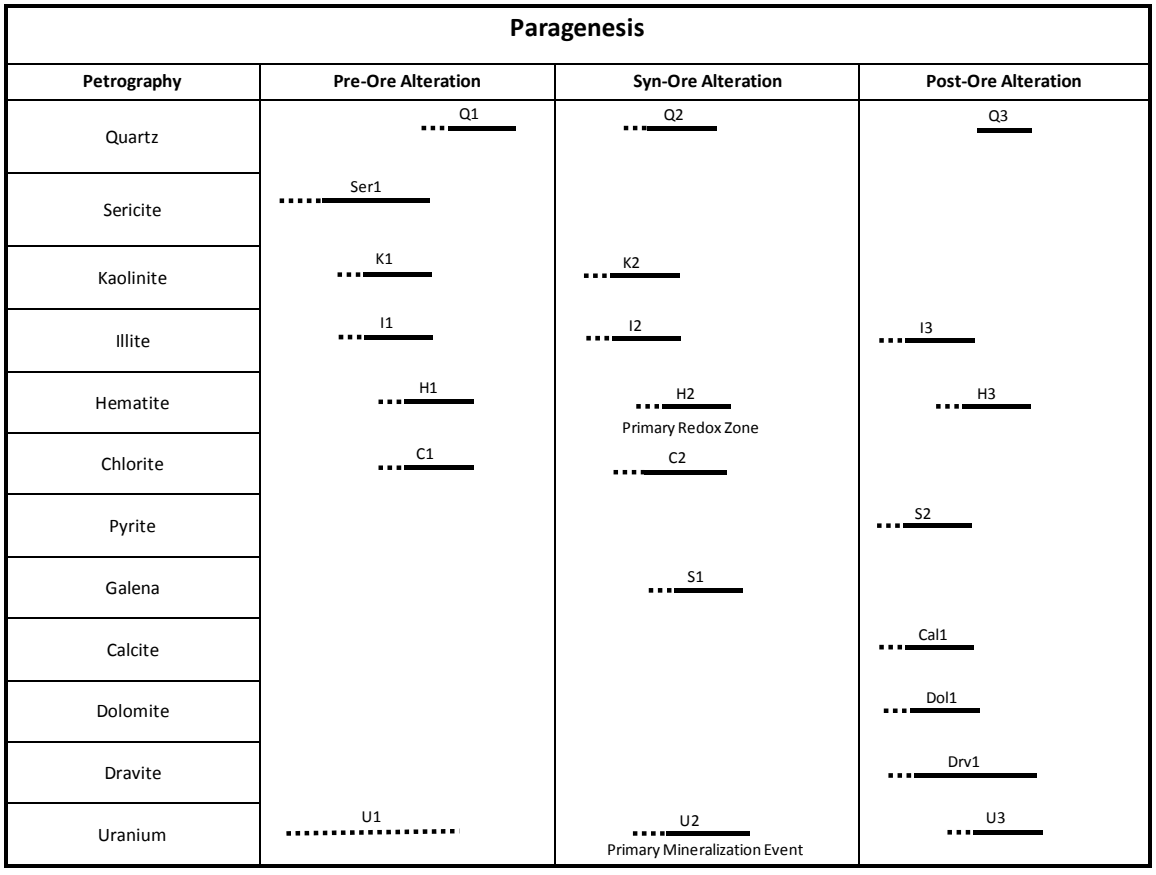

Figure 4.18: Fluid-mineral relationships within the basement rocks of the Millennium deposit. Letters correspond to specific generations of minerals described in the text.

4.3 Fluid-Rock interaction

4.3.1 Fe Speciation

The hydrothermal alteration associated with uranium mineralization in the basement rocks of the Millennium deposit has produced extensive chlorite and hematite overprints in mineralized drill core. The Fe^{2+} /Fe^{3+} ratios of whole-rock samples were measured by Mössbauer Spectroscopy, to determine the effect of hydrothermal alteration on the Fe-oxidation state of mineralized and unmineralized drill core samples. Major and trace element geochemistry on whole rock samples were also completed on mineralized and unmineralized basement samples. Due to the detection limit associated with the Mössbauer ^{57}Co (Rh) point source, only samples that contained >3.5 wt% Fe_2O_3 were selected (based on whole-rock geochemistry).

For whole-rock samples that did not meet the requirements for Mössbauer spectroscopy (>3.5 wt% Fe_2O_3) the Fe^{2+} /Fe^{3+} ratio was calculated from Fe_2O_3 and FeO values measured by Fusion ICP and Fe- titration. The mole% Fe was determined for each Fe-oxide and then normalized to determine the Fe^{2+} /Fe^{3+} ratio (See tables 5 and 6 in Appendix A for Fe values). These values were then compared to values obtained by Mössbauer Spectroscopy. Figure 4.19a shows the Fe^{2+}/Fe^{3+} ratio obtained by Mössbauer spectroscopy versus depth for mineralized and unmineralized drill-holes. The shaded region in Figure 4.19 represents the intersection of uranium mineralization (main zone) in drill core from DDH's CX-44-1 and CX-56-1 (See Appendix B). Mineralized drill-core shows low Fe^{2+}/Fe^{3+} ratios within the "main zone" of uranium mineralization, while the unmineralized drill-core is has higher Fe^{2+}/Fe^{3+} ratios within the same interval. Figure 4.19b shows the Fe^{2+} / Fe^{3+} ratio versus depth for the remaining whole rock samples.

Comparatively there is a pronounced abundance in Fe^{2+} in unmineralized basement rocks relative to the mineralized basement rocks in the main uranium ore zone when Fe species are measured by Mössbauer Spectroscopy.

The Fe^{2+} and Fe^{3+} concentrations in two samples from unmineralized drill hole CX-58 were measured by both methods to determine the feasibility of using whole-rock geochemistry in Fe species determination. The first sample CX-58 625.6 m has (73.37% Fe^{2+} and 26.63% Fe^{3+}) and (47.87% Fe^{2+} and 52.13% Fe^{3+}) measured by Mössbauer and Fe titration respectively. The second sample CX-58 636.0 m has (72.7% Fe^{2+} and 27.3% Fe^{3+}) and (51.69% Fe^{2+} and 48.31% Fe^{3+}) measured by Mössbauer and Fe titration respectively (See Table 9 Appendix A for data). There is a ~3:1 ratio of Fe^{2+} vs. Fe^{3+} concentration measured by Mössbauer while the Fe titration method gives ~1:1 ratio for the same sample. The significant decrease in the Fe^{2+} values measured by Fe titration when compared to Fe^{2+} measured by Mössbauer suggests that Fe^{2+} may have been oxidized during Fe titration, or the oxidation of Fe^{2+} in whole-rock samples after crushing were exposed to air. Therefore, Fe titration may be a less accurate method for determination of Fe^{2+} and Fe^{3+} values. The small sample size and sensitivity of the Mössbauer spectrometer provides a more accurate method for Fe species determination.

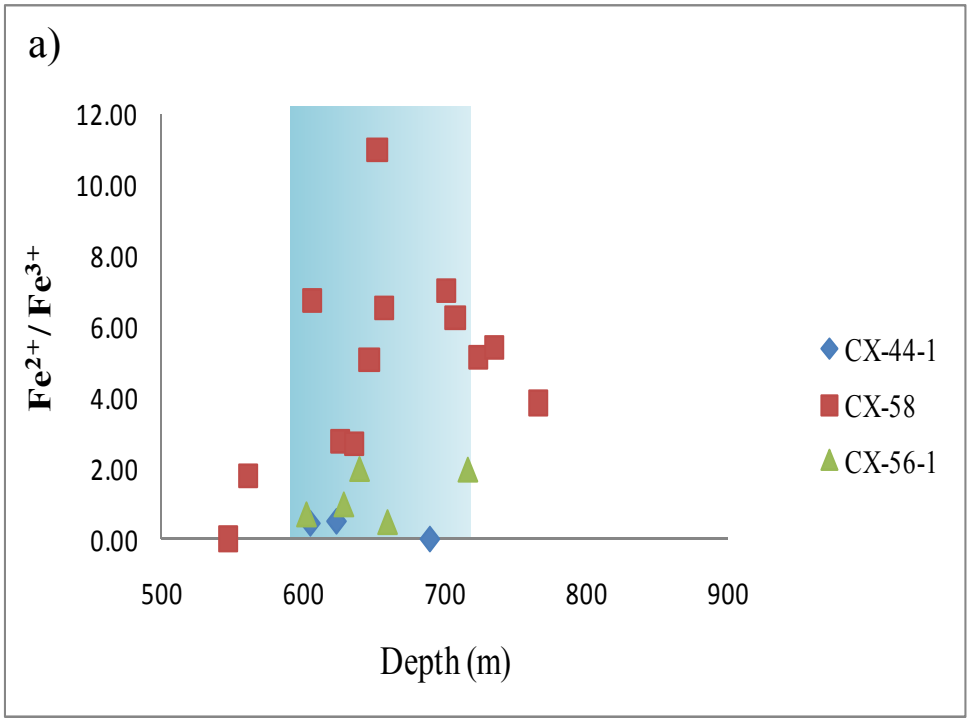

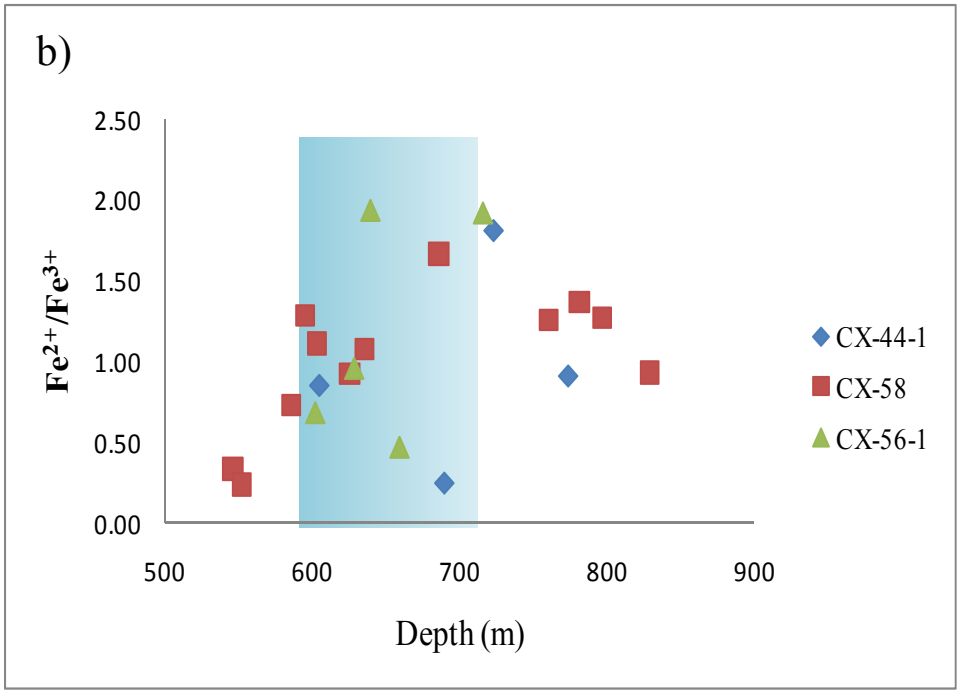

Figure 4.19: a) Whole-rock Fe^{2+}/Fe^{3+} ratio measured by Mossbauer *vs.* depth for mineralized and unmineralized drill-core. b) calculated whole-rock Fe^{2+}/Fe^{3+} ratio *vs.* depth for mineralized and unmineralized drill-core. The shaded region represents the intersection of uranium mineralization in drill core from DDH's CX-44-1 and CX-56-1 (See Appendix B).

4.4. Fluid Inclusions

Detailed thin section petrography on the quartz-uraninite veins showed that euhedral quartz grains contain primary and secondary two phase fluid inclusions (*vapor + liquid*) (Fig.4.20). Phase changes during freezing studies indicate that these inclusions are represented by the H_2O-NaCl system. Within this system fluid salinities can be determined from the ice-melting temperature (Bodnar, 2003). The salinity can be calculated using equation [1].

[1] Salinity (wt. %) = $0.00 + 1.78\theta - 0.0442\theta^2 + 0.000557\,\theta^3$

Where θ is the absolute value of the freezing temperature (e.g. -10°C is 10°C).

The equation is valid in the temperatures range from 0.0°C to -21.2°C, and corresponds to the eutectic temperature of the H_2O-NaCl system (Bodnar, 2003). Calculation of salinities was completed on primary and secondary fluid inclusions within metamorphic quartz and secondary euhedral quartz grains from the vein sample. Two fluid types were identified; the first is characterized by moderate salinities 4-15 wt. % NaCl, and the second set is highly saline inclusions with 22-24 wt. % NaCl (Fig.4.21). The moderately saline fluid represents primary fluid inclusions located within the core of euhedral and metamorphic quartz grains. The highly saline fluid inclusions represent primary fluid inclusions located along growth planes in euhedral quartz, and secondary inclusions located along fractures in metamorphic quartz (Fig.4.20). The highly saline fluid inclusions are similar in composition to basinal brines that are associated with unconformity-hosted uranium deposits in the Athabasca Basin (Derome, *et. al*, 2005).

Heating experiments on both the moderately saline and highly saline fluid inclusions were not successful. Both moderately saline and highly saline fluid inclusions

decrepitated at temperatures between 200-225°C. Petrographic analysis of these inclusions indicated the inclusions had variable vapor to fluid ratios. These observations, suggest the fluid inclusions may have leaked prior to heating experiments, due to radiation induced damage to the quartz. This type of damage would weaken the crystal structure, cause the inclusions to leak, and decrepitate as the vapor pressure increases during the heating process. Therefore, heating measurements can only provide minimum temperatures. Although the homogenization temperature was not determined, the decrepitation temperature is still within the temperature range for basinal brines (200 ± 20°C) reported by Kotzer and Kyser (1995).

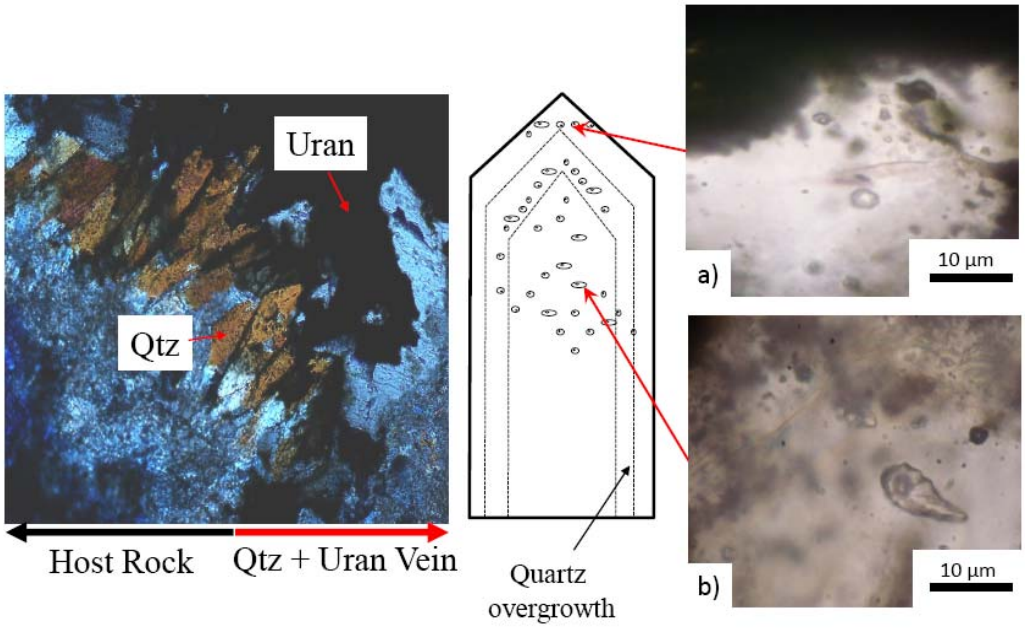

Figure 4.20: Transmitted light image of euhedral quartz- uraninite vein in psammopelitic schist CX-56-1 644.5 m. With schematic representation of euhedral quartz crystal showing the relative locations of: a) 22 - 24 wt.% NaCl fluid inclusions located along inferred growth plane near quartz termination; b) 4 – 15 wt.% NaCl fluid inclusions in crystal interior..

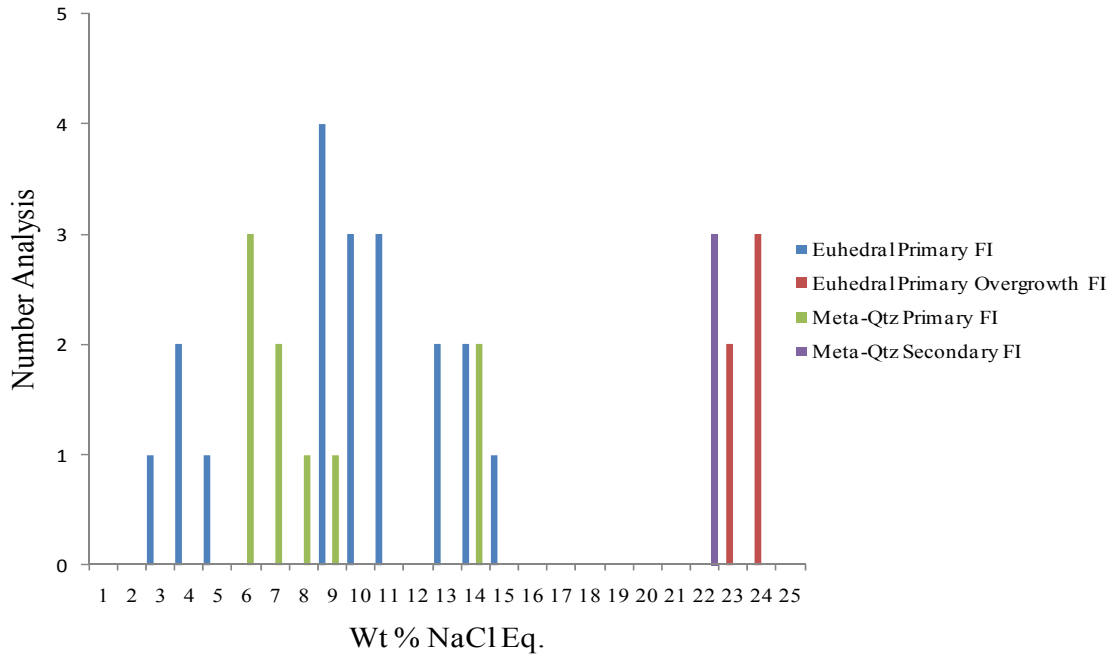

Figure 4.21: Plot of fluid inclusion salinities in metamorphic and secondary euhedral quartz grains associated with vein type mineralization. Analysis of data show that there are two fluids preserved within the sample; 1) moderately saline fluid comprised of 6-15wt.% NaCl equivalent and 2) highly saline 22-24 wt.% NaCl equivalent. Abbreviations: Meta-Qtz- metamorphic quartz.

4.5 Stable Isotopes

The $\delta^{18}O$ values of uraninites from massive replacement and vein type uraninite were measured by secondary ion mass spectrometry (SIMS). The $\delta^{18}O$ values of massive uraninite from the Millennium deposit range from -25.9‰ to -15.7‰ whereas vein uraninite has $\delta^{18}O$ values from -23.0‰ to -18.5‰ (Table 4, Appendix A).

Thin section petrography identified a vein of intergrown uraninite and euhedral quartz crystals (Fig. 4.21a). The $\delta^{18}O$ values of euhedral and metamorphic quartz were measured by SIMS (Fig. 4.22b). Euhedral quartz grains have $\delta^{18}O$ values that range from

16.2‰ to 19.1‰ whereas metamorphic quartz has $\delta^{18}O$ values from 11.1‰ to 15.1‰. Assuming the euhedral quartz and uraninite are in textural equilibrium, an equilibrium temperature can be calculated using the quartz-water and uraninite-water fractionation factors from [1] Zheng (1991) and [2] Kawabe (1978):

[1] $1000*\ln\alpha_{UO2\text{-}H2O} = A * 10^6/T^2 + B * 10^3/T + C$ (Uraninite)
Where, A = 2.630, B = -12.97, C = 3.86

[2] $1000*\ln\alpha_{Quartz\text{-}H2O} = A * 10^6/T^2 + B * 10^3/T + C$ (Quartz)
Where, A = 3.280, B = 0.00, C = -5.50

The calculated equilibrium temperatures for euhedral quartz and uraninite are ~43°C. Using the equilibrium temperature in the uraninite-water fractionation factor of Zheng (1991), the calculated $\delta^{18}O$ value for the fluid that precipitated both the uraninite and euhedral quartz was -10‰. However, the isotope equilibrium temperature is much lower than the minimum decrepitation temperature from fluid inclusion analysis. Kotzer and Kyser (1993) and Fayek and Kyser (1997) suggest that the low $\delta^{18}O$ values of uraninites from unconformity-type uranium deposits are the result of the interaction between late stage low temperature meteoric water, which results in negligible modification of the chemical composition and texture. These data suggest that meteoric fluids affected the Millennium deposit similar to other basement and unconformity-hosted uranium deposits in the Athabasca Basin (Fayek and Kyser, 1997). Oxygen isotopic analysis of style 3 uraninite is in progress and the $\delta^{18}O$ values of style 4 uraninite are difficult to obtain because of small grain size and the lack of a suitable Secondary Ion Mass Spectrometer (SIMS) standard. However, due to the rapid diffusion of oxygen

through the uraninite structure (Fayek *et. al*, in prep), it is unlikely that the $\delta^{18}O$ values of style 3 uraninite will be outside the range of values obtained for styles 1 and 2 uraninite from the Millennium deposit.

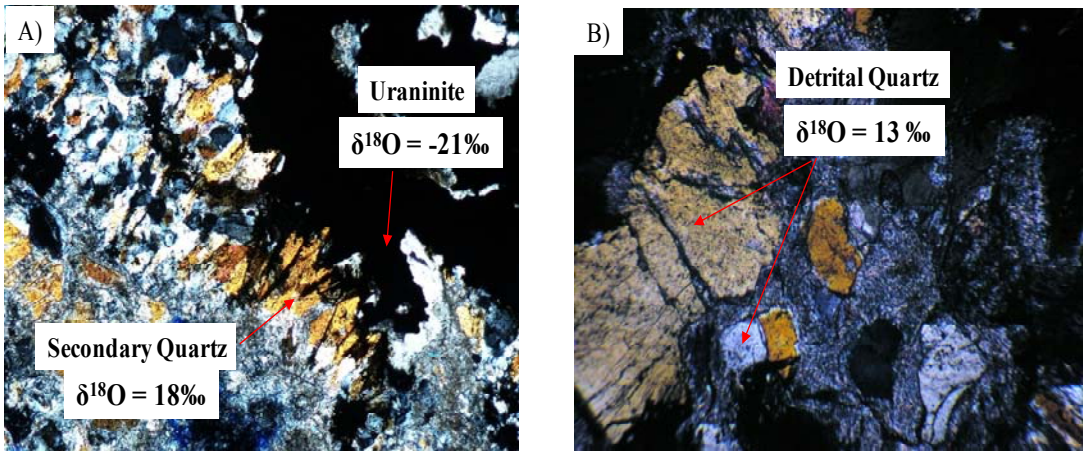

Vein 644.5 M Transmitted Light Image FOV 2mm Vein 644.5 M Transmitted Light Image FOV 2mm

Figure 4.22: Transmitted light image of quartz-uraninite vein from CX-56-1 644.5 M. a) $\delta^{18}O$ values for secondary euhedral quartz and uraninite vein, b) $\delta^{18}O$ values of detrital quartz grains. *Note the listed $\delta^{18}O$ values are averages for each mineral*.

4.6 Geochronology

4.6.1 Chemical Pb Ages

Uraninite occurs in several mineralization styles within the Millennium deposit these include: massive replacement, vein-type mineralization, "bleb-like" aggregates and centimeter-scale roll-fronts. The mineralization styles were examined by SEM back scattered electron (BSE) imaging to determine their homogeneity. Grains that appeared homogenous were analyzed by electron microprobe (EMP) to determine their chemical composition. The concentrations of U and Pb in uraninite were then used to calculate chemical Pb ages. Th content was negligible (generally below 0.1 wt % detection limit, see Table 1 Appendix A) and had no effect on age calculations. The disadvantage of this

method is that all lead is assumed to be radiogenic. Any common lead present in the system or Pb loss would yield unrealistically old or young ages, respectively (Bowles, 1990). Equation [1] shown below was used to calculate chemical lead ages:

[1] $t = \lambda_1^{-1} \ln [(1.104Pb/U) + 1]$

Where λ_1 is the decay constant of ^{238}U; the constant 1.104 accounts for the relative abundance of ^{238}U, ^{235}U, ^{206}Pb and ^{207}Pb; it also allows the proportions of Pb and U to be expressed in wt % (Bowles, 1990).

Bowles (1990) noted that the age (Ma) of a sample is related to the total percent of Pb in the sample in the following equation:

[2] $t = 100Pb$

The approximate relation between time (t) and Pb in equation [2] is derived by simplification of the formula of Ranchin (1968) (see Bowles, 1990). This equation applies only to uraninite or other uranium minerals that contain >50% U. In uraninite the relationship provides a method to determine the error associated with the age calculation. Bowles noted that the age and associated error is highly dependent on the quality of the Pb analysis. Bowles (1990) stated that a sample with an error of ~0.01% Pb is equivalent to ± 1 Ma.

The massive replacement and vein-type uraninites yield a range of ages from 322 to 1413 Ma (Table 11, Appendix A). The oldest recorded age is ~1400 Ma (primary mineralization age) while, recorded ages of 1300, 1250-1200, 1100, 1000, and 900 Ma (Fig.4.23) indicates lead loss and/or recrystallization of uraninites by post-depositional

fluids. The analysis of U and Pb for Millennium uraninite has an error of 0.1 %. Thus all reported ages have an error of ± 10 Ma.

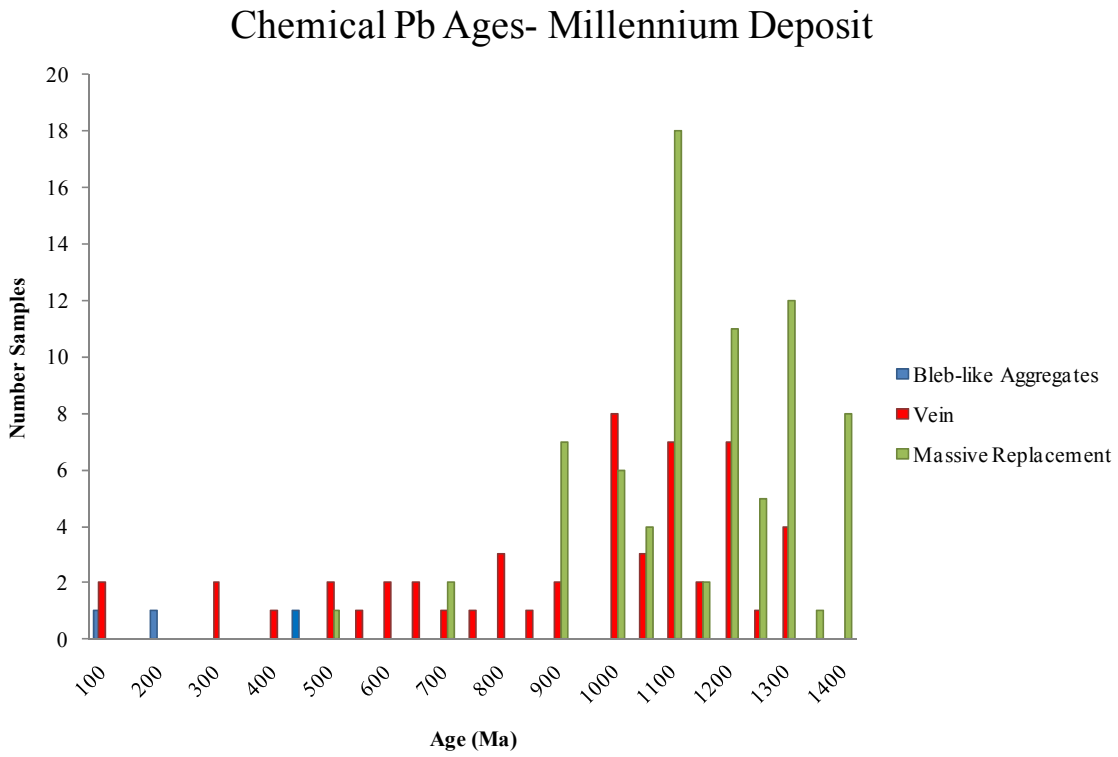

Figure 4.23: Chemical lead age distribution for Millennium deposit uranium mineralization styles. Note primary mineralization occurs at ~1400 Ma and resetting of uranium minerals by late fluid events at 1300, 1250-1200, 1100, 1000, and 900 Ma.

4.6.2 Pb-Pb Isotopic Ages

The $^{207}Pb/^{206}Pb$ isotopic ages of uraninite from the various styles of uranium mineralization within the Millennium deposit were measured by SIMS. The relationship between $^{207}Pb/^{206}Pb$ ratio and time is a result of the different half-life of their parent isotopes [1].

$$(^{207}Pb/^{206}Pb)^* = {}^{235}U/^{238}U\ (e^{\lambda 2t} - 1/e^{\lambda 1t} - 1) \qquad [1]$$

Where t is time, λ_1, and λ_2 are the decay constants of ^{238}U and ^{235}U, respectively. The $^{235}U/^{238}U$ ratio is a constant equal to 1/137.88 for all uranium of normal isotopic composition in the Earth, Moon and meteorites at the present time (Faure, 1986).

Therefore,

$$(^{207}Pb/^{206}Pb)^* = 1/137.88\ (e^{\lambda 2t} - 1/e^{\lambda 1t} - 1) \qquad [2]$$

This equation is solved by iteration until the solution converges. Additionally, the equation cannot be solved for t=0, due to the low abundance of ^{235}U on Earth today. Therefore, the minimum $(^{207}Pb/^{206}Pb)^*$ ratio one would expect would be the present day ratio (Faure, 1986).

Any mineral that contains an appreciable amount of radioactive material (i.e. U, Th) can be dated as long as the system remains closed (Anderson, 2002). However, if non-radiogenic Pb is incorporated into the mineral at the time of closure or during a later fluid event, the lead present in the mineral is no longer attributed exclusively due to *in situ* radiogenic accumulation. If common lead is present, the ages determined from observed U-Th-Pb isotope ratios no longer reflect the true age for the sample and will be older (Anderson, 2002). Where common lead is identified corrections must be applied to isotopic ratios to determine the "true age" for the mineral. Minimal common lead was detected in Millennium uraninites and therefore no correction was necessary (See Table 7 Appendix A).

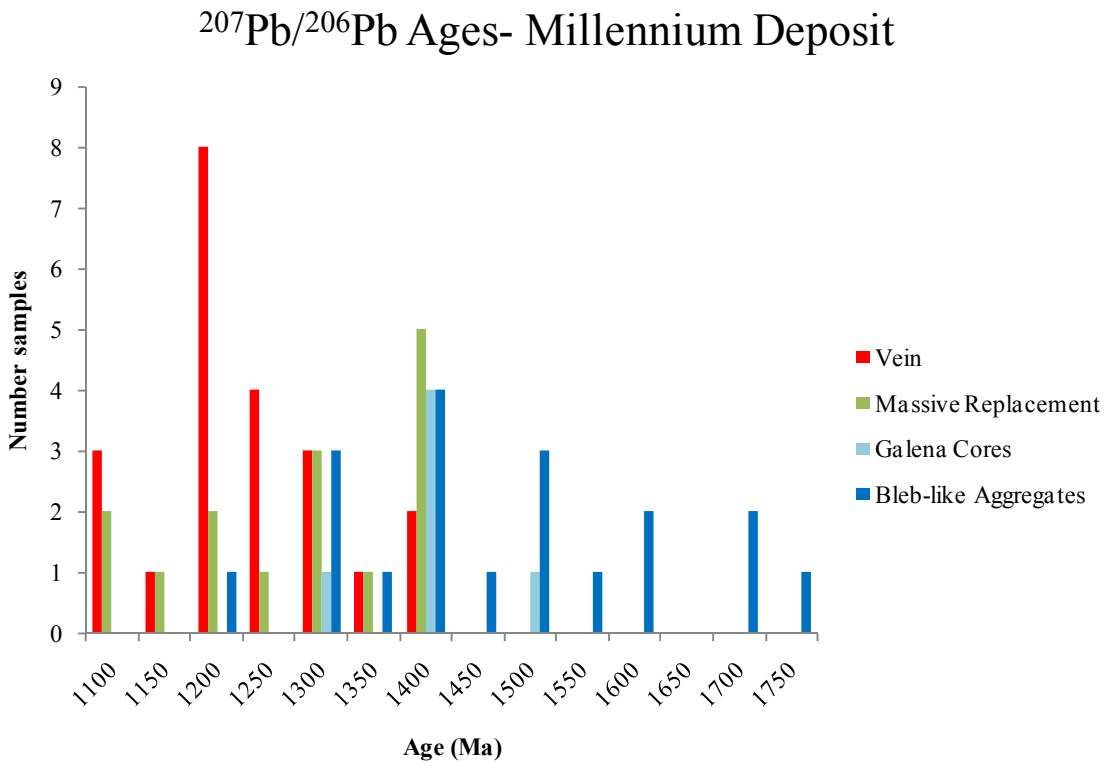

Figure 4.24: distribution of $^{207}Pb/^{206}Pb$ ages in various mineralization styles within the Millennium Deposit, Athabasca Basin, Saskatchewan, Canada.

The massive replacement and vein type uraninite yield ages that cluster at 1300 ± 7 Ma, 1250-1200 ± 8 Ma and 1100 ± 7 Ma (Fig.4.24). These ages indicate partial resetting by post-depositional fluids. Calculated $^{207}Pb/^{206}Pb$ ages for the "bleb-like" uraninite are in the range of 1750-1650 ± 97 Ma. Galena associated with the "bleb-like" uraninite yield an age of 1400 ± 83 Ma. This indicates that the "bleb-like" uraninites were partially reset during the emplacement of massive replacement and vein type uraninite at ~1400 Ma. A late fluid event remobilized some of the radiogenic lead within the "bleb-like" uraninites and formed the galena. Figure 4.25 shows the SIMS analysis spot and $^{207}Pb/^{206}Pb$ age in millions of years for Millennium uraninites. The oldest age group 1750-1650 Ma is similar to reported ages of uranium minerals from Beaverlodge vein-

type uranium deposits. This suggests that uranium mineralization processes have been active in the basement rocks far earlier than has been reported within unconformity-hosted deposits in the Athabasca Basin.

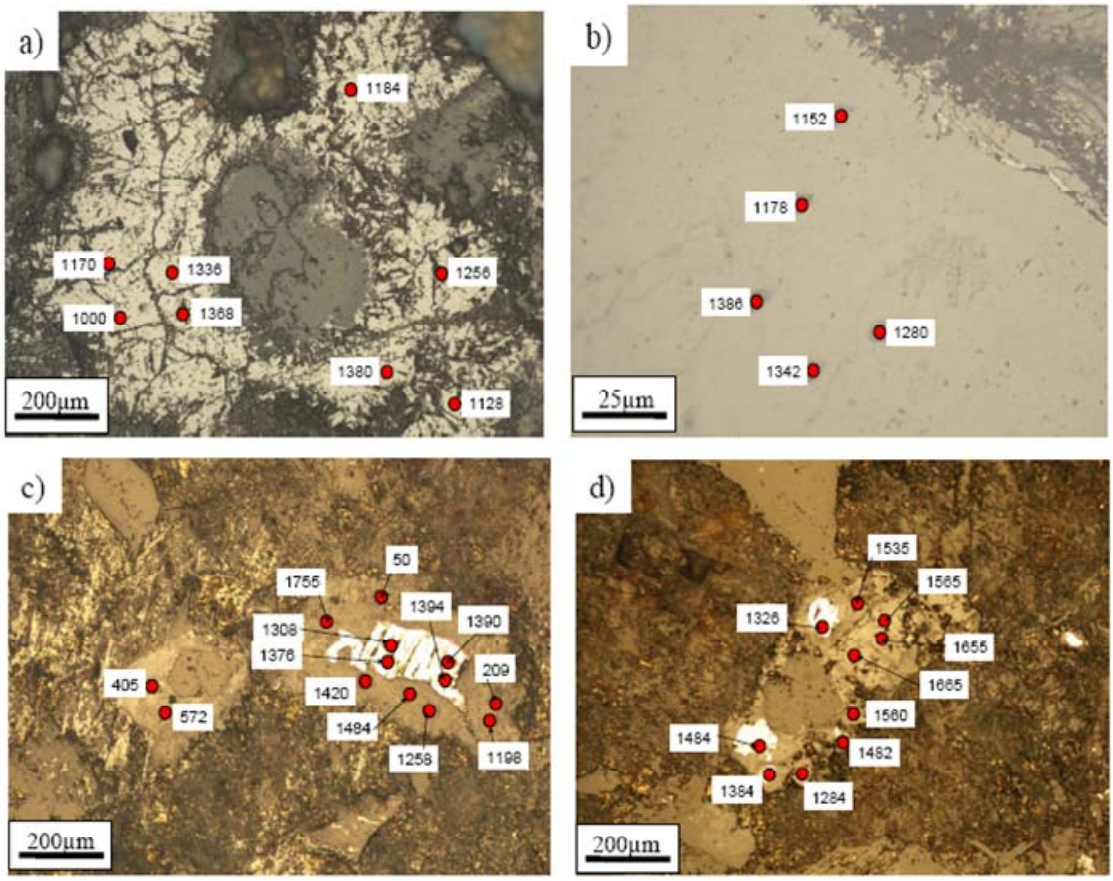

Figure 4.25: Reflected light images uranium minerals and sulphides with SIMS analysis spots and ages (in millions of years). a) vein type mineralization CX-56-1 644.5 m, b) massive replacement mineralization CX-56-1 663.4 m, c and d) bleb-like aggregate CX-47-1 758.2 m

4.6.3 Comparison of Chemical and Isotopic Lead Ages

Both chemical and isotopic Pb ages from the Millennium deposit indicate the primary mineralization event occurred at approximately 1500-1400 Ma. Both methods also indicate lead loss at 1300, 1250-1200, 1100, 1000, and 900 Ma. These ages coincide with major worldwide tectonic and fluid events within the Athabasca Basin (Kotzer and

Kyser, 1990). The only major difference between chemical Pb and isotopic ages was 1750-1650 Ma isotopic ages obtained for the "bleb-like" uraninites. Chemical Pb ages are calculated using the concentrations of U, Th and Pb in uraninite assuming there was no loss or gain of U, Th, and Pb, and that all Pb was produced from the decay of U. The chemical Pb method cannot distinguish between common and radiogenic Pb. Therefore, Pb loss during alteration of uranium minerals would produce erroneously young chemical Pb ages (e.g., 450-100 Ma chemical Pb ages for disseminated uraninite). However, chemical Pb ages of many grains can provide a record of events that have caused Pb loss.

Chapter 5: Discussion

5.1 A comparison between other basement-hosted uranium deposits and the Millennium Uranium deposit, Athabasca Basin.

The Rabbit Lake, Eagle Point, Sue C, Dominique-Peter, and Millennium uranium deposits are hosted within the crystalline basement rocks of the Athabasca Basin, and are interpreted as a derivative of the unconformity deposit model (Thomas, *et. al,* 1998; Roy, *et. al*, 2005). The Rabbit Lake, Eagle Point, Sue C, and Millennium uranium deposits are located within the Wollaston Domain along the eastern margin of the Athabasca Basin. The Dominique-Peter deposit is located approximately 1 km to the N-NE of the Cluff Lake mine within the Carswell Structure in the western Athabasca Basin. Unlike their unconformity-associated counterparts, the basement-hosted uranium deposits do not have well constrained genetic models. In particular, the role of the basement rocks in the development of these basement-hosted uranium deposits is not well understood (Alexandre, *et. al,* 2005). The Millennium Deposit provides an opportunity to define the role of the basement rock in the development of these basement hosted uranium deposits.

5.1.1 Geology

The Rabbit Lake, Eagle Point, Sue C, and Millennium deposit are situated within the lower pelitic dominated unit of the Wollaston Group. The host rocks consist of graphitic and non-graphitic pelitic to semi-pelitic gneisses/schists, quartz rich psammites, calc-silicates, amphibolites and minor marbles interlayered with anatectic pegmatites derived from partial melting at upper amphibolite-granulite facies metamorphism during the Trans-Hudson Orogeny (Sibbald, 1985; Bruneton, 1993). The Dominique-Peter deposit is situated ~1 km north-northeast of Cluff Lake near the southwest margin of the

Carswell structure basement core (Blaise and Koning, 1985). The deposit is hosted within aluminous and felsic gneisses which make up the Peter River Gneiss and the Earl River Complex (Blaise and Koning, 1985; Baudemont and Fedorowich, 1996).

5.1.2 Structural controls on uranium mineralization

Structurally all of the basement–hosted deposits are associated with major post-Athabasca Group reverse faults. Open voids and fractures along and adjacent to these fault zones increase the permeability of the basement rocks allowing uraniferous fluids (i.e. basinal brines) to penetrate into the basement rocks.

For example, the Eagle Point deposits are located within the hanging wall block of the Collins Bay Fault. Uranium mineralization occurs as a series of steeply dipping tabular veins and lenses that are both concordant and discordant to the foliation of the host rocks. A structural control on the mineralization has been inferred based on the discordant nature of veins and the lack of consistent relationship between mineralization and lithological contacts (Gilboy and Vigrass, 1986).

Within the Millennium deposit, increased brecciation of the basement units is attributed to an inferred dilational jog created by movement along two sub-parallel reverse faults.

5.1.3 Host-rock alteration

The basement rocks hosting uranium mineralization have all been affected by pre-, syn-, and post-depositional fluids. The main alteration assemblages within the basement-hosted deposits include chloritization of Fe-rich mafic minerals, the sericitization/illitization of feldspars and micas, and hematization.

At the Rabbit Lake deposit, alteration is characterized by two chloritization events both of which occur after the primary mineralization event. The first chloritization event has been termed the "red alteration" and occurred under oxidizing conditions which remobilized uranium minerals. The second is the "green alteration" event that is associated with precipitation of secondary uranium minerals such as sooty pitchblende and coffinite (Hoeve and Sibbald, 1976). The relationship between chlorite and uranium mineralization, within the Millennium deposit, provides evidence of the changing oxidation and reduction conditions, responsible for the remobilization and precipitation of uranium minerals in the basement rocks in the Millennium area.

5.1.4 Uranium Mineralization

Unconformity-related uranium mineralization within the Athabasca Basin can also be classified as either simple or complex. This classification is based on the spatial relationship between uranium mineralization and sulphide and arsenide mineral assemblages (Fayek and Kyser, 1997). Uranium mineralization hosted at the Athabasca Group unconformity is often classified as complex-type deposit, because uranium mineralization is associated with Ni- Co- As- Fe- Cu- Pb sulfides and arsenides. Within some complex deposits, associated metals can occur in economic concentrations (Midwest U-Ni deposit). The basement-hosted deposits located within the Wollaston Group (Rabbit Lake, Eagle Point, Sue C, and Millennium) fall into the simple-type uranium deposit classification proposed by Fayek and Kyser (1997) because uranium mineralization is generally monominerallic with only trace amounts of sulfides and arsenides. Within the Millennium deposit, Ni, As, Cu and Co contents are generally less

than 200 ppm, which are interpreted to be weakly elevated to background concentrations (Roy, *et. al,* 2005).

The basement-hosted Dominique-Peter deposit does not fall into the classification of simple-type uranium deposits. Uranium mineralization within the Dominique-Peter deposit occurs in three uraniferous assemblages. The first of which is composed of uraninite-sulphide-selenides, the second by uraninite-sulphides, and the third by pitchblende-carbonate (Blaise and Koning, 1985; Baudemont and Fedorowich, 1996). The difference between the simple-type mineralization for basement-hosted uranium deposits located in the Wollaston Domain and the uraniferous assemblages within the Dominique-Peter deposit is most likely associated with differences in host rocks of the Wollaston Group in the eastern Athabasca versus those in the Carswell Structure in the west.

5.1.5 Geochronology basement-hosted uranium deposits

The emplacement of primary uranium mineralization within the basement-hosted uranium deposits is generally accepted to have occurred between 1500-1400 Ma (Bell, 1985; Blaise and Koning, 1985; Baudemont and Fedorowich, 1996; Fayek and Kyser, 1997; Gilboy and Vigrass, 1986; and references therein). This is generally contemporaneous with the primary mineralization within the unconformity-hosted deposits (Fayek and Kyser, 1997, 2002; Kotzer and Kyser, 1990, 1992, 1993; and references therein).

For example, the primary mineralization event within the Eagle Point deposit occurred at 1400 ± 25 Ma (Gilboy and Vigrass, 1986). Primary uranium mineralization at the Millennium deposit is constricted within the 1500-1400 Ma mineralization event

recorded at other deposits in the Athabasca Basin. However, at the Millennium deposit there appears to be an earlier uranium mineralization event, which gives an age of 1750-1650 Ma. These ages are older than the Athabasca Basin, which is estimated at ~1700 Ma (Armstrong and Ramaekers, 1985; Kotzer and Kyser, 1990). Therefore, these old ages obtained from the Millennium deposit suggests that there was proto-ore in the basement rocks prior to the primary uranium mineralization event at 1500-1400 Ma.

5.2 Genesis of the Millennium Uranium Deposit

5.2.1 Basement-hosted uranium deposit models

Since, the first discovery of basement-hosted uranium mineralization at Rabbit Lake in the late 1960s, significant effort has gone into the development of the unconformity-associated uranium deposit model. Early work on the Rabbit Lake deposit was completed by Knipping (1974). Knipping proposed a supergene model which was based on 1) the proximity of the deposit to the unconformity, 2) the decrease in uranium mineralization with depth, 3) the alteration envelop is older than the initial uranium emplacement, 4) the mineralization occurs only in the hanging wall of the Rabbit Lake fault.

Hoeve and Sibbald (1976, 1978) indicate that several arguments for Knipping's model are not valid. These include observations that primary mineralization occurred before chloritic alteration and the presence of uranium mineralization footwall to the Rabbit Lake fault.

Hoeve and Sibbald (1976, 1978) proposed a diagenetic model which involves basinal fluids that circulate along the unconformity and become, heated under the influence of the geothermal gradient with in the Athabasca Basin, as the fluid migrated

downwards. They also state the oxidized nature of the Athabasca Group would have allowed uranium to be transported and leached from the sandstone and deposited where reducing conditions were optimal. Further work by Wilson and Kyser (1987); Kotzer and Kyser (1990, 1992, 1993, 1995); and Fayek and Kyser (1997), using stable and radiogenic isotope studies on diagenetic clays and uranium minerals, confirmed that diagenetic basinal brines were responsible for the transport and deposition of uranium at the sub-Athabasca unconformity.

While, a clear link between unconformity and basement-hosted uranium mineralization has been established, there is still contention about the uranium precipitation mechanism in basement-hosted uranium deposits. Multiple precipitation mechanisms have been proposed and include: 1) fluid mixing (Wilson and Kyser, 1987) and 2) fluid-rock interaction (Fayek and Kyser, 1997; Alexandre, *et. al*, 2005).

Wilson and Kyser (1987), Kotzer and Kyser (1995), developed a model for the Key Lake uranium deposit based on the δD and $\delta^{18}O$ values of diagenetic clay minerals. Mg-chlorite in altered basement gneisses was formed from basinal fluids with δD near -20‰ and $\delta^{18}O$ value of +5‰ and a temperature of ~200°C. Illite in the sandstone alteration halo was produced from basinal brine with δD -65‰ and $\delta^{18}O$ value of +5‰ at ~200°C. Uranium was concentrated along the unconformity by the mixing of the two distinct fluids. Most unconformity-type uranium deposits particularly the basement-hosted uranium deposits (e.g. Deilmann at Key Lake) occur in close proximity (i.e. within 5 meters) to the unconformity. However, the Millennium deposit is unique because the main orebody is located approximately 100 M below the unconformity (Roy, *et. al,* 2005). This is likely due to the unique structural setting of the Millennium deposit,

where a dilational jog enhanced the permeability and allowed the uraniferous fluids to infiltrate the basement rocks.

Fayek and Kyser (1997), proposed a model for the formation of the Sue C uranium deposit in which uraniferous basinal brines entered the basement along a reverse fault. The interaction between the oxidizing basinal brines and reducing basement rocks sufficiently changed the geochemical characteristics of the basinal brine and, resulted in precipitation of uraninite within planar orebodies in the fault system. However, the Millennium deposit is not situated in the fault structure, but within an adjacent dilational zone. In which uraniferous fluids were allowed to move laterally away from the fault in fractures and voids until it encountered the proper geochemical conditions to precipitate uranium.

Alexandre, *et. al.* (2005) proposed a model for basement-hosted uranium deposits based on common alteration assemblages from the McArthur River, Dawn Lake and Rabbit Lake uranium deposits. Pre-ore alteration consists of illitization of feldspar and amphibole, and the chloritization of biotite. Alexandre stated that the illitization of feldspar results in the formation of open void spaces, thereby increasing the permeability of the basement rocks. While, the conversion of biotite to chlorite in the basement rocks would consume Mg and release Fe which could act as a reductant during the syn-ore stage. The potassium and silica released during chloritization of biotite would contribute to the silica and illite alteration halos. Alexandre, also noted that pre-, and syn-ore alteration is directly attributed to basinal fluids intruding into the basement rocks.

The rocks that host the Millennium deposit consist of pelitic to psammopelitic gneisses and schists interlayered with minor amphibolite and pegmatites. The host pelitic

and psammopelitic units are composed of quartz, biotite, muscovite and their clay alteration products. In mineralized drill holes, the Fe-rich silicate minerals have been chloritized. The main ore zone within the Millennium deposit is spatially associated with a zone of dark green chlorite. Therefore, based on empirical observation, the uranium depositional mechanism proposed by Alexandre, *et. al.* (2005) is a possible mechanism for uranium precipitation at the Millennium deposit.

The composition of chloritized Fe-rich silicate minerals (hornblende and biotite) in mineralized and unmineralized basement drill core samples from the Millennium deposit, were measured by EMP. Results from the analysis showed linear relationship between FeO and MgO concentrations in biotite and amphiboles from the unmineralized basement units, whereas the FeO and MgO concentrations within altered biotite from mineralized basement units are much lower and highly variable (See Figure 4.14).

Mössbauer spectroscopy was conducted on whole-rock samples from mineralized and unmineralized drill core to determine the relative abundance of ferric and ferrous iron within the host rocks. Mineralized drill-core shows low Fe^{2+}/Fe^{3+} ratios within the main zone of uranium mineralization, while the unmineralized drill-core has higher Fe^{2+}/Fe^{3+} ratios within the same interval (see Figure 4.17). The higher Fe^{2+}/Fe^{3+} ratios and the correlation between MgO and FeO in the unmineralized core, and the lower Fe^{2+}/Fe^{3+} ratios and lack of correlation between MgO and FeO relationship in mineralized core suggests that chloritization and iron oxidation of Fe^{2+} -rich minerals (such as biotite and hornblende) in the basement rocks could have created the proper environment for reduction of U^{6+} in solution to U^{4+}, which lead to the precipitation of uraninite [1].

$$U^{6+} + 5H_2O + 2Fe^{2+} \rightarrow UO_2 + Fe_2O_3 + 10H^+ \qquad [1]$$

However, there is a lack of uranium mineralization in highly altered amphibolite within the ore zone, which initially contained a tremendous amount (up to 25 wt %) of Fe^{2+}. Therefore, Fe-oxidation may not be the dominant mechanism for uranium reduction.

The graphitic "marker unit" is typically associated with the first ore grade uranium mineralization. The "marker unit" contains up to several weight percent graphite. Where uraniferous fluids interact with the "marker unit" carbon reacts with U^{6+} in solution to precipitate U^{4+} in the following reaction [2]:

$$U^{6+} + 3H_2O + \tfrac{1}{2}C \rightarrow UO_2 + \tfrac{1}{2}CO_2 + 6H^+ \qquad [2]$$

In addition, fine-grain uraninite appears to be associated with small disseminated titanium oxides (Fig. 5.1). In aqueous environments, the surface of TiO_2 is composed of non-stoichiometric hydrated and hydroxyl phases. The adsorption of U (VI) onto the hydrated surface causes a reaction with the non-stoichiometric surface phases to undergo chemical reduction to form solid UO_2 (Bonato, et. al, 2008). While none of the precipitation mechanisms within the Millennium deposit appears to be clearly dominant, a combination of several mechanisms could have contributed to uraninite precipitation in the Millennium deposit.

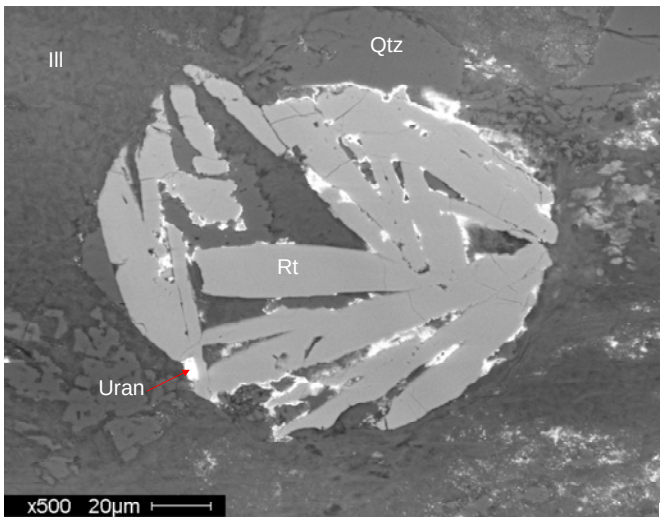

Figure 5.1: Uraninite rim on rutile in psammopelitic schist CX-44-1 741 m. Abbreviations: Ill = illite; Qtz = quartz; Uran = uraninite; Rt = rutile.

5.2.2 Source of fluids and temperatures of uranium mineral precipitation

Fluid inclusion analysis of primary fluid inclusions from euhedral and metamorphic quartz show that there are two dominant fluids associated with the Millennium deposit: 1) a moderately saline (5-15 wt% NaCl) metamorphic fluid and 2) a highly saline (22-24 wt% NaCl) basinal brine that precipitated euhedral quartz overgrowths. Both fluid inclusion sets decrepitated upon heating and gave minimum temperatures between 200-225°C. These relatively high decrepitation temperatures are consistent with isotope equilibrium temperatures for clay minerals obtained for other deposits in the Athabasca Basin (Kotzer and Kyser, 1995). However, these temperatures are considerably higher than the equilibrium isotope temperature obtained for euhedral quartz- uraninite (~ 43°C). Using this low temperature for vein uraninite precipitation, the calculated $\delta^{18}O$ for the fluid that precipitated the uraninite is -10‰. This is significantly different from the calculated $\delta^{18}O$ for basinal brines (0 ± 4‰; Kotzer and Kyser, 1992, 1995) and meteoric water ($\delta^{18}O$ -20‰; Kotzer and Kyser, 1990) that were involved in the

formation and post-depositional modification of unconformity-type uranium deposits in the Athabasca Basin (Kotzer and Kyser, 1995; Fayek and Kyser, 1997).

Therefore, the quartz and uraninite are likely not in isotopic equilibrium. There are two possible scenarios for the formation of the euhedral quartz with a $\delta^{18}O$= 16-19‰ and uraninite with a $\delta^{18}O$= ~ -22‰. The first scenario is that the uraninite and euhedral quartz were co-precipitated at 200°C, but the uraninite was overprinted by late meteoric fluids ($\delta^{18}O$ -20‰) that did not affect the $\delta^{18}O$ of the quartz. A similar model was proposed by Fayek and Kyser (1997). The second scenario is that the euhedral quartz and uraninite formed in a closed system at 200°C. The precipitation of the euhedral quartz ($\delta^{18}O$= 16-19‰) would have depleted the fluid in ^{18}O and resulted in the precipitation of uraninite with a $\delta^{18}O$ of ~ -22‰, because the uraninite water fractionation at 200°C is ~ -12.5‰ (Fayek and Kyser, 2000).

5.2.3 Basement source

Based on the petrography and $^{207}Pb/^{206}Pb$ ages of the uranium minerals there appears to be uranium mineralization at the Millennium deposit that pre-dates the Athabasca Basin sediments (~1710 Ma; Jefferson et al., 2007) and a main ore depositional event that is geochemically and geochronologically similar to mineralizing events associated with unconformity-type uranium deposits elsewhere in the Athabasca basin (Fayek and Kyser, 1997; Alexander et al., 2005).

Uraniferous metasediments are not uncommon in the Wollaston Group. The Karpinka Lake uranium prospect is an uneconomic deposit located approximately 30 km south of the Athabasca Basin and 50 km southwest of the Key Lake deposit (Fig.5.2). The deposit is hosted within graphitic metapelites of the Wollaston Group and uranium

mineralization is comprised of small disseminated uraninite and brannerite. U-Pb ages for uraninite and brannerite range between 1770-1730 Ma (Williams-Jones and Sawiuk, 1985). While there is no genetic link between the Karpinka Lake uranium prospect and the Athabasca Basin unconformity-type uranium deposits, $^{207}Pb/^{206}Pb$ ages of 1750-1650 Ma obtained from the disseminated uraninite are comparable to the U-Pb dates obtained for uranium mineralization at the Karpinka Lake uranium prospect. Although it is not unusual to find uranium mineralization with similar ages in the Wollaston/Mudjatik Groups along the periphery of the Athabasca basin (e.g., Beaverlodge, Rabbit L.). Hecht and Cuney (2000) have suggested that monazite alteration in basement rocks can be a source of uranium associated with unconformity-type uranium deposits, the 1750-1650 Ma ages of uraninite from the Millennium deposit are the first documented pre-Athabasca ages from an unconformity-type deposit and establish the presence of a basement source for uranium mineralization which predates the primary mineralization events within the Athabasca Basin.

Fluid inclusion analysis suggests that a basinal brine was primarily responsible for the alteration of the basement rocks and deposition of the massive and vein-type uranium mineralization at the Millennium deposit. Subsequent to the main ore depositional event, several fluid events between 1450 and 900 Ma, likely related to distal tectonic events affected the U-Pb systematics of the uranium mineralization, including recent low-temperature meteoric fluids. Therefore, there are two possible sources of uranium at the Millennium deposit, the uraniferous basinal brines that leached uranium from the Athabasca sedimentary package and the uraniferous basement metasediments.

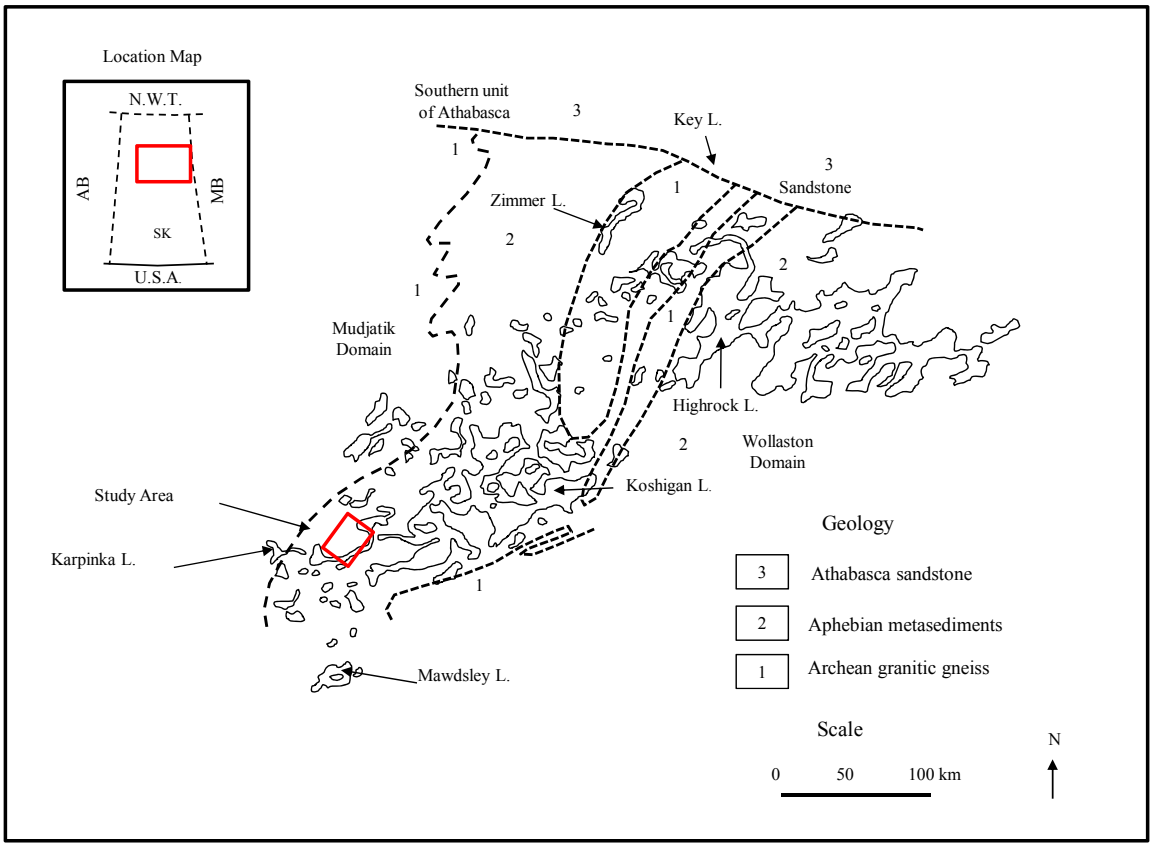

Figure 5.2: Location of Karpinka Lake uranium prospect, south of southern margin of the Athabasca Basin, Saskatchewan, Canada, with major lithostructural domains. Abbreviations: L= Lake (Modified from Williams-Jones and Sawiuk, 1985).

5.3 Depositional Model for the Millennium Deposit

There are three stages in the formation of the Millennium uranium deposit. Stage 1 (Fig.5.3a) started at the onset of peak diagenesis (>1500 Ma; Fayek et al. 2002; Alexandre et. al., 2005) where two Hudsonian age reverse faults were re-activated to form a dilational jog and a zone of brecciation. This increased the permeability of the basement units in the hanging wall block of the Millennium deposit (Fig. 5.3b). During stage 1, basinal fluids began to penetrate deep into the basement rocks, remobilizing the proto-ore and forming bleb-style uraninite. Alteration of the basement host rocks resulted

in the precipitation of sericite (Ser1), kaolinite (K1), illite (I1), hematite (H1), quartz (Q1), and chlorite (C1). Continued diagenesis (~1500 Ma; Kotzer and Kyser, 1995) produced increased uraniferous basinal fluid flow into the basement rocks, which resulted in increased chemical brecciation and alteration of the basement rocks (Stage 2; Fig. 5.3b; Alexandre et. al., 2005; Lorilleux et. al., 2003). The massive replacement and vein uranium ore was precipitated during stage 2 (1500-1400 Ma) in addition to kaolinite (K2), quartz (Q2), illite (I2), hematite (H2), and chlorite (C2). Electron microprobe analysis of altered Fe-rich silicates suggests that the uraniferous fluids altered the biotite and hornblende to chlorite (Alexandre et. al., 2005), which would release Fe^{2+} and created a geochemical redox zone and caused uranium precipitation (Stage 2 Fig. 5.3b). The main uranium orebody within the Millennium deposit is spatially related with a dark chloritic alteration, and located foot-wall to the orebody is a zone of intense hematization. This supports the interpretation of Fe reduction of uranium in solution. But the lack of uranium mineralization in amphibolite units suggests that this may not be the dominant mechanism for uranium precipitation. Other precipitation mechanisms within the Millennium area are graphitic pelite which would have provided a source for carbon reduction. Locally the graphitic "marker unit" is mineralized. Small titanium oxides disseminated within the host pelite/semipelite units are the sites of uranium precipitation. Stage 3 (Fig. 5.3c) involved post depositional fluids which resulted in variable bleaching and argillic alteration (Fig. 4.18), which overprints the primary mineralization as well as the alteration of uraninite of coffinite.

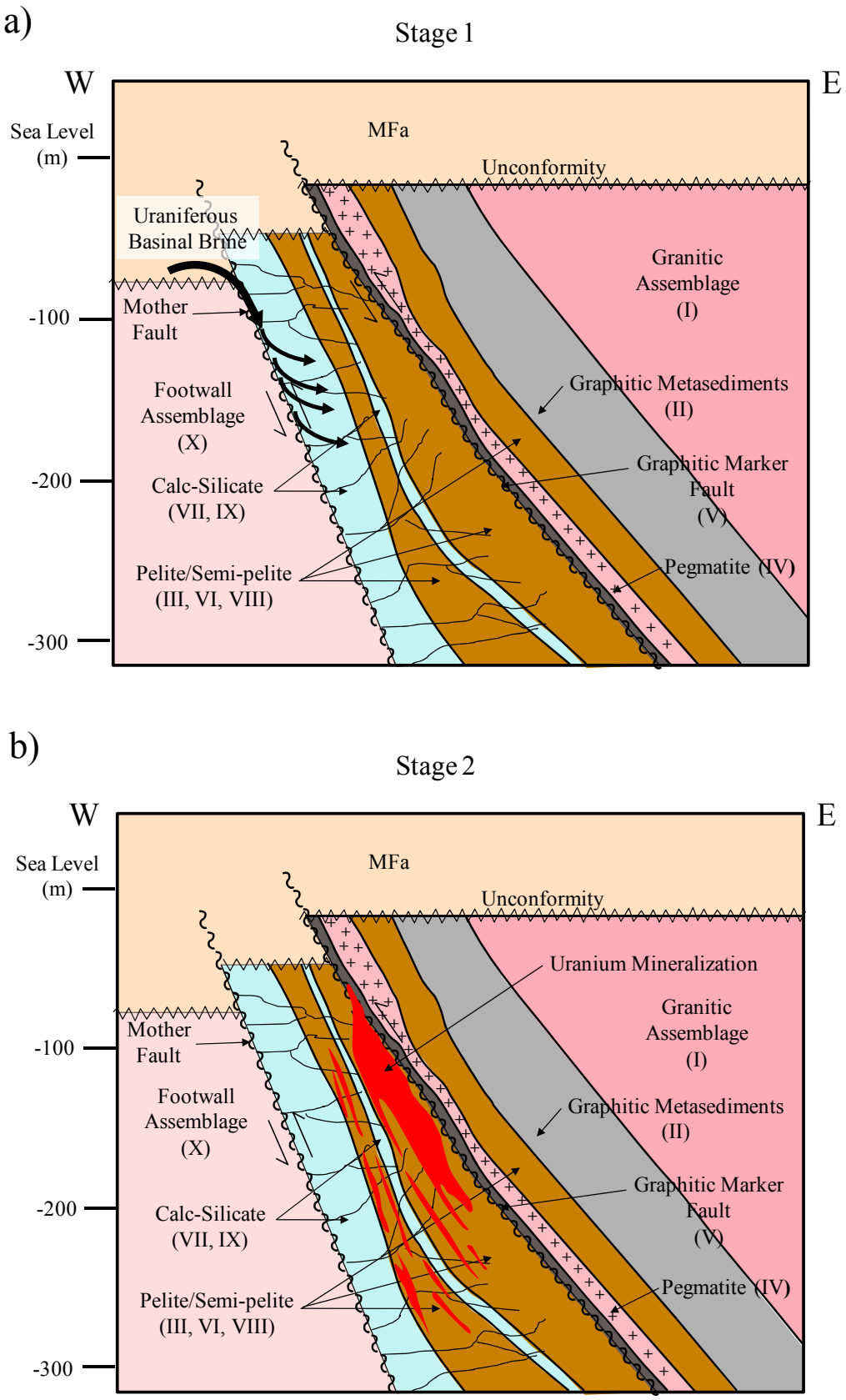
a)
Stage 1
W
E
Sea Level
(m)
MFa
Unconformity
Uraniferous
Basinal Brine
Granitic
Assemblage
(I)
Mother
Fault
-100
Graphitic Metasediments
(II)
Footwall
Assemblage
(X)
Graphitic Marker
Fault
(V)
-200
Calc-Silicate
(VII, IX)
Pegmatite (IV)
Pelite/Semi-pelite
(III, VI, VIII)
-300
b)
Stage 2
W
E
Sea Level
(m)
MFa
Unconformity
Uranium Mineralization
Granitic
Assemblage
(I)
Mother
Fault
-100
Graphitic Metasediments
(II)
Footwall
Assemblage
(X)
Graphitic Marker
Fault
(V)
-200
Calc-Silicate
(VII, IX)
Pegmatite (IV)
Pelite/Semi-pelite
(III, VI, VIII)
-300

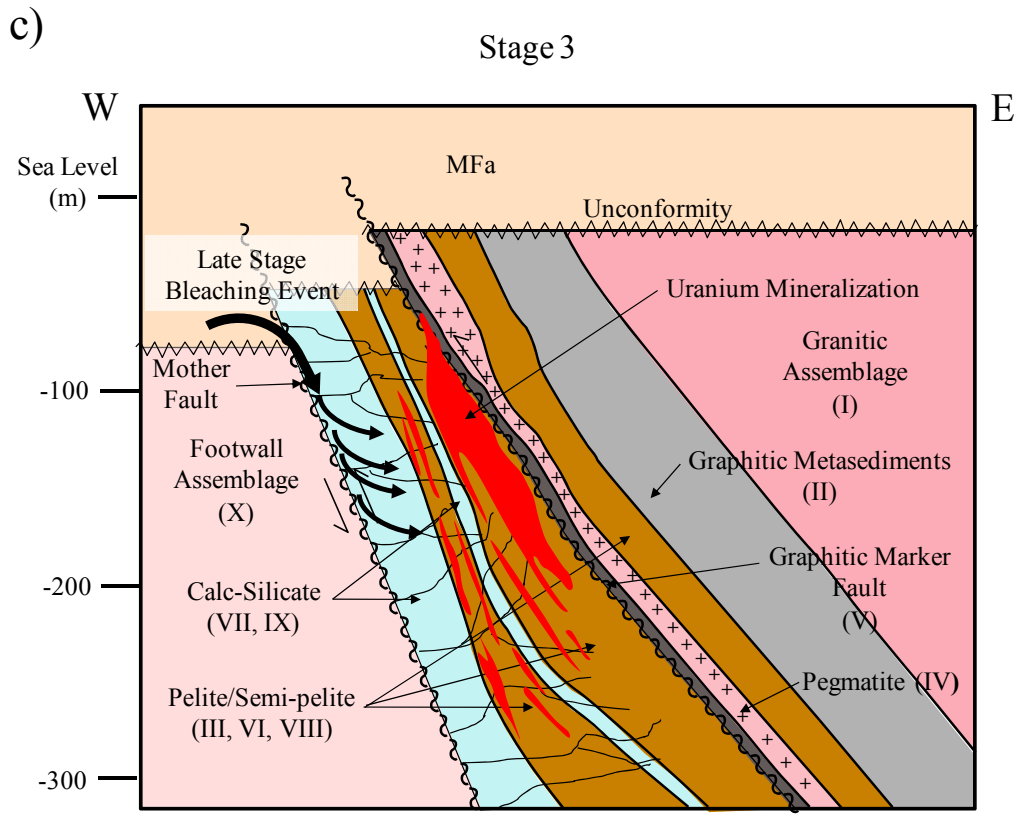

Figure 5.3: Depositional model for the Millennium deposit: a) stage 1- uplift along two sub-parallel reverse fault resulted in the development of a dilational structure enhancing permeability of basement rocks, b) stage 2- uraniferous basinal brines moved along the unconformity and down the reverse fault. Brecciation of the basement units would have allowed lateral dispersion of uraniferous fluids into the basement rocks, where geochemical conditions were optimal uranium mineralization would have precipitated, c) stage 3- post-depositional modification results in increased argillic alteration, bleaching, and development of secondary uranium minerals.

Chapter 6: Conclusions

This study aimed to determine the paragenetic relationship between basement alteration and uranium mineralization. In order to understand the mechanisms responsible for the formation of the basement hosted Millennium deposit. The Millennium deposit is situated within a dilational structure produced by movement along two sub-parallel reverse faults. The increased permeability allowed pre, syn and post depositional fluids to penetrate into the basement rocks in the Millennium area. Pre- and syn-depositional alteration of basement rocks in the Millennium area produced the ideal geochemical environment for the precipitation of uranium mineralization in the basement rocks. The analysis of Fe-rich silicate minerals by EMP in conjunction with Mössbauer spectroscopy identified one of three possible uranium precipitation mechanisms (i.e. Fe reduction). The others are carbon reduction in graphitic pelites, and minor TiO_2 adsorption.

Massive and vein-type uraninites have low $\delta^{18}O$ values from -35‰ to -15‰, which are typical of oxygen isotopic values of uraninite from unconformity hosted uranium deposits in the Athabasca basin. Relict metamorphic and secondary euhedral quartz grains associated with vein-type uraninite have $\delta^{18}O$ values of 11.1‰ to 15.1‰ and 16.2‰ to 19.1‰ respectively. The low $\delta^{18}O$ values for uraninite and the high $\delta^{18}O$ values for quartz suggest that the original isotopic composition of both minerals have been modified by recent low-temperature meteoric waters.

Fluid inclusion analysis suggests that basinal brine was primarily responsible for the alteration of the basement rocks and deposition of the massive and vein-type uranium mineralization at the Millennium deposit. Prior to the main ore depositional event, several fluid events between 1450 and 900 Ma, likely related to distal tectonic events

affected the U-Pb systematics of the uranium mineralization, including recent low-temperature meteoric fluids. Therefore, there are two possible sources of uranium at the Millennium deposit, the uraniferous basinal brines that leached uranium from the Athabasca sedimentary package and the uraniferous basement metasediments. The ultimate nature for the formation of basement hosted uranium deposits depends on several key factors which include (1) the appropriate structural setting, (2) a favorable geochemical environment and (3) timing.

Recommendations:

- Stable isotope and age dating of clay alteration minerals to better define the paragenetic relationship between host-rock alteration and uranium mineralization.
- Detailed analysis of structural features related to uranium mineralization in order to develop a more detailed understanding of structural controls on uranium mineralization.

Chapter 7: References

Alexandre, P., Kyser, T.K., Polito, P., and Thomas, D. (2005): Alteration mineralogy and stable isotope geochemistry of Paleoproterozoic basement-hosted unconformity-type uranium deposits in the Athabasca Basin, Canada. *Economic Geology*. **100**, 1547-1563.

Anderson, T. (2002): Correction of common lead in U-Pb analyses that do not report ^{204}Pb. *Chemical Geology*. **192**, 59-79.

Armstrong, R.L. and Ramaekers, P. (1985): Sr isotopic study of Helikian sediment and diabase dikes in the Athabasca Basin, northern Saskatchewan. *Canadian Journal of Earth Sciences*. **22**, 344-407.

Baudemont, D., and Fedorowich, J. (1996): Structural control of uranium mineralization at the Dominique-Peter deposit, Saskatchewan, Canada. *Economic Geology*. **91**, 855-874.

Bruneton, P. (1993): Geological environment of the Cigar lake uranium deposit. *Can. J. Earth Sci*. **30**, 653-673.

Bell, K. (1985): Geochronology of the Carswell area, northern Saskatchewan. *In* R. Lainé, D. Alonso, and M. Svab, eds., The Carswell Structure Uranium Deposits, Saskatchewan. *Geological Association of Canada,* Special Paper **29**, 33-46.

Blaise, J.R., and Koning, E. (1985): Mineralogical and structural aspects of the Dominique-Peter uranium deposit. *In* R. Lainé, D. Alonso, and M. Svab, eds., The Carswell Structure Uranium Deposits, Saskatchewan. *Geological Association of Canada,* Special Paper **29**, 139-151.

Bodnar, R.J. (2003) Introduction to Aqueous-Electrolyte Fluid Inclusions, *In* Samson, I., Anderson, A., Marshall, D., (Eds.) Fluid Inclusions- Analysis and Interpretation. *Mineralogical Association of Canada*. Short course Volume **32**, 81-101.

Bonato, M., Allen, G.C. and Scott, T.B. (2008): Reduction of U(VI) to U(IV) on the surface of TiO_2 anatase nanotubes. *Micro and Nano Letters*, Vol. **3**, No. 2, 57-61.

Bowles, J.F.W. (1990): Age dating of individual grains of uraninite in rocks from electron microprobe analysis. *Chemical Geology*. **83**, 47-53.

Cuney, M., and Kyser, K. (Eds.) (2008): Recent and not -so recent developments in uranium deposits and implications for exploration. *Mineral. Assoc. Can., Short Course* **39**, 1-15.

Derome, D., Cathelineau, M., Cuney, M., Fabre, C., Lhomme, T., and Banks, D.A. (2005): Mixing of Sodic and Calcic brines and uranium deposition at McArthur River,

Saskatchewan, Canada: A Raman and laser-induced breakdown spectroscopic study of fluid inclusions. *Economic Geology*. **100**, 1529-1545.

Energy Information Administration, (2007): International Energy Outlook 2007. Department of Energy, Washington, D.C., www.eia.doe.gov/oiaf/ioe/index.html.

Ey, F., Piquard, J.P., and Zimmerman, J. (1993): The Sue uranium deposits, Saskatchewan, Canada. *Exploration and Mining Geology*. 1993 **vol. 2, no.3**, 179-202.

Faure, G. Principles of Isotope Geology. New York: John Wiley and Sons, 1986. 287-291

Fayek, M., Anovitz, L.M., Cole, D.C., Bostick, D. (in prep).

Fayek, M., Kyser, K.T., and Riciputi, L.R. (2002): U and Pb isotope analysis of uranium minerals by ion microprobe and the geochronology of the McArthur River and Sue Zone uranium deposits, Saskatchewan, Canada. *Canadian Mineralogist*. **40**, 1553-1569.

Fayek, M., and Kyser, T.K., 2000. Low temperature oxygen isotopic fractionation in the uraninite–UO2–CO2–H2O system. *Geochimica et Cosmochimica Acta.* **64**, 2185– 2197.

Fayek, M., and Kyser, T.K. (1997): Characterization of multiple fluid-flow events and rare-earth-element mobility associated with formation of unconformity-type uranium deposits in the Athabasca Basin, Saskatchewan. *Canadian Mineralogist*. **35**, 627-658.

Fayek, M., Janeczek, J., and Ewing, R.C. (1997): Mineral chemistry and oxygen isotopic analyses of uraninite, pitchblende, and uranium alteration minerals from the Cigar Lake deposit, Saskatchewan, Canada. *Applied Geochemistry*. **12**, 549-565.

Gilboy, C.F., and Vigrass, L.W., Eds. (1986) The Eagle Point uranium deposits, Northern Saskatchewan. *In* Economic Minerals of Saskatchewan. *Saskatchewan Geological Society*, Special Publication **no. 8**, 78-98.

Gilboy, C.F. (1985): Basement Geology, Part of the Cree Lake (South) area. *Saskatchewan Energy and Mines*, Report **203**, 47 p.

Hattori, K., and Halas, S. (1982): Calculation of oxygen isotope fractionation between uranium dioxide, uranium trioxide and water. *Geochimica et Cosmochimica Acta*. **46**, 1863-1868

Hecht, L., and Cuney, M. (2000): Hydrothermal alteration on monazite in the Precambrian crystalline basement of the Athabasca Basin (Saskatchewan, Canada): Implications for the formation of unconformity-related uranium deposits. *Mineralium Deposita*. **35**, 791-795.

Hoeve, J., and Sibbald, T.I.I. (1978): On the Origin of Rabbit Lake and other unconformity-type uranium deposits in northern Saskatchewan. *Economic Geology*. **73**, 1450- 1473.

Hove, J., and Sibbald, T.I.I. (1976): The Rabbit Lake uranium mine. *In* Uranium is Saskatchewan. (Dunn, C.E., Ed.). *Saskatchewan Geological Society*, Special Publication. **No. 3**, 331-354.

International Atomic Energy Agency (2001): Analysis of Uranium Supply to 2050. *IAEA, Vienna*, Austria. STI/PUB/1104. 112 Pages.

Jefferson, C.W., Thomas, D.J., Gandhi, S.S., Ramekers, P., Delaney, G., Brisbin, D., Cutts, C., Portella, P. and Olson, R.A. (2007): Unconformity Associated Uranium Deposits- *Draft*.

Kawabe, I. (1978): Calculation of oxygen isotope fractionation in quartz-water system with special reference to the low temperature fractionation. *Geochemica et Cosmochimica Acta* 42, pp 613-621.

Kotzer, T.G., and Kyser, T.K. (1995): Petrogenesis of the Proterozoic Athabasca Basin, northern Saskatchewan, Canada, and its relation to Diagenesis, hydrothermal uranium mineralization and paleohydrogeology. *Chemical Geology*. **120**, 45-89.

Kotzer, T.G., and Kyser, T.K. (1993): O, U, and Pb isotopic and chemical variations in uraninite: Implications for determining the temporal and fluid history of ancient terrains. *American Mineralogist*. **78**, 1262-1274.

Kotzer, T.G., and Kyser, T.K. (1992): Isotopic, mineralogic and chemical evidence for multiple episodes of fluid movement during prograde and retrograde diagenesis in a Proterozoic Basin. *In* Kharaka, Y.K., Maest, A.S., eds. *Proc. 7th Inter, Symp. On Water-Rock Interaction*. July 13-18, Utah, 1177-1181.

Kotzer, T.G., and Kyser, T.K. (1990): The use of stable and radiogenic isotopes in the identification of fluids and processes associated with unconformity-type uranium deposits. *In* Modern Exploration Techniques, *Saskatchewan Geological Society Special Publication*, **10**, 115-131.

Lewry, J.F., and Sibbald, T.I.I. (1980): Thermotectectonic Evolution of the Churchill province in northern Saskatchewan, *Tectonphysics* **68**, 45-82

Lewry, J.F., and Sibbald, T.I.I. (1977): Variation in lithology and tectonometamorphic relationships in the Precambrian basement of northern Saskatchewan, *Canadian Journal of Earth Sciences*. **14**, 1453-1467.

Lorilleux, G., Cuney, M., Jébrak, M., Rippert, J.C., Portella, P. (2003): Chemical; brecciation processes in the Sue unconformity-type uranium deposits, Eastern Athabasca Basin (Canada). *Journal of Geochemical Exploration.* **80**. 241-258.

Portella, P. and Annesley, I.R., (2000): Paleoproterozoic tectonic evolution of the eastern sub-Athabasca basement, northern Saskatchewan: Integrated magnetic, gravity, and geological data; extended abstract *in* GeoCanada: The Millennium Geoscience Summit; Joint meeting of the Canadian Geophysical Union, Canadian Society of Exploration Geophysicists, Canadian Society of Petroleum Geologists, Canadian Well Logging Society, *Geological Association of Canada, and the Mineralogical Association of Canada, Program with Abstracts*, **25**, 4 p.

Ramekers, P. (1979): Stratigraphy of the Athabasca basin. *In* Summary of investigations 1979. Christopher, J.E., and MacDonald, R., (Eds.). *Saskatchewan Geological Survey, Miscellaneous Report* **79-10**, 154-160.

Ramekers, P. (1980): Stratigraphy and tectonic history of the Athabasca Group (Helikian) of northern Saskatchewan. *In* Summary of investigations 1980. *Saskatchewan Geological Survey, Miscellaneous Report* **80-4**, 99-106.

Ramekers, P. (1981): Hudsonian and Helikian basins of the Athabasca region, northern Saskatchewan. *In* Campbell, F.H.A. (Ed.). Proterozoic basins of Canada. *Geological Survey of Canada*, Paper **81-10**, 219-233.

Ramekers, P. (1990): Geology of the Athabasca Group (Helikian) in northern Saskatchewan. *Saskatchewan Energy and Mines*, Report **195**, 49 p.

Rancourt, D.G. and Ping, J.Y. (1991) Voigt-based methods for arbitrary-shape static hyperfine parameter distributions in Mössbauer spectroscopy. *Nuclear Instruments and Methods in Physics Research* **B58**, 85-97.

Riciputi, L.R., Paterson, B.A. and Ripperdan, R.L. (1998): Measurement of light stable isotope ratios by SIMS: matrix effects for oxygen, carbon, and sulfur isotopes in minerals. *International Journal of Mass Spectrometry*. **178**, 81-112.

Roy, C., Halaburda, J., Thomas, D., and Hirsekorn, D. (2005): Millennium deposit – basement-hosted derivative of the unconformity uranium model. *In* Uranium production and raw materials for the nuclear fuel cycle- Supply and demand, economics, the environment and energy security. *IAEA Proceedings of an international symposium, Vienna, 20-24 June, 2005*. 111-121.

Sibbald, T.I.I. (1985): Geology and genesis of the Athabasca Basin uranium deposits. *In* Summary of Investigations 1985, *Saskatchewan Geological Survey, Sask. Energy Mines*, **Misc. Rept. 85-4**, 45 pages.

Thomas, D. (2002): Observations on structural and alteration features- Millennium Zone, Cree Extension Project: Insights into a Basement-hosted Uranium Model. *Cameco Corporation- unpublished report, 37 pages.*

Thomas, D.J., Matthews, R.B., and Sopuck, V.J., (1998): Athabasca basin unconformity-type uranium deposits: A synopsis of the empirical model and review of exploration and production trends (abs.). Canadian Institute of Mining, Metallurgy and Petroleum Meeting, Montreal, May 3-7, Proceedings (CD-ROM).

Tran, H.T. and Yeo, G.M. (1997): Geology of the Burbidge Lake- northern Upper Foster Lake area, eastern Wollaston Domain (NTS 74A-14). *In* Summary of Investigations 1997, *Saskatchewan Geological Survey, Sask. Energy Mines*, Misc**. Rept. 97-4**, 72-89.

Tran, H.T., Yeo, G.M., Bradley, S., and Lewry, J.F. (1998): Geology of the Daly-Suttle-Middle Foster Lakes area, eastern Wollaston Domain (NTS 74A-5, -11, and -12). *In* Summary of Investigations 1998, *Saskatchewan Geological Survey, Sask. Energy Mines*, **Misc. Rept. 98-4**, 48-65.

Wakita H., Rey P., and Schmitt R. A. (1971): Elemental abundances of major, minor, and trace elements in Apollo 11 lunar rocks, soil and core samples. *Proc. Apollo 11 Lunar Sci. Conf.*, 1685-1717.

Williams-Jones, and A.E., Sawiuk, M. (1985): The Karpinka Lake uranium prospect, Saskatchewan: A possible metamorphosed Middle Precambrian sandstone-type uranium deposit. *Economic Geology*. **80**, 1927-1941.

Yeo, G.M. (1998): A systems tract approach to the stratigraphy of paragneisses in the southeastern Wollaston Domain. *In* Summary of Investigations 1998, *Saskatchewan Geological Survey, Sask. Energy Mines*, **Misc. Rept. 98-4**, 36-47.

Zheng, Y., (1995): Isotope fractionation in uranium oxides. *Nucl Sci.Technol*. **6**,193–197.

Zheng, Y., (1991): Calculation of oxygen isotope fractionation in metal oxides *Geochemica et Cosmochimica Acta*, Vol. **55**, pp. 2299- 2307.

APPENDIX A

TABLE 1. MINERALOGICAL AND CHEMICAL COMPOSITION OF URANIUM MINERALS FROM THE MILLENNIUM DEPOSIT, ATHABASCA BASIN, SASKATCHEWAN, CANADA

Sample No. (DDH/depth)	Remarks	SiO_2	UO_2	SO_2	TiO_2	Fe_2O_3	PbO	CaO	Al_2O_3	P_2O_5	ThO_2	Total
*47-1 758-1a	Ca-U	5.81	82.18	0.02	0.05	0.0	0.05	3.29	0.85	0.11	0.02	92.38
*47-1 758-1b	galena	0.04	0.0	29.35	0.0	0.03	95.13	0.0	0.0	0.0	0.0	124.55
*47-1 758-1c	Alt. Uran	5.39	83.52	0.02	0.01	0.0	0.11	3.73	0.82	0.08	0.07	93.75
*47-1 758-2a	Coff	11.25	75.85	0.02	0.0	0.08	0.0	3.84	1.09	0.05	0.13	92.30
*47-1 758-2b	Coff	17.47	68.44	0.02	0.04	0.0	4.10	2.08	1.66	0.17	0.09	94.06
*47-1 758-2c	galena	0.02	0.0	29.52	0.0	0.0	94.77	0.04	0.01	0.0	0.03	124.38
*47-1 758-3a	Ca-U	6.84	81.35	0.0	0.0	0.0	0.08	3.41	20.0	0.06	0.0	93.76
*47-1 758-3b	galena	0.04	0.0	29.56	0.0	0.0	95.24	0.04	0.0	0.01	0.0	124.88
*47-1 758-3c	Coff	16.55	74.38	0.0	0.03	0.0	0.15	3.35	1.63	0.15	0.0	96.24
*47-1 758-3d	galena	0.01	0.0	29.33	0.0	0.0	95.0	0.03	0.0	0.0	0.06	124.43
*47-1 758-3e	Alt. Uran	6.09	80.81	0.01	0.02	0.0	0.51	3.87	0.74	0.06	0.0	92.11
*47-1 758-3f	Alt. Uran	4.14	82.84	0.0	0.01	0.01	0.81	3.92	0.56	0.04	0.0	92.33
*47-1 758-3g	Alt. Uran	4.37	81.99	0.03	0.04	0.01	0.98	4.0	0.63	0.05	0.0	92.10
*47-1 758-3h	Alt. Uran	4.25	79.74	0.12	0.04	0.01	2.02	3.79	0.57	0.05	0.0	90.60
*47-1 758-3i	galena	0.0	0.0	29.63	0.0	0.01	94.49	0.02	0.01	0.0	0.0	124.15
*47-1 758-4a	Alt. Uran	9.31	75.23	0.01	0.0	0.08	0.0	5.49	2.28	0.10	0.11	92.59
*47-1 758-4b	Alt. Uran	5.21	82.10	0.0	0.02	0.11	0.0	5.85	3.23	0.10	0.14	96.76
*47-1 758-4c	galena	0.03	0.0	29.50	0.0	0.0	94.29	0.03	0.0	0.0	0.0	123.84
*47-1 758-5a	Coff	20.02	53.95	0.03	0.01	0.42	0.13	3.30	13.41	0.03	0.0	91.30
*47-1 758-5b	Alt. Uran	5.12	80.43	0.0	0.02	0.05	0.11	5.56	1.67	0.08	0.0	93.04
*47-2 708-4a	Coff	12.81	73.27	0.01	0.07	0.0	0.0	2.34	1.13	0.90	0.0	90.51
*56-1 663-1a	Uran	0.04	77.13	0.30	0.15	0.08	14.16	2.40	0.01	0.21	0.03	94.50
*56-1 663-1b	Uran	0.07	77.84	0.0	0.09	0.32	14.21	1.80	0.02	0.20	0.0	94.56
*56-1 663-1c	Uran	0.09	78.32	0.0	0.03	0.04	14.94	1.70	0.03	0.30	0.0	95.45
*56-1 663-1d	Uran	0.18	78.43	0.03	0.05	0.20	15.16	1.95	0.02	0.34	0.0	96.36
*56-1 663-1e	Uran	0.07	76.72	0.02	0.06	0.07	14.47	1.58	0.02	0.25	0.0	93.26
*56-1 663-1f	Uran	0.61	81.32	0.19	0.06	0.45	7.94	3.38	0.06	0.29	0.13	94.41

*56-1 663-1a1	Uran	0.15	80.41	0.08	0.28	0.31	13.39	1.98	0.0	0.20	0.0	96.80
*56-1 663-1b1	Uran	0.21	80.12	0.03	0.17	0.32	11.88	2.05	0.01	0.27	0.0	95.05
*56-1 663-1c1	Uran	0.21	77.89	0.03	0.06	0.19	12.73	2.13	0.03	0.28	0.0	93.55
*56-1 663-1d1	Uran	0.22	79.17	0.03	0.21	0.40	12.12	2.27	0.02	0.26	0.0	94.70
*56-1 663-1e1	Uran	0.26	80.11	0.02	0.04	0.13	11.65	2.50	0.03	0.29	0.0	95.03
*56-1 663-1f1	Uran	0.26	78.66	0.25	0.29	0.53	12.15	2.18	0.04	0.18	0.0	94.54
*56-1 663-2a	Uran	0.04	79.22	0.03	0.03	0.22	13.64	2.11	0.02	0.29	0.0	95.61
*56-1 663-2b	Uran	0.05	78.11	0.0	0.04	0.09	13.95	2.17	0.02	0.33	0.0	94.76
*56-1 663-2c	Uran	0.10	79.37	0.0	0.10	0.08	11.58	2.29	0.01	0.33	0.0	93.86
*56-1 663-2d	Uran	0.23	79.23	0.03	0.19	0.41	12.61	2.29	0.01	0.22	0.04	95.24
*56-1 663-2**e**	Uran	0.09	78.16	0.02	0.07	0.20	14.57	1.85	0.01	0.26	0.06	95.28
*56-1 663-2f	Alt. Uran	2.18	77.41	0.03	0.41	1.07	8.57	2.57	0.45	0.19	0.04	92.92
*56-1 663-3a	Uran	0.45	81.14	0.01	0.73	0.46	10.46	2.25	0.03	0.21	0.07	95.79
*56-1 663-3b	Uran	0.11	76.68	0.06	0.03	0.15	15.79	1.61	0.01	0.32	0.0	94.74
*56-1 663-3c	Uran	0.08	78.61	0.01	0.0	0.04	12.99	1.94	0.02	0.31	0.0	93.99
*56-1 663-3d	Uran	0.07	76.99	0.0	0.02	0.16	15.91	1.69	0.0	0.29	0.04	95.18
*56-1 663-3e	Uran	0.10	78.34	0.0	0.02	0.16	12.75	2.23	0.02	0.40	0.0	94.02
*56-1 663-3f	Uran	0.33	79.40	0.18	0.20	0.36	11.09	2.62	0.03	0.23	0.08	94.52
*56-1 663-3g	Uran	0.12	78.65	0.04	0.02	0.35	12.64	1.91	0.0	0.21	0.0	93.95
*56-1 663-3h	Uran	0.11	77.39	0.02	0.05	0.14	14.92	1.69	0.02	0.32	0.0	94.65
*56-1 663-3i	Uran	0.09	78.59	0.04	0.02	0.14	14.10	1.73	0.03	0.26	0.0	94.99
*56-1 663-3j	Uran	0.05	76.30	0.52	0.05	0.18	16.09	1.65	0.02	0.26	0.0	95.11
*56-1 663-4a	Uran	0.16	78.79	0.10	0.06	0.35	13.66	1.99	0.0	0.20	0.05	95.36
*56-1 663-4b	Uran	0.07	76.25	0.03	0.07	0.07	15.98	1.44	0.04	0.29	0.0	94.23
*56-1 663-4c	Uran	0.23	78.86	0.12	0.11	0.31	12.08	2.50	0.03	0.28	0.0	94.51
*56-1 663-4d	Uran	0.17	76.85	0.0	0.07	0.17	15.17	2.10	0.01	0.29	0.0	94.82
*56-1 663-4e	Uran	0.21	77.14	0.02	0.13	0.22	14.35	1.98	0.01	0.29	0.0	94.34
*56-1 663-5a	Uran	0.10	79.20	0.12	0.05	0.24	12.86	1.89	0.02	0.23	0.0	94.72
*56-1 663-5b	Uran	0.38	82.22	0.01	0.19	0.32	10.13	2.34	0.03	0.27	0.0	95.88
*56-1 663-5c	Uran	0.06	77.40	0.07	0.02	0.10	15.96	1.42	0.01	0.24	0.13	95.40
*56-1 663-5d	Uran	0.09	76.79	0.0	0.04	0.03	14.96	1.88	0.01	0.36	0.0	94.15
*56-1 663-5e	Uran	0.08	79.71	0.02	0.38	0.13	12.49	2.27	0.01	0.24	0.26	95.59
*56-1 663-5f	Uran	0.43	79.23	0.02	0.22	0.37	10.98	2.72	0.03	0.19	0.02	94.20
*56-1 663-5g	Alt. Uran	4.02	79.63	0.01	0.45	2.14	0.31	6.17	0.20	0.10	0.0	93.03

*56-1 663-6a	Uran	0.29	80.46	0.07	0.16	0.51	10.77	2.58	0.01	0.22	0.0	95.06
*56-1 663-6b	Uran	0.21	79.61	0.07	0.11	0.40	12.10	2.05	0.01	0.21	0.0	94.75
*56-1 663-6c	Uran	0.07	77.80	0.0	0.03	0.11	13.90	1.78	0.03	0.29	0.01	94.03
*56-1 663-6d	Uran	0.07	77.94	0.02	0.06	0.11	14.54	1.95	0.03	0.31	0.0	95.04
*56-1 663-6e	Uran	0.31	80.82	0.22	0.03	0.41	10.95	2.54	0.06	0.39	0.0	95.71
*56-1 663-7a	Uran	0.21	77.32	0.03	0.03	0.20	15.25	1.75	0.03	0.30	0.02	95.16
*56-1 663-7b	Uran	0.45	80.62	0.0	0.21	0.48	10.35	2.80	0.05	0.30	0.0	95.26
*56-1 663-7c	Uran	0.60	82.24	0.01	0.08	0.57	10.43	2.66	0.03	0.22	0.14	96.97
*56-1 663-7d	Uran	0.25	75.54	0.05	0.03	0.15	13.91	2.16	0.05	0.33	0.01	92.47
*56-1 663-7e	Uran	0.09	77.03	0.01	0.13	0.14	14.92	1.90	0.01	0.30	0.0	94.52
*56-1 663-7f	Uran	0.08	77.37	0.01	0.05	0.10	14.68	1.91	0.01	0.29	0.0	94.47
*56-1 663-8a	Uran	0.16	77.80	0.36	0.04	0.17	14.72	1.75	0.02	0.26	0.0	95.28
*56-1 663-8b	Uran	0.85	82.33	0.0	0.27	0.86	6.09	4.22	0.07	0.17	0.0	94.87
*56-1 663-8c	Uran	0.10	79.27	0.04	0.13	0.31	13.80	1.73	0.0	0.21	0.24	95.82
*56-1 663-8d	Uran	0.73	80.81	0.40	0.20	0.79	8.42	3.81	0.04	0.18	0.04	95.41
*56-1 663-8e	Uran	0.48	78.51	0.02	0.37	0.45	12.50	2.31	0.06	0.08	0.02	94.80
*56-1 663-8a1	Uran	0.10	78.48	0.0	0.15	0.29	13.95	1.79	0.02	0.26	0.0	95.05
*56-1 663-8b1	Uran	0.18	78.30	0.03	0.06	0.15	13.26	2.07	0.04	0.31	0.0	94.38
*56-1 663-8c1	Uran	0.31	80.96	0.08	0.12	0.47	10.86	2.63	0.03	0.24	0.10	95.80
*56-1 663-8d1	Uran	0.08	76.87	0.0	0.05	0.08	16.23	1.77	0.07	0.32	0.0	95.46
*56-1 663-8e1	Uran	0.16	79.41	0.08	0.15	0.35	13.22	2.06	0.0	0.21	0.17	95.80
*56-1 663-9a	Uran	0.12	80.00	0.01	0.07	0.32	12.94	1.93	0.0	0.21	0.0	95.60
*56-1 663-9b	Uran	0.09	77.00	0.01	0.04	0.10	14.71	1.61	0.03	0.29	0.20	94.07
*56-1 663-9c	Uran	0.08	76.42	0.01	0.03	0.11	15.88	1.86	0.04	0.36	0.0	94.77
*56-1 663-9d	Uran	0.28	78.97	0.11	0.07	0.33	13.34	2.27	0.03	0.30	0.0	95.70
*56-1 663-9e	Uran	0.09	77.13	0.02	0.02	0.07	14.44	1.56	0.03	0.32	0.06	93.73
*56-1 663-10a	Uran	0.18	78.34	0.03	0.07	0.35	12.81	2.15	0.02	0.24	0.07	94.27
*56-1 663-10b	Uran	0.14	79.46	0.14	0.11	0.29	13.12	2.13	0.02	0.24	0.0	95.64
*56-1 663-10c	Uran	0.18	79.55	0.31	0.04	0.42	12.72	2.31	0.0	0.27	0.06	95.86
*56-1 663-10d	Uran	0.08	77.05	0.01	0.02	0.12	14.36	1.82	0.02	0.35	0.0	93.82
*56-1 663-10e	Uran	0.28	79.12	0.11	0.37	0.33	11.44	2.42	0.03	0.24	0.0	94.33
*56-1 663-10f	Uran	0.14	79.28	0.03	0.41	0.20	14.41	1.29	0.0	0.17	0.0	95.93
*56-1 663-10a1	Uran	0.13	77.14	0.07	0.02	0.17	15.07	1.72	0.04	0.30	0.03	94.69
*56-1 663-10b1	Uran	0.11	77.84	0.06	0.03	0.13	14.03	1.93	0.05	0.35	0.07	94.59

*56-1 663-10c1	Uran	0.20	79.95	0.06	0.13	0.27	12.56	2.07	0.03	0.28	0.0	95.55
*56-1 663-10d1	Uran	0.20	79.83	0.02	0.10	0.42	12.26	1.99	0.01	0.21	0.01	95.05
*56-1 663-10e1	Uran	0.09	76.72	0.03	0.02	0.04	15.52	1.77	0.03	0.33	0.03	94.58
*56-1 682-1a	Alt. Uran	3.31	86.31	0.02	0.07	0.22	0.32	3.07	0.53	0.23	0.12	94.12
*56-1 682-1b	Alt. Uran	3.19	85.45	0.0	0.04	0.26	0.32	3.25	0.54	0.25	0.0	93.29
*56-1 682-2a	Alt. Uran	4.36	86.06	0.03	0.02	0.14	0.20	1.87	0.96	0.27	0.0	93.90
*56-1 682-2b	Alt. Uran	4.41	85.95	0.0	0.0	0.05	0.16	1.77	0.71	0.24	0.0	93.28
*56-1 682-2c	Alt. Uran	4.34	86.05	0.01	0.25	0.07	0.22	1.72	0.75	0.27	0.0	93.68
*56-1 682-2d	Alt. Uran	4.08	85.50	0.02	0.08	0.11	0.09	1.83	0.65	0.27	0.01	92.63
*56-1 682-2e	Alt. Uran	3.91	87.19	0.0	0.03	0.06	0.07	1.89	0.66	0.23	0.10	94.13
*56-1 682-2f	Alt. Uran	4.19	85.64	0.02	0.03	0.07	0.05	1.91	0.70	0.25	0.06	92.93
*56-1 682-3a	Alt. Uran	3.17	85.92	0.02	0.32	0.22	0.35	2.86	0.48	0.26	0.02	93.59
*56-1 682-3b	Alt. Uran	3.38	86.39	0.0	0.13	0.19	0.44	2.99	0.65	0.32	0.0	94.49
*56-1 644-1a	Uran	0.28	79.12	0.01	0.78	0.19	12.01	1.19	0.01	0.11	0.0	93.70
*56-1 644-1b	Uran	0.19	78.78	0.21	0.73	0.19	14.27	0.99	0.0	0.13	0.0	95.48
*56-1 644-1c	Coff	24.90	58.92	0.01	0.0	0.03	0.20	2.89	1.62	0.13	0.09	88.77
*56-1 644-1d	Uran	0.71	79.05	0.10	0.12	0.36	9.70	2.48	0.03	0.12	0.0	92.68
*56-1 644-1e	Alt. Uran	2.68	79.42	0.02	0.30	0.0	3.74	4.78	0.14	0.23	0.06	91.36
*56-1 644-1f	Uran	0.49	79.70	0.21	0.19	0.55	10.49	2.39	0.03	0.18	0.0	94.22
*56-1 644-2a	Uran	0.18	79.07	0.01	0.08	0.24	12.04	2.18	0.0	0.19	0.05	94.04
*56-1 644-2b	Uran	0.31	79.40	0.08	0.10	0.46	11.43	2.20	0.02	0.13	0.07	94.20
*56-1 644-2c	Uran	0.27	79.45	0.14	0.02	0.38	11.71	2.20	0.04	0.23	0.16	94.59
*56-1 644-2d	Uran	0.37	80.38	0.05	0.05	0.40	8.53	3.20	0.02	0.09	0.06	93.16
*56-1 644-3a	Uran	0.19	78.61	0.04	0.28	0.41	12.88	1.68	0.0	0.18	0.06	94.30
*56-1 644-3b	Uran	0.37	78.02	0.02	0.35	0.37	11.81	1.88	0.02	0.13	0.0	92.98
*56-1 644-3c	Alt. Uran	8.55	60.42	0.07	1.19	0.40	5.44	3.93	1.11	0.17	0.0	81.29
*56-1 644-3d	Uran	0.28	78.71	0.12	0.02	0.22	14.61	2.12	0.02	0.25	0.08	96.43
*56-1 644-3e	Uran	0.20	78.44	0.06	0.12	0.40	14.88	1.50	0.03	0.12	0.0	95.74
*56-1 644-3f	Uran	0.12	79.78	0.06	0.10	0.28	13.65	1.63	0.01	0.13	0.0	95.75
*56-1 644-3g	Uran	0.68	77.46	0.09	0.18	0.61	12.13	1.96	0.04	0.14	0.0	93.28
*56-1 644-3h	Uran	0.11	78.36	0.05	0.08	0.26	15.44	1.25	0.0	0.10	0.01	95.65
*56-1 644-3i	Uran	0.77	77.48	0.11	0.06	0.51	13.11	2.18	0.01	0.18	0.03	94.44
*56-1 644-3j	Uran	0.18	83.22	0.16	0.14	0.22	9.73	2.90	0.02	0.18	0.03	96.78
*56-1 644-3k	Uran	0.11	79.04	0.02	0.10	0.28	15.22	1.43	0.0	0.12	0.0	96.32

*56-1 644-6a	Uran	0.67	81.96	0.0	0.16	0.19	9.83	2.66	0.04	0.14	0.0	95.64
*56-1 644-6b	Uran	0.13	80.88	0.01	0.03	0.13	13.33	2.56	0.02	0.22	0.0	97.32
*56-1 644-6c	Coff	41.18	0.76	0.01	0.01	0.97	0.05	1.54	5.63	0.01	0.08	50.22
*56-1 644-6d	Uran	0.91	82.30	0.0	0.06	0.29	6.88	3.58	0.05	0.19	0.10	94.36
*56-1 644-e	Uran	0.25	78.80	0.05	0.03	0.22	13.82	2.28	0.06	0.22	0.09	95.81
*56-1 644-6f	Uran	0.28	79.51	0.10	0.08	0.39	12.70	2.27	0.02	0.19	0.02	95.56
*56-1 644-6g	Uran	0.40	81.02	0.03	0.16	0.42	11.78	2.36	0.02	0.14	0.14	96.46
*56-1 644-6h	Uran	0.59	79.40	0.03	0.23	0.52	9.32	2.79	0.04	0.15	0.08	93.14
*56-1 644-7a	Uran	0.33	79.50	0.18	0.17	0.46	11.61	2.28	0.04	0.12	0.0	94.69
*56-1 644-7b	Uran	0.14	80.09	0.05	0.12	0.26	13.82	1.44	0.03	0.12	0.0	96.06
*56-1 644-7c	Uran	0.33	79.30	0.10	0.05	0.54	12.04	2.16	0.04	0.15	0.0	94.71
*56-1 644-7d	Alt. Uran	10.16	64.77	0.02	0.01	0.0	2.85	5.70	1.55	0.33	0.0	85.39
*56-1 644-7e	Uran	0.16	79.51	0.03	0307	0.26	12.97	2.52	0.01	0.18	0.0	95.69
*56-1 644-7f	Uran	0.35	79.17	0.04	0.34	0.47	12.19	2.01	0.03	0.15	0.04	94.78
*56-1 644-8a	Uran	0.20	80.53	0.02	0.06	0.16	11.49	2.70	0.01	0.22	0.03	95.40
*56-1 644-8b	Uran	0.13	79.43	0.04	0.25	0.21	15.38	1.05	0.0	0.10	0.0	96.58
*56-1 644-8c	Alt. Uran	5.11	65.30	0.01	0.97	0.03	4.65	5.72	0.03	0.36	0.0	82.19
*56-1 644-8d	Uran	0.23	78.76	0.01	0.01	0.17	13.17	2.36	0.04	0.25	0.06	95.06
*56-1 644-9a	Uran	0.11	82.19	0.0	0.0	0.10	10.32	3.03	0.0	0.20	0.0	95.96
*56-1 644-9b	Alt. Uran	4.78	70.29	0.01	0.83	0.0	3.95	6.45	0.29	0.41	0.09	87.10
*56-1 644-9c	Uran	0.21	83.86	0.01	0.05	0.31	7.81	3.22	0.02	0.24	0.0	95.09
*56-1 644-9d	Uran	0.02	82.97	0.0	0.03	0.15	8.42	3.41	0.01	0.26	0.0	95.27
*56-1 644-9e	Uran	0.12	81.10	0.06	0.0	0.03	12.17	2.48	0.04	0.27	0.0	96.27
*56-1 644-9f	Uran	0.17	79.92	1.07	0.02	0.20	13.92	2.84	0.06	0.26	0.11	98.57
*56-1 644-9g	Coff	17.80	62.38	0.01	0.02	0.0	0.43	2.27	0.86	0.10	0.0	83.85
*56-1 644-10a	Uran	0.11	84.18	0.0	0.09	0.26	7.55	3.37	0.02	0.31	0.03	95.90
*56-1 644-10b	Uran	0.35	80.15	0.10	0.11	0.45	11.65	2.20	0.0	0.12	0.0	95.13
*56-1 644-10c	Uran	0.13	84.00	0.0	0.0	0.21	6.55	0.17	0.04	0.0	0.08	91.19
*56-1 644-10d	Uran	0.27	78.75	0.05	0.13	0.38	12.66	2.22	0.09	0.19	0.07	94.81
*56-1 644-10e	Uran	0.22	79.00	0.04	0.25	0.35	14.41	1.36	0.02	0.12	0.0	95.77

Note: all values are reported in wt%. Abbreviations: **Uran**: uraninite, **Coff**: coffinite, **DDH**: diamond drill hole. *Cree Extension Project (CX). Depths are in meters.

TABLE 2. MINEROLOGY AND CHEMICAL COMPOSITION OF SILICATE MINERALS FROM UNMINERALIZED DRILL CORE

Sample No. (DDH/depth)	Remarks	Na_2O	Al_2O_3	SiO_2	F	MgO	K_2O	CaO	FeO	TiO_2	Cr_2O_3	Cl	MnO	Total
*58 686-1a	Bt	0.0	18.60	26.35	0.03	12.99	0.03	0.02	29.84	0.13	0.0	0.01	0.17	88.18
*58 686-1b	Alt. Bt	0.09	28.47	48.33	0.60	4.74	8.31	0.06	3.43	0.01	0.0	0.03	0.0	94.06
*58 686-1c	Fsp	0.39	18.30	64.05	0.26	0.0	16.27	0.02	0.04	0.0	0.0	0.01	0.0	99.34
*58 686-2a	Bt	0.02	16.72	24.11	0.04	12.16	0.02	0.04	22.15	0.07	0.0	0.01	0.16	75.15
*58 686-2b	Fsp	1.17	16.69	57.78	0.0	0.01	12.36	0.05	0.03	0.0	0.0	0.01	0.0	88.09
*58 686-2c	Dol	0.0	0.22	0.73	0.01	17.70	0.17	23.48	3.25	0.0	0.0	0.01	0.11	45.69
*58 686-3a	Bt	0.06	18.51	26.50	0.0	13.35	0.02	0.03	29.37	0.09	0.0	0.02	0.20	88.16
*58 686-4a	Bt	0.0	18.81	26.21	0.38	13.03	0.05	0.04	29.49	0.15	0.02	0.02	0.17	88.38
*58 686-4b	Alt. Bt	0.11	27.61	53.08	0.66	3.79	8.55	0.16	0.96	0.02	0.02	0.07	0.0	95.03
*58 686-4c	Fsp	0.77	18.06	63.97	0.0	0.01	15.76	0.06	0.05	0.0	0.01	0.02	0.0	98.72
*58 657-1a	Bt	0.09	14.80	35.82	0.41	12.24	5.98	0.01	19.35	3.16	0.0	0.05	0.13	95.63
*58 657-1b	Fsp	6.33	27.29	56.70	0.16	0.0	0.30	9.44	0.03	0.0	0.0	0.01	0.01	100.27
*58 657-2a	Bt	0.10	14.72	36.23	1.15	12.84	9.39	0.01	18.39	3.25	0.06	0.05	0.10	96.28
*58 657-2b	Fsp	6.37	27.53	56.25	0.0	0.01	0.21	9.54	0.05	0.01	0.0	0.0	0.0	99.97
*58 657-3a	Bt	0.03	14.92	36.37	0.22	12.20	9.57	0.01	19.62	2.81	0.06	0.04	0.09	95.94
*58 657-3b	Fsp	5.88	27.95	55.26	0.65	0.12	0.54	9.56	0.20	0.01	0.0	0.0	0.0	100.18
*58 657-3c	Bt	0.02	15.22	29.59	0.49	15.42	0.07	0.11	26.80	0.01	0.0	0.02	0.27	88.01
*58 657-4a	Bt	0.06	5.15	6.80	0.49	6.45	2.99	0.0	9.27	0.48	0.0	0.02	0.05	31.76
*58 657-4b	Fsp	1.95	6.96	7.86	0.09	2.26	0.56	2.05	0.69	0.0	0.02	0.0	0.01	22.46
*58 700-1a	Fsp	1.98	9.56	12.42	0.87	0.43	2.78	1.61	0.88	0.01	0.02	0.05	0.0	30.62
*58 700-1b	Bt	0.48	2.21	11.33	0.23	7.64	0.03	3.77	11.50	0.16	0.27	0.0	0.23	37.86
*58 700-2a	Bt	0.01	19.84	26.60	0.07	16.04	0.01	0.01	25.29	0.03	0.01	0.05	0.35	88.29
*58 700-2b	Fsp	6.91	27.13	56.44	0.12	0.02	0.13	8.88	0.13	0.0	0.0	0.01	0.0	99.78
*58 700-3a	Bt	0.01	18.98	27.01	0.42	16.97	0.02	0.04	24.36	0.05	0.26	0.03	0.31	88.45
*58 700-3b	Dol	0.01	0.10	0.58	0.80	15.77	0.0	28.83	7.83	0.0	0.02	0.04	0.0	55.08
*58 646-1a	Amph	0.89	3.72	8.99	0.20	4.50	0.47	3.43	15.82	0.54	0.04	0.04	0.15	38.78
*58 646-1b	Fsp	3.40	10.18	11.82	0.0	0.0	0.08	3.33	0.07	0.0	0.02	0.01	0.0	28.90

*58 646-2a	Amph	0.97	4.0	9.50	0.35	4.63	0.51	3.61	16.06	0.61	0.04	0.04	0.16	40.48
*58 646-2b	Fsp	3.26	9.99	11.67	0.0	0.08	0.07	3.38	0.30	0.01	0.0	0.0	0.0	28.77
*58 646-2c	Bt	0.0	6.12	5.91	0.14	8.63	0.11	0.01	21.05	0.05	0.0	0.0	0.17	42.20
*58 646-3a	Amph	1.33	10.09	42.84	0.13	8.59	1.07	11.07	20.47	2.02	0.03	0.04	0.17	97.84
*58 646-3b	Fsp	5.57	27.25	54.33	0.06	0.64	0.29	10.03	1.17	0.01	0.02	0.0	0.0	99.38

Note: all values are reported in wt%. Abbreviations: **Bt**: biotite, **Fsp**: feldspar, **Amph**: Amphibolite; **Dol:** dolomite **DDH**: diamond drill hole. *Cree Extension Project (CX). Depths are in meters.

TABLE 3. MINERALOGICAL AND CHEMICAL COMPOSITION OF SILICATE MINERALS FROM MINERALIZED DRILL CORE

Sample No. (DDH/depth)	Remarks	Na_2O	Al_2O_3	SiO_2	F	MgO	K_2O	CaO	FeO	TiO_2	Cr_2O_3	Cl	MnO	Total
*56-1 644-3	Bt	0.09	22.67	47.75	0.38	12.65	1.89	0.78	0.10	0.0	0.02	0.01	0.05	86.37
*56-1 644-3a	Cal	0.05	0.0	0.0	0.27	1.58	0.0	55.72	0	0.01	0.0	0.0	0.02	57.66
*56-1 644-3b	Cal	0.04	0.21	0.67	0.0	1.90	0.08	55.83	0.03	0.01	0.03	0.0	0.03	58.82
*56-1 644-3c	Bt	0.22	26.17	47.60	1.18	3.81	5.56	0.67	1.63	0.03	0.0	0.02	0.04	86.91
*47-2 708-1	Bt	0.18	31.05	43.87	0.20	5.63	4.88	0.42	2.36	0.01	0.01	0.17	0.04	88.83
*47-2 708-1a	Bt	0.22	29.61	46.86	1.08	2.73	7.41	0.43	2.51	0.0	0.03	0.20	0.0	91.09
*47-2 708-3	Bt	0.19	26.19	47.70	0.33	4.12	5.16	0.75	5.59	0.0	0.03	0.14	0.02	90.22
*47-2 708-10a	Qtz	0.0	0.0	98.91	0.0	0.0	0.01	0.0	0.0	0.0	0.02	0.0	0.0	98.94
*47-2 708-10b	Bt	0.19	25.08	48.31	0.18	3.47	5.76	0.56	6.63	0.0	0.02	0.05	0.0	90.26
*47-1 758-1a	Bt	0.08	34.95	40.21	0.68	9.92	2.37	0.30	0.97	0.0	0.06	0.09	0.0	89.62
*47-1 758-1b	Bt	0.13	31.70	42.83	0.27	7.63	3.45	0.45	1.75	0.0	0.15	0.12	0.0	88.48
*47-1 758-1c	Bt	0.15	21.68	35.01	0.17	3.23	4.45	0.35	1.18	0.0	0.04	0.28	0.0	66.54
*47-1 758-2b	Bt	0.04	30.91	34.30	0.30	15.55	0.15	0.16	4.88	0.01	0.05	0.07	0.0	86.42
*47-1 758-2c	Bt	0.10	32.24	42.76	0.30	7.69	3.27	0.45	1.64	0.02	0.10	0.12	0.0	88.68
*47-1 758-2d	Bt	0.12	33.00	44.79	0.61	7.57	3.28	0.51	1.72	0.0	0.14	0.15	0.01	91.87
*47-1 758-4a	Bt	0.03	32.72	35.92	0.66	13.55	0.53	0.22	3.97	0.01	0.03	0.13	0.0	87.76
*47-1 758-4b	Bt	0.14	28.70	44.15	0.05	7.38	3.88	0.82	3.75	0.04	0.01	0.50	0.01	89.44
*56-1 663-1a	Bt	0.20	22.71	41.53	0.23	4.50	6.24	0.31	11.26	0.0	0.02	0.04	0.04	87.09
*56-1 663-1b	Bt	0.27	27.36	45.30	0.12	2.56	7.77	0.22	4.75	0.0	0.06	0.04	0.01	88.46
*56-1 663-2a	Bt	0.15	22.37	44.52	0.12	4.32	6.49	0.38	9.64	0.01	0.01	0.01	0.01	88.02
*56-1 663-2b	Bt	0.15	5.53	30.06	0.05	8.05	0.94	5.77	3.86	0.84	0.07	0.19	0.02	55.52
*56-1 682-5a	Hem	0.10	15.11	17.03	0.0	0.72	0.91	0.22	46.69	0.14	0.01	0.07	0.02	81.00

Note: all values are reported in wt%. Abbreviations: **Bt**: biotite, **Qtz**: quartz, **Hem**: hematite, **Cal:** calcite **DDH**: diamond drill hole.
*Cree Extension Project (CX). Depths are in meters.

TABLE 4. $\delta^{18}O$ VALUES FOR QUARTZ AND URANINITE

Sample No. (DDH/depth)	Remarks	Mineral	$\delta^{18}O_{V\text{-}SMOW}$
CX-56-1 644.5_1sp1	VN	Uran.	-23.0
CX-56-1 644.5_1sp1	VN	Uran.	-21.9
CX-56-1 644.5_3sp1	VN	Uran.	-18.7
CX-56-1 644.5_3sp2	VN	Uran.	-18.5
CX-56-1 644.5_3sp3	VN	Uran.	-21.7
CX-56-1 663.4_8sp1	MR	Uran.	-19.3
CX-56-1 663.4_8sp2	MR	Uran.	-15.7
CX-56-1 663.4_8sp3	MR	Uran.	-20.0
CX-56-1 663.4_8sp4	MR	Uran.	-25.5
CX-56-1 663.4_8sp5	MR	Uran.	-27.4
CX-56-1 663.4_4sp1	MR	Uran.	-22.6
CX-56-1 663.4_4sp2	MR	Uran.	-22.7
CX-56-1 663.4_4sp3	MR	Uran.	-19.4
CX-56-1 663.4_10sp1	MR	Uran.	-21.7
CX-56-1 663.4_10sp2	MR	Uran.	-25.9
CX-56-1 663.4_10sp3	MR	Uran.	-14.5
CX-56-1 663.4_1sp1	MR	Uran.	-24.8
CX-56-1 663.4_1sp2	MR	Uran.	-23.7
CX-56-1 663.4_1sp3	MR	Uran.	-25.4
CX-56-1 644.5_1sp1	SD.	Qtz	18.1
CX-56-1 644.5_1sp2	SD.	Qtz	16.2
CX-56-1 644.5_1sp3	SD.	Qtz	18.1
CX-56-1 644.5_1sp4	SD.	Qtz	18.3
CX-56-1 644.5_1sp5	SD.	Qtz	18.5
CX-56-1 644.5_1sp6	SD.	Qtz	18.9
CX-56-1 644.5_1sp7	SD.	Qtz	17.8
CX-56-1 644.5_1sp8	SD.	Qtz	18.1
CX-56-1 644.5_1sp1	SD.	Qtz	19.1

Note: DDH- Diamond Drill Hole. Depths are in Meters. Abbreviations: MR-massive replacement, VN- vein type, SD- secondary euhedral quartz, Uran-uraninite.

TABLE 5. Fe SPECIES BY MÖSSBAUER SPECTROSCOPY

Rock Type	Sample Depth (m)	Fe^{2+}%	Fe^{3+}%	Fe^{3+}% hematite	Fe(0)	Fe total	Fe^{2+}/ Fe^{3+}
	CX-44-1						
PELT	604.70	7.43	17.58	75.00	0.00	100.01	0.42
SMPL	623.20	7.90	16.60	43.80	31.80	100.10	0.48
SMPL	689.50	0.00	6.60	93.40	0.00	100.00	0.00
	CX-56-1						
PELT (PLO WTHR)	591.20	17.50	23.90	0.00	58.60	100.00	0.73
SMPL	612.00	22.10	18.30	0.00	59.60	100.00	1.21
PELT (HEM. CAP)	683.20	0.00	5.01	89.20	5.80	100.01	0.00
PEGM (HEM)	690.50	11.30	7.10	81.60	0.00	100.00	1.59
	CX-58						
PEGM (HEM)	546.60	0.00	6.00	88.86	5.14	100.00	0.00
GPELT	560.70	43.00	24.00	0.00	32.90	99.90	1.79
CSMPL	606.00	87.00	13.00	0.00	0.00	100.00	6.69
MARKER	625.60	73.37	26.63	0.00	0.00	100.00	2.76
PEGM/PELT	636.00	72.70	27.30	0.00	0.00	100.00	2.66
PELT	646.50	83.44	16.56	0.00	0.00	100.00	5.04
PELT (W/ VNS)	652.00	81.00	7.40	0.00	10.60	99.00	10.95
PELT	657.00	86.70	13.30	0.00	0.00	100.00	6.52
UP CALC	700.70	87.50	12.50	0.00	0.00	100.00	7.00
BRACKETED UNIT	707.50	86.20	13.80	0.00	0.00	100.00	6.25
LOW CALC	724.00	83.70	16.30	0.00	0.00	100.00	5.13
CPELT	735.00	84.34	15.66	0.00	0.00	100.00	5.39
PELT/PEGM	765.70	79.30	20.70	0.00	0.00	100.00	3.83

Notes: Abbreviations: PELT- pelite, SMPL- semipelite, PEGM- pegmatite, CSMPL- calc-semipelite, GPELT- graphitic pelite, CPELT- calc-pelite, CALC- calc-silicate, VNS- veins, HEM- hematite, PLO WTHR- paleo-weathering.

TABLE 6. IRON SPECIATION BY WHOLE-ROCK GEOCHEMISTRY AND MÖSSBAUER SPECTROSCOPY

Analysis Method		Whole-Rock mol % Fe					Whole-Rock Normalized			Mossbauer			
Rock Type	**Drill hole**	FeO	Fe_2O_3	**Fe^{2+}**	**Fe^{3+}**	**Fe^{2+}/Fe^{3+}**	**Fe^{2+}**	**Fe^{3+}**	**Fe^{2+}/Fe^{3+}**	**Fe^{2+}**	**Fe^{3+}**	**Fe^{3+} total**	**Fe^{2+}/Fe^{3+}**
	CX-44-1												
PELT	604.7		6.24							7.43	17.58	92.58	0.42
SMPL	623.2		6.08							7.9	16.6	60.4	0.48
MARKER	651	2.5	2.96	1.75	2.07	0.84	45.79	54.21	0.84				
PELT	680.4		4										
SMPL	689.5		4.26							0.0	6.6	100.0	0.00
CPELT	722.9		3.43										
CSMPL	773.5	0.16	0.67	0.11	0.47	0.24	19.28	80.72	0.24				
SIL. BRC	795.4	4.35	2.41	3.04	1.69	1.80	64.35	35.65	1.80				
GRAN	822.6	1.12	1.24	0.78	0.87	0.90	47.46	52.54	0.90				
	CX-56-1												
PELT	591.2		3.71							17.5	23.9	23.9	0.73
PEGM	602	0.47	0.69	0.33	0.48	0.68	40.52	59.48	0.68				
SMPL	612		3.66							22.1	18.3	18.3	1.21
PELT	628.5	0.66	0.69	0.46	0.48	0.96	48.89	51.11	0.96				
PEGM	639.6	3.62	1.87	2.53	1.31	1.94	65.94	34.06	1.94				
CSMPL	659.4	0.42	0.9	0.29	0.63	0.47	31.82	68.18	0.47				
PELT	683.2		15.04							0	5.01	94.21	0.00
PEGM	690.5		5.5							11.3	7.1	88.7	1.59
SIL. BRC	716.3	2.65	1.38	1.85	0.97	1.92	65.76	34.24	1.92				
	CX-58												
PELT	546.4	0.8	2.42	0.56	1.69	0.33	24.84	75.16	0.33				
PEGM	546.6		4.5							0.0	6.0	94.9	0.00
PELT	552	2.14	9.1	1.50	6.37	0.24	19.04	80.96	0.24				
GPELT	560.7		3.4							43.0	24.0	24.0	1.79
PELT	586	2.16	2.97	1.51	2.08	0.73	42.11	57.89	0.73				
GSMPL	595.4	4.43	3.45	3.10	2.41	1.28	56.22	43.78	1.28				
PEGM	603.7	2.31	2.08	1.62	1.45	1.11	52.62	47.38	1.11				
CSMPL	606		10.3							87	13	13	6.69
MARKER	625.6	6.4	6.97	4.48	4.88	0.92	47.87	52.13	0.92	73.37	26.63	26.63	2.76
PEGM	636	5.66	5.29	3.96	3.70	1.07	51.69	48.31	1.07	72.7	27.3	27.3	2.66
PELT	646.5		12.69							83.44	16.56	16.56	5.04

PELT	652		3.58							81.0	7.4	7.4	10.95
PELT	657		4.98							86.7	13.3	13.3	6.52
PEGM	686	4.39	2.64	3.07	1.85	1.66	62.45	37.55	1.66				
CPELT	700.7		9.37							87.5	12.5	12.5	7.00
AMPH	707.5		12.36							86.2	13.8	13.8	6.25
AMPH	724		11.6							83.7	16.3	16.3	5.13
CPELT	735		11.88							84.34	15.66	15.66	5.39
PEGM	760.6	0.6	0.48	0.42	0.34	1.25	55.56	44.44	1.25				
PELT	765.7		4.89							79.3	20.7	20.7	3.83
PEGM	781.7	0.71	0.52	0.50	0.36	1.37	57.72	42.28	1.37				
GRAN	797.1	3.42	2.7	2.39	1.89	1.27	55.88	44.12	1.27				
GRAN	829	1.32	1.42	0.92	0.99	0.93	48.18	51.82	0.93				

Notes: Abbreviations: PELT- pelite, SMPL- semipelite, PEGM- pegmatite, CSMPL- calc-semipelite, GPELT- graphitic pelite, CPELT- calc-pelite, CALC- calc-silicate, AMPH- amphibole, GRAN- granite, SIL BRC- resilicified breccia.

TABLE 7. RADIOGENIC ISOTOPE FROM THE BASEMENT HOSTED MILLENNIUM DEPOSIT, ATHABASCA BASIN, SASKATCHEWAN, CANADA

SAMPLE	$^{206}Pb/^{204}Pb$	±%	$^{207}Pb/^{204}Pb$	±%	$^{207}Pb/^{206}Pb$	±%	$^{208}Pb/^{204}Pb$	±%	$^{235}U/^{238}U$	±%	$^{206}Pb/^{238}U$	±%	$^{207}Pb/^{235}U$	±%	$^{238}U^{16}O/^{238}U$	±%	$^{238}U/^{238}U+^{1}H$	±%
MR-1 sp1	3.02E+04	0.00	2.44E+03	0.00	8.07E-02	0.00	6.00E+00	0.00	7.56E-03	1.20	3.26E-01	0.30	3.47E+00	1.50	2.78E+00	0.04	1.66E+02	1.30
MR-1 sp2	2.04E+04	1.20	1.56E+03	2.70	7.53E-02	0.01	2.50E+00	60.00	7.55E-03	0.50	2.11E-01	0.50	2.09E+00	0.40	2.67E+00	0.20	1.64E+02	2.10
MR-1 sp3	3.22E+04	2.80	2.73E+03	2.10	8.48E-02	0.07	6.50E+00	7.70	7.93E-03	2.00	3.45E-01	4.00	3.66E+00	1.10	2.72E+00	0.20	1.95E+02	0.20
MR-1 sp4	2.28E+04	0.70	1.71E+03	2.40	7.49E-02	0.30	7.00E+00	0.00	7.65E-03	1.30	2.31E-01	0.60	2.26E+00	1.30	2.73E+00	0.04	1.92E+02	1.20
MR-1 sp5	3.02E+04	0.00	2.50E+03	0.00	8.63E-02	0.50	6.00E+00	0.00	7.47E-03	0.70	3.11E-01	0.80	3.59E+00	0.40	2.71E+00	0.07	1.96E+02	0.10
MR-1 sp6	2.93E+04	1.10	2.34E+03	1.30	8.13E-02	0.20	7.50E+00	6.70	7.51E-03	2.70	3.17E-01	1.70	3.44E+00	1.20	2.73E+00	0.50	1.60E+02	0.80
MR-1 sp7	3.02E+04	0.00	2.55E+03	0.00	8.51E-02	0.50	5.00E+00	0.00	7.78E-03	0.40	3.12E-01	1.50	3.43E+00	0.90	2.71E+00	0.40	1.69E+02	1.60
MR-1 sp8	3.10E+04	0.10	2.68E+03	3.40	8.58E-02	0.40	6.00E+00	16.70	7.76E-03	0.70	3.33E-01	0.30	3.72E+00	2.00	2.66E+00	0.04	1.67E+02	1.20
MR-1 sp9	2.43E+04	8.60	2.11E+03	9.20	8.65E-02	0.50	3.92E+00	41.40	7.62E-03	0.20	2.87E-01	0.30	3.27E+00	0.60	2.70E+00	0.10	1.62E+02	0.20
MR-1 sp10	3.28E+04	1.70	2.83E+03	0.50	8.70E-02	0.20	5.75E+00	47.80	7.66E-03	0.50	3.36E-01	0.30	3.82E+00	0.10	2.67E+00	0.50	1.75E+02	1.40
MR-1 sp11	n/a	n/a	n/a	n/a	8.81E-02	0.50	n/a	n/a	7.65E-03	0.40	3.54E-01	0.60	4.11E+00	1.20	2.82E+00	0.10	1.44E+02	1.60
MR-1 sp12	n/a	n/a	n/a	n/a	7.82E-02	0.30	n/a	n/a	7.70E-03	1.10	2.12E-01	0.10	2.17E+00	0.80	2.78E+00	0.40	1.51E+02	0.10
MR-1 sp13	3.00E+04	1.50	2.41E+03	0.30	7.92E-02	0.10	8.00E+00	0.00	7.93E-03	1.90	3.34E-01	3.00	3.36E+00	0.90	2.77E+00	0.40	1.49E+02	0.70
MR-1 sp14	2.65E+04	0.20	2.16E+03	0.10	8.34E-02	1.00	5.50E+00	45.50	7.59E-03	0.50	2.89E-01	2.10	3.15E+00	2.10	2.74E+00	0.40	1.67E+02	1.40
MR-1 sp15	2.29E+04	0.00	2.07E+03	0.00	8.61E-02	0.60	3.00E+00	0.00	7.47E-03	0.10	3.24E-01	0.60	3.74E+00	0.40	2.75E+00	0.02	1.63E+02	0.50
BA-1 sp1	1.69E+03	0.60	1.57E+02	0.60	9.28E-02	0.10	5.69E+01	0.40	n/a	n/a	2.05E+01	33.20	1.86E+03	1.50	2.41E+00	0.70	2.81E+02	47.10
BA-1 sp2	1.54E+03	6.00	1.35E+02	6.70	8.80E-02	0.40	4.91E+01	6.30	n/a	n/a	1.25E+02	4.30	n/a	n/a	1.23E+00	5.90	4.20E+01	2.30
BA-1 sp3	2.60E+02	0.00	1.90E+01	0.00	8.35E-02	4.30	1.00E+01	0.00	7.58E-03	0.70	2.84E-03	2.50	3.13E-02	2.70	2.20E+00	0.70	5.09E+02	1.80
BA-1 sp4	8.00E+00	0.00	n/a	n/a	9.27E-02	9.80	2.00E+00	0.00	7.65E-03	1.10	1.25E-04	7.70	1.47E-03	34.30	2.25E+00	0.10	5.05E+02	2.50
BA-1 sp5	9.50E+00	5.30	1.50E+00	33.30	9.66E-02	19.80	1.00E+00	0.00	7.76E-03	1.10	1.34E-04	0.80	1.87E-03	25.60	2.13E+00	0.40	5.27E+02	5.50
BA-1 sp6	n/a	n/a	n/a	n/a	1.02E-01	10.60	n/a	n/a	7.51E-03	0.10	3.13E-04	4.90	4.53E-03	11.00	2.07E+00	0.70	6.19E+02	5.20
BA-1 sp7	n/a	n/a	n/a	n/a	1.02E-01	6.10	n/a	n/a	7.46E-03	0.90	9.81E-04	0.30	1.38E-02	11.40	2.07E+00	0.50	6.96E+02	2.20
BA-1 sp8	4.20E+01	0.00	3.00E+00	0.00	9.69E-02	7.10	2.00E+00	0.00	7.56E-03	1.10	4.87E-04	8.00	6.44E-03	4.70	1.88E+00	0.20	8.28E+02	0.10
BA-1 sp9	1.17E+03	3.00	1.03E+02	0.90	8.54E-02	0.80	3.83E+01	6.00	7.74E-03	0.60	1.94E-02	2.10	2.15E-01	2.60	1.99E+00	0.40	7.15E+02	1.40
BA-1 sp10	1.78E+02	0.00	2.30E+01	0.00	9.53E-02	3.90	1.15E+01	0.00	7.64E-03	1.40	1.48E-03	2.10	1.86E-02	1.60	2.13E+00	0.70	8.16E+02	2.00
BA-2 sp1	5.30E+01	0.90	6.75E+00	40.70	8.97E-02	13.80	3.00E+00	16.60	7.63E-03	1.30	7.57E-04	3.10	8.94E-03	15.30	2.06E+00	0.80	6.60E+02	2.70
BA-2 sp2	6.80E+01	0.00	7.00E+00	0.00	9.28E-02	8.50	3.00E+00	0.00	7.70E-03	0.20	1.34E-03	5.80	1.58E-02	1.30	1.95E+00	0.60	9.28E+02	0.05
BA-2 sp3	n/a	n/a	n/a	n/a	8.25E-02	11.40	n/a	n/a	7.39E-03	0.60	1.38E-03	10.20	1.60E-02	7.90	1.79E+00	0.40	1.14E+03	4.80
BA-2 sp4	4.33E+01	0.00	5.00E+00	0.00	1.07E-01	2.30	2.25E+00	0.00	7.66E-03	1.70	1.03E-03	5.90	1.43E-02	7.10	1.80E+00	0.10	1.14E+00	2.70
BA-2 sp5	1.79E+03	1.00	1.52E+02	2.40	8.46E-02	1.10	5.51E+01	2.30	n/a	n/a	5.03E+02	3.70	1.09E+03	4.50	5.84E-01	13.00	1.35E+01	25.80
BA-2 sp6	1.64E+03	3.60	1.44E+02	3.40	8.77E-02	0.20	5.21E+01	3.40	n/a	n/a	4.60E+02	2.60	1.68E+03	0.00	2.79E-01	11.80	1.68E+01	27.10
BA-2 sp7	1.82E+03	0.60	1.61E+02	1.60	8.85E-02	0.80	5.69E+01	2.10	n/a	n/a	5.30E+02	1.00	1.64E+03	0.00	3.53E-01	12.20	1.02E+01	19.10
BA-2 sp8	1.77E+03	7.50	1.57E+02	6.90	8.83E-02	0.03	5.71E+01	7.00	n/a	n/a	2.64E+02	11.40	1.40E+03	0.00	6.82E-01	9.60	1.86E+01	16.20
BA-2 sp9	n/a	n/a	n/a	n/a	2.56E-02	22.00	n/a	n/a	7.74E-03	0.80	7.83E-04	1.60	2.57E-03	24.00	1.84E+00	0.40	9.43E+02	0.60
BA-2 sp10	6.51E+01	29.00	3.88E+00	67.70	5.03E-02	7.30	3.63E+00	38.00	7.64E-03	0.40	8.96E-04	11.30	6.06E-03	2.90	1.63E+00	0.40	9.47E+02	2.00
BA-2 sp11	n/a	n/a	n/a	n/a	5.91E-02	6.90	n/a	n/a	7.69E-03	0.40	1.77E-03	2.20	1.35E-02	9.30	1.63E+00	0.30	1.25E+03	2.70
BA-2 sp12	1.39E+02	3.40	9.25E+00	24.30	5.48E-02	11.00	2.50E+00	60.00	7.56E-03	0.80	1.49E-03	1.40	1.07E-02	9.60	1.70E+00	0.40	1.06E+03	0.50
BA-2 sp13	5.00E+01	0.00	4.00E+00	0.00	4.70E-02	7.60	3.00E+00	0.00	7.53E-03	0.90	4.70E-04	3.50	3.13E-03	1.30	1.99E+00	0.20	1.05E+03	0.30
BA-2 sp14	5.95E+02	5.38	4.93E+01	0.50	8.00E-02	0.40	1.75E+01	8.60	7.72E-03	0.70	5.81E-03	1.40	5.97E-02	2.60	2.08E+00	0.90	7.37E+02	0.30
VN- 1 sp1	2.43E+04	0.00	1.90E+03	0.00	7.89E-02	0.40	5.00E+00	0.00	7.54E-03	0.80	2.25E-01	1.00	2.34E+00	2.50	2.58E+01	0.50	6.91E+01	0.30
VN- 1 sp2	2.01E+04	0.40	1.49E+03	2.00	7.25E-02	0.04	4.50E+00	11.10	7.65E-03	0.30	1.94E-01	0.40	1.85E+00	0.03	2.55E+00	0.60	8.43E+01	0.06
VN- 1 sp3	n/a	n/a	n/a	n/a	8.58E-02	0.60	n/a	n/a	7.62E-03	0.80	2.43E-01	0.30	2.75E+00	0.60	2.59E+00	0.10	9.96E+01	0.10
VN- 1 sp4	2.96E+04	1.50	2.56E+03	1.30	8.70E-02	0.01	1.50E+00	33.30	7.64E-03	1.70	2.86E-01	0.30	3.29E+00	0.70	2.57E+00	0.20	1.09E+02	0.80
VN- 1 sp5	2.37E+04	1.10	2.06E+03	3.50	8.80E-02	1.70	2.50E+00	20.00	7.56E-03	0.10	2.25E-01	1.90	2.59E+00	1.10	2.39E+00	0.30	1.17E+02	1.50
VN- 1 sp6	2.44E+04	1.30	1.88E+03	0.70	7.69E-02	1.00	4.50E+00	33.30	7.70E-03	1.90	2.19E-01	0.90	2.21E+00	0.50	2.48E+00	0.20	1.31E+02	0.20
VN- 1 sp7	2.70E+04	0.00	2.30E+03	0.00	8.26E-02	0.40	3.00E+00	0.00	7.62E-03	0.01	2.34E-01	0.20	2.58E+00	0.90	2.58E+00	0.20	1.39E+02	3.70
VN- 1 sp8	2.61E+04	0.00	2.02E+03	0.00	7.95E-02	0.50	1.00E+00	0.00	7.61E-03	0.08	2.54E-01	0.20	2.67E+00	0.60	2.62E+00	0.03	1.36E+02	0.30
VN- 1 sp9	2.29E+04	0.00	1.87E+03	0.00	8.24E-02	0.20	4.00E+00	0.00	7.47E-03	0.20	2.25E-01	0.08	2.49E+00	0.40	2.53E+00	0.20	1.39E+02	1.20
VN- 1 sp10	2.15E+04	0.10	1.75E+03	4.00	8.09E-02	0.08	1.25E+00	20.00	7.60E-03	1.10	2.10E-01	0.10	2.24E+00	1.60	2.48E+00	0.07	1.50E+02	2.30
VN- 1 sp11	2.26E+04	3.40	1.81E+03	1.40	7.99E-02	0.90	3.50E+00	14.30	7.70E-03	0.20	2.23E-01	0.70	2.30E+00	0.90	2.52E+00	0.20	1.54E+02	1.10
VN- 1 sp12	2.30E+04	0.00	1.90E+03	0.00	8.30E-02	0.20	3.00E+00	0.00	7.44E-03	1.80	2.55E-01	0.10	2.83E+00	1.10	2.56E+00	0.20	3.12E+02	2.10
VN- 1 sp13	2.12E+04	0.00	1.67E+03	0.00	7.87E-02	0.10	6.00E+00	0.00	7.47E-03	1.30	2.29E-01	1.50	2.42E+00	0.30	2.45E+00	0.30	4.09E+02	3.00
VN- 1 sp14	n/a	n/a	n/a	n/a	7.55E-02	0.20	n/a	n/a	7.64E-03	0.80	2.14E-01	2.10	2.13E+00	2.00	2.38E+00	0.60	5.34E+02	2.50
VN- 1 sp15	1.53E+04	0.80	1.19E+03	2.80	8.00E-02	1.50	1.50E+00	33.30	7.72E-03	1.60	2.05E-01	1.70	2.13E+00	1.60	2.40E+00	0.10	5.16E+02	0.30
VN- 1 sp16	1.57E+04	0.00	1.25E+03	0.00	8.10E-02	0.90	1.00E+00	0.00	7.68E-03	1.20	1.66E-01	0.60	1.75E+00	0.10	2.33E+00	0.06	5.85E+02	1.20

VN- 1 sp17	1.95E+04	0.60	1.59E+03	1.20	8.07E-02	0.80	2.50E+00	2.00	7.64E-03	0.40	2.05E-01	0.30	2.18E+00	0.70	2.41E+00	0.10	7.95E+02	2.00
VN- 1 sp18	n/a	n/a	n/a	n/a	8.15E-02	1.20	n/a	n/a	7.65E+03	1.30	1.43E-01	0.70	1.51E+00	1.40	2.39E+00	0.10	8.95E+02	4.50
VN- 1 sp19	1.69E+04	0.00	1.32E+03	0.00	7.89E-02	0.01	3.33E-01	0.00	7.67E-03	0.10	1.88E-01	0.50	1.93E+00	0.60	2.36E+00	0.03	8.36E+02	4.70
VN- 1 sp20	1.57E+04	0.00	1.19E+03	0.00	7.55E-02	1.00	n/a	n/a	7.55E-03	0.80	1.65E-01	0.50	1.65E+00	2.10	2.33E+00	0.03	8.62E+02	1.00
VN- 1 sp21	n/a	n/a	n/a	n/a	8.32E-02	1.00	n/a	n/a	7.49E-03	2.40	1.76E-01	1.40	1.96E+00	0.30	2.31E+00	0.10	8.45E+02	1.30

Notes: Abbreviations: MR- Massive replacement mineralization CX-56-1 663 m, BA- Bleb-like aggregates CX-41-1 758 m, VN- Fracture filling vein mineralization CX-56-1 644 m, sp- spot#.

Table 8. CHEMICAL Pb and ISOTOPIC Pb-Pb AGES FROM THE MILLENNIUM DEPOSIT, ATHABASCA BASIN, SASKATCHEWAN, CANADA.

Isotopic Pb-Pb				Chemical Pb							
Spot #	**$^{207}Pb/^{206}Pb$**	**Age**	**± Ma**	**Spot #**	**Age**	**Spot #**	**Age**	**Spot #**	**Age**	**MR cont**	**Age**
MR.sp1	0.0881	1386	3.2	BA sp1	4.6	VN sp1	1048	MR sp1	1247	MR sp51	1285
MR.sp2	0.0782	1152	3.1	BA sp2	9.5	VN sp2	1232	MR sp2	1241	MR sp52	1281
MR.sp3	0.0792	1178	3.1	BA sp3	433.9	VN sp3	26	MR sp3	1291	MR sp53	532
MR.sp4	0.0834	1280	3.2	BA sp4	7.4	VN sp4	860	MR sp4	1307	MR sp54	1188
MR.sp5	0.0861	1342	3.2	BA sp5	15.1	VN sp5	343	MR sp5	1278	MR sp55	737
MR.sp6	0.0813	1230	3.1	BA sp6	46.8	VN sp6	918	MR sp6	693	MR sp56	1094
MR.sp7	0.0851	1318	3.2	BA sp7	73.1	VN sp7	1051	MR sp7	1141	MR sp57	1211
MR.sp8	0.0858	1334	3.2	BA sp8	88.5	VN sp8	998	MR sp8	1025	MR sp58	1158
MR.sp9	0.0865	1350	3.2	BA sp9	187.5	VN sp9	1020	MR sp9	1122	MR sp59	935
MR.sp10	0.0870	1362	3.2	BA sp10	18.0	VN sp10	750	MR sp10	1056	MR sp60	1415
MR.sp11	0.0807	1216	3.1	BA sp11	9.9	VN sp11	1124	MR sp11	1007	MR sp61	1140
MR.sp12	0.0753	1078	3.1	BA sp1	4.6	VN sp12	1045	MR sp12	1065	MR sp62	1111
MR.sp13	0.0848	1312	3.2	BA sp2	9.5	VN sp13	641	MR sp13	1176	MR sp63	1293
MR.sp14	0.0749	1066	3.1	BA sp3	433.9	VN sp14	1285	MR sp14	1216	MR sp64	1395
MR.sp15	0.0863	1346	3.2			VN sp15	1169	MR sp15	1010	MR sp65	1156
VN_sp1	0.0789	1170	3.1			VN sp16	1078	MR sp16	1094	MR sp66	1269
VN_sp2	0.0725	1000	3.1			VN sp17	1329	MR sp17	1264	MR sp67	1122
VN_sp3	0.0859	1336	3.2			VN sp18	1158	MR sp18	781	MR sp68	1132
VN_sp4	0.0873	1368	3.2			VN sp19	821	MR sp19	900	MR sp69	1099
VN_sp5	0.0878	1380	3.2			VN sp20	1302	MR sp20	1383	MR sp70	1264
VN_sp6	0.0772	1128	3.1			VN sp21	1259	MR sp21	1133	MR sp71	1002
VN_sp7	0.0824	1256	3.1			VN sp22	841	MR sp22	1388	MR sp72	1236
VN_sp8	0.0794	1184	3.1			VN sp23	1130	MR sp23	1117	MR sp73	1319
VN_sp9	0.0823	1254	3.1			VN sp24	468	MR sp24	970	MR sp74	1226
VN_sp10	0.0804	1208	3.1			VN sp25	598	MR sp25	1104	MR sp75	1082
VN_sp11	0.0799	1196	3.1			VN sp26	1196	MR sp26	1304	MR sp76	1059
VN_sp12	0.0830	1270	3.2			VN sp27	1098	MR sp27	1221	MR sp77	1362
VN_sp13	0.0787	1166	3.1			VN sp28	1007	MR sp28	1413		
VN_sp14	0.0755	1082	3.1			VN sp29	824	MR sp29	1184		
VN_sp15	0.0800	1198	3.1			VN sp30	1011	MR sp30	1406		
VN_sp16	0.0810	1222	3.1			VN sp31	1179	MR sp31	1056		

VN_sp17	0.0807	1216	3.1
VN_sp18	0.0815	1234	3.1
VN_sp19	0.0789	1170	3.1
VN_sp20	0.0755	1082	3.1
VN_sp21	0.0832	1274	3.2
BA2_sp1	0.0897	1420	3.2
BA2_sp2	0.0928	1484	3.2
BA2_sp3	0.0825	1258	3.1
BA2_sp4	0.1074	1755	3.3
BA2_sp5	0.0846	1308	3.2
BA2_sp6	0.0877	1376	3.2
BA2_sp7	0.0885	1394	3.2
BA2_sp8	0.0883	1390	3.2
BA2_sp9	0.0256	n/a	
BA2_sp10	0.0503	209	2.8
BA2_sp11	0.0591	572	2.9
BA2_sp12	0.0548	405	2.9
BA2_sp13	0.0470	50	2.8
BA2_sp14	0.0800	1198	3.1
BA1_sp1	0.0928	1484	3.2
BA1_sp2	0.0880	1384	3.2
BA1_sp3	0.0835	1282	3.2
BA1_sp4	0.0927	1482	3.2
BA1_sp5	0.0966	1560	3.3
BA1_sp6	0.1021	1665	3.3
BA1_sp7	0.1016	1655	3.3
BA1_sp8	0.0969	1565	3.3
BA1_sp9	0.0854	1326	3.2
BA1_sp10	0.0953	1535	3.3

VN sp32	1048	MR sp32	1331
VN sp33	322	MR sp33	1262
VN sp34	1120	MR sp34	1115
VN sp35	1061	MR sp35	863
VN sp36	989	MR sp36	1385
VN sp37	1309	MR sp37	1316
VN sp38	513	MR sp38	1079
VN sp39	1145	MR sp39	963
VN sp40	878	MR sp40	29
VN sp41	408	MR sp41	932
VN sp42	612	MR sp42	1049
VN sp43	719	MR sp43	1217
VN sp44	1036	MR sp44	1265
VN sp45	1189	MR sp45	943
VN sp46	51	MR sp46	1331
VN sp47	639	MR sp47	897
VN sp48	1006	MR sp48	886
VN sp49	560	MR sp49	1251
VN sp50	1105	MR sp50	1309
VN sp51	1240		

Notes: Abbreviations: MR- Massive replacement mineralization CX-56-1 663 m, BA- Bleb-like aggregates CX-41-1 758 m, VN- Fracture filling vein mineralization CX-56-1 644 m, sp- spot#.

Appendix B

Millennium Deposit Drill Core Logs

1

Legend

Manitou Falls Formation

MFd
MFc
MFb } 0-572 Meters
MFa

Symbols

BH-bleaching
CHL-chloritization
SAUS-suaseritization
SE-serritization
HE-hematite
HEB-hematite (secondary)
SIL-silicification
CY-clay
NOX-black oxide
QZ-quartz
UX-uranium
DV-dravite
VN-vein
HX-hydrothermal breccia
LI-limonite

Alteration

Highly altered

Moderately altered

Weakly altered

Litograghic Unit Shorthand:

MGRAN- micro-granite
GRAN-granite
GPELT-graphitic pelite
GSMPL-graphitic semi-pelite
PELT-pelite
SMPL-semi-pelite
PEGM-pegmatite
AMPH-amphibolite
CPELT-calc-pelite
CSMPL- calc-semi-pelite

Uranium Mineralization:

Strong-3000+CPS
Moderate-500-3000 CPS
Weak-150-500 CPS
Background <150 CPS

Uranium Occurrence

DISS-disseminated
VN-vein
BX-breccia fill
REPL-replacement

CX- 44: 569.5- 778.0 METERS

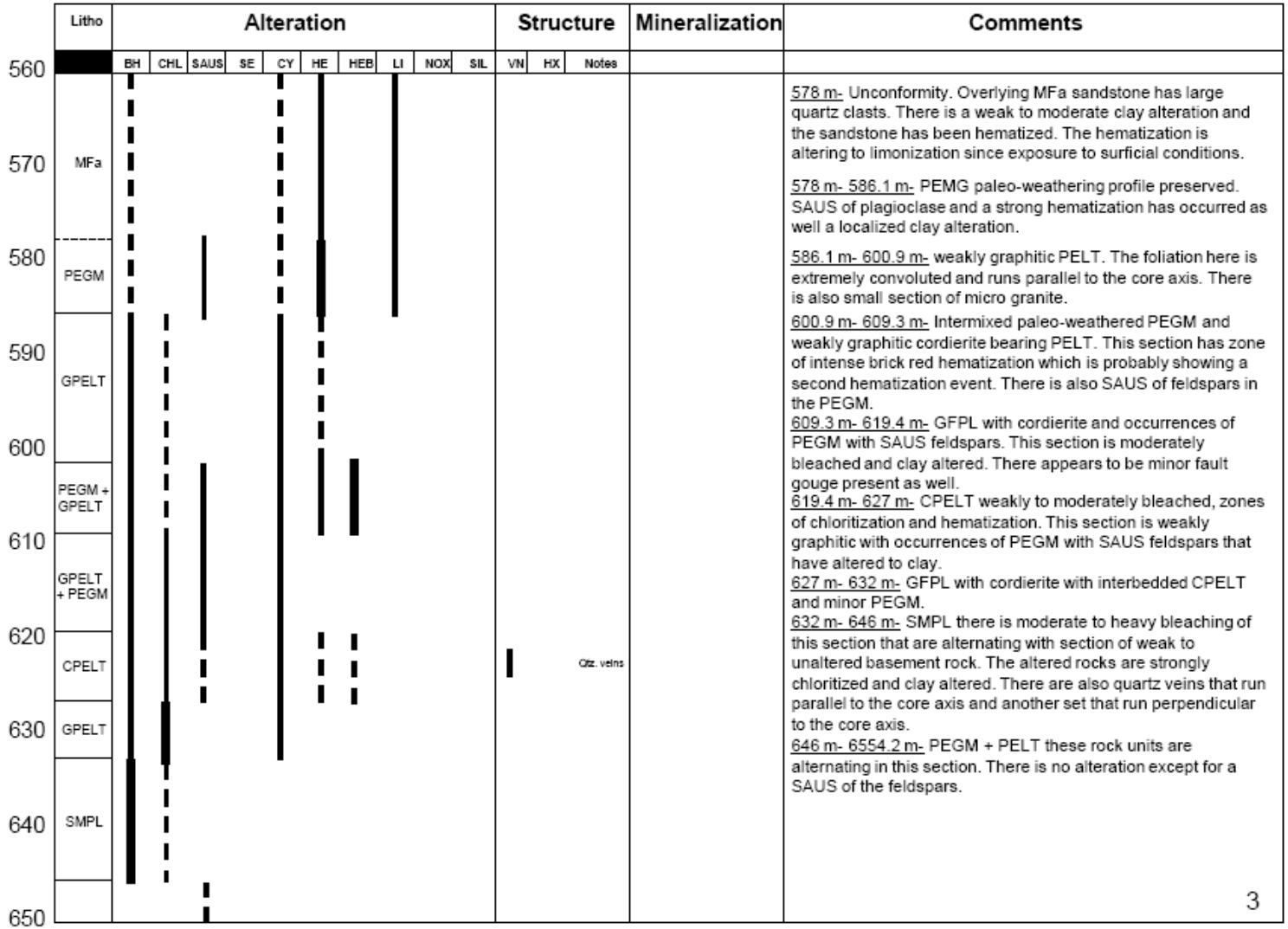

578 m- Unconformity. Overlying MFa sandstone has large quartz clasts. There is a weak to moderate clay alteration and the sandstone has been hematized. The hematization is altering to limonization since exposure to surficial conditions.

578 m- 586.1 m- PEMG paleo-weathering profile preserved. SAUS of plagioclase and a strong hematization has occurred as well a localized clay alteration.

586.1 m- 600.9 m- weakly graphitic PELT. The foliation here is extremely convoluted and runs parallel to the core axis. There is also small section of micro granite.

600.9 m- 609.3 m- Intermixed paleo-weathered PEGM and weakly graphitic cordierite bearing PELT. This section has zone of intense brick red hematization which is probably showing a second hematization event. There is also SAUS of feldspars in the PEGM.

609.3 m- 619.4 m- GFPL with cordierite and occurrences of PEGM with SAUS feldspars. This section is moderately bleached and clay altered. There appears to be minor fault gouge present as well.

619.4 m- 627 m- CPELT weakly to moderately bleached, zones of chloritization and hematization. This section is weakly graphitic with occurrences of PEGM with SAUS feldspars that have altered to clay.

627 m- 632 m- GFPL with cordierite with interbedded CPELT and minor PEGM.

632 m- 646 m- SMPL there is moderate to heavy bleaching of this section that are alternating with section of weak to unaltered basement rock. The altered rocks are strongly chloritized and clay altered. There are also quartz veins that run parallel to the core axis and another set that run perpendicular to the core axis.

646 m- 6554.2 m- PEGM + PELT these rock units are alternating in this section. There is no alteration except for a SAUS of the feldspars.

3

CX- 44: 569.5- 778.0 METERS

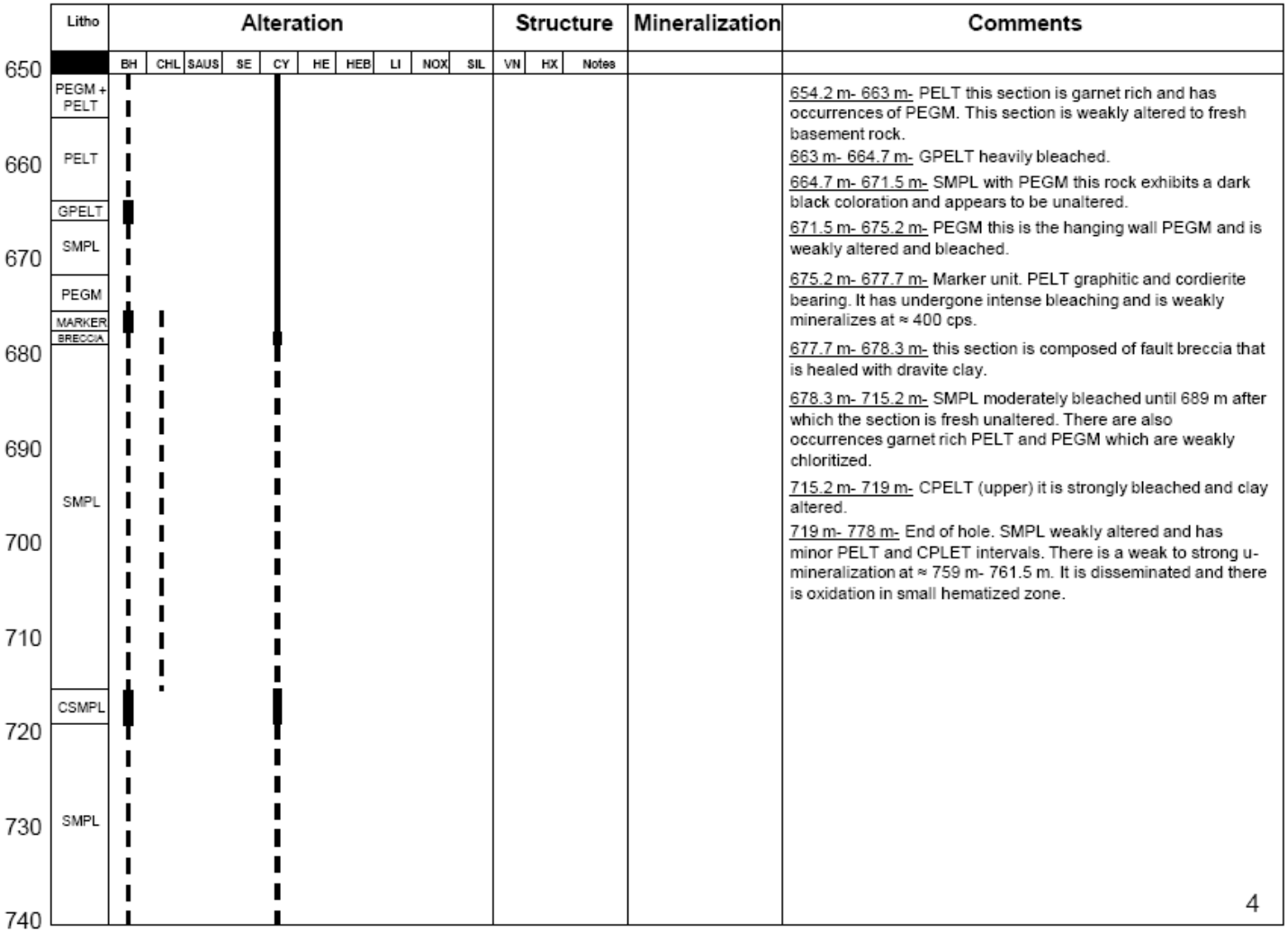

654.2 m- 663 m- PELT this section is garnet rich and has occurrences of PEGM. This section is weakly altered to fresh basement rock.

663 m- 664.7 m- GPELT heavily bleached.

664.7 m- 671.5 m- SMPL with PEGM this rock exhibits a dark black coloration and appears to be unaltered.

671.5 m- 675.2 m- PEGM this is the hanging wall PEGM and is weakly altered and bleached.

675.2 m- 677.7 m- Marker unit. PELT graphitic and cordierite bearing. It has undergone intense bleaching and is weakly mineralizes at ≈ 400 cps.

677.7 m- 678.3 m- this section is composed of fault breccia that is healed with dravite clay.

678.3 m- 715.2 m- SMPL moderately bleached until 689 m after which the section is fresh unaltered. There are also occurrences garnet rich PELT and PEGM which are weakly chloritized.

715.2 m- 719 m- CPELT (upper) it is strongly bleached and clay altered.

719 m- 778 m- End of hole. SMPL weakly altered and has minor PELT and CPLET intervals. There is a weak to strong u-mineralization at ≈ 759 m- 761.5 m. It is disseminated and there is oxidation in small hematized zone.

4

CX- 44: 569.5- 778.0 METERS

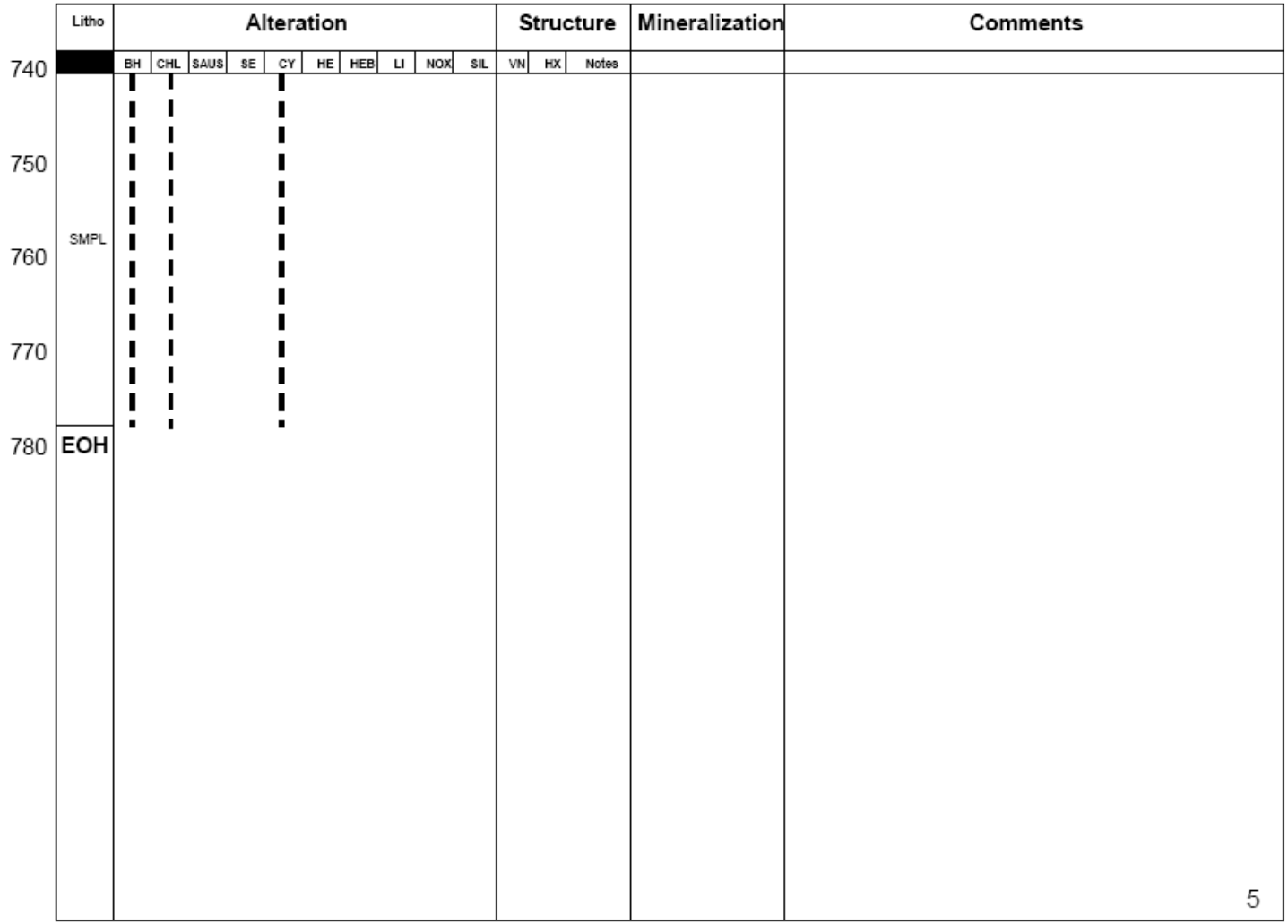

CX- 44- 1: 592.5- 827.0 METERS

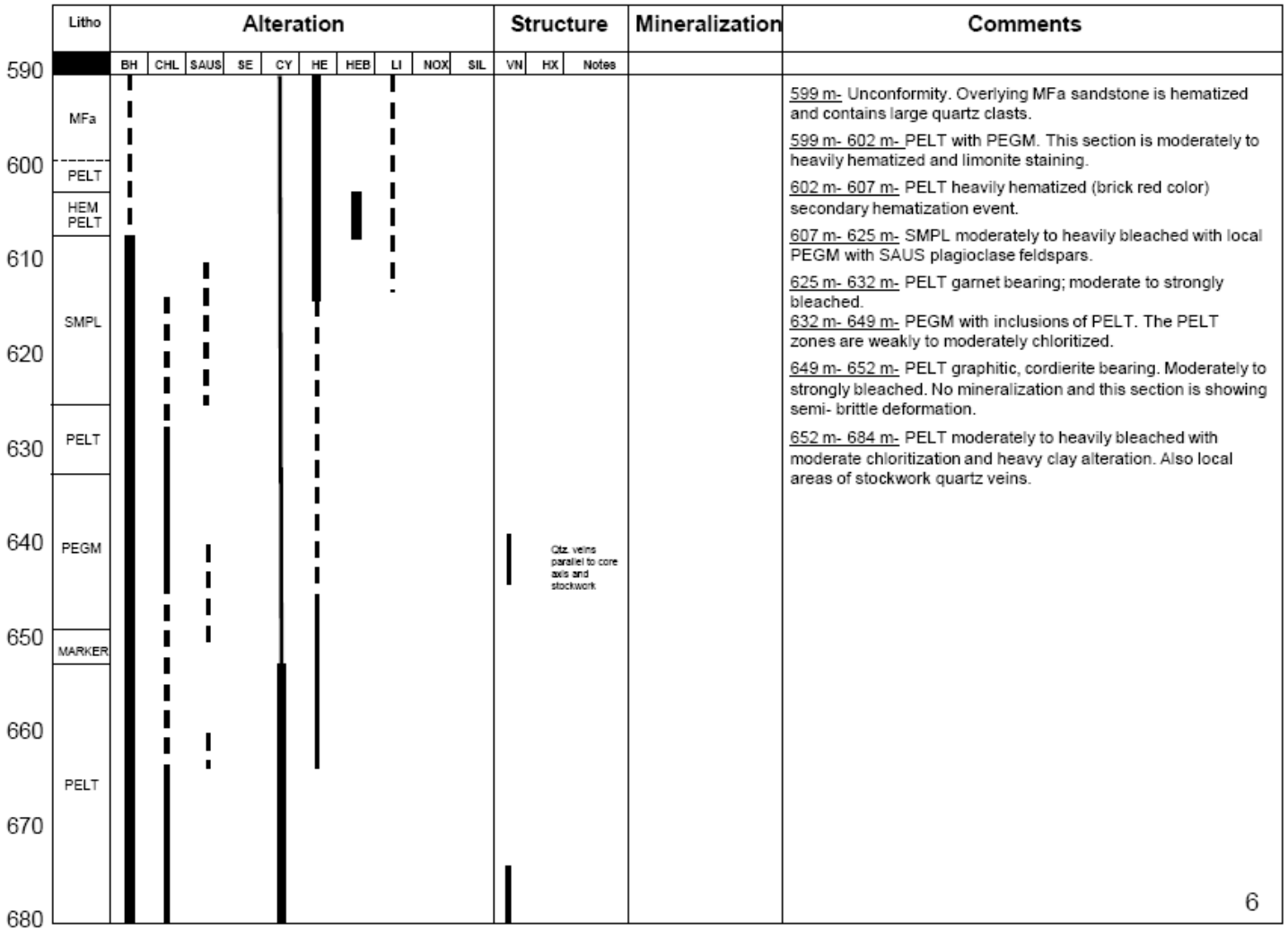

599 m- Unconformity. Overlying MFa sandstone is hematized and contains large quartz clasts.

599 m- 602 m- PELT with PEGM. This section is moderately to heavily hematized and limonite staining.

602 m- 607 m- PELT heavily hematized (brick red color) secondary hematization event.

607 m- 625 m- SMPL moderately to heavily bleached with local PEGM with SAUS plagioclase feldspars.

625 m- 632 m- PELT garnet bearing; moderate to strongly bleached.

632 m- 649 m- PEGM with inclusions of PELT. The PELT zones are weakly to moderately chloritized.

649 m- 652 m- PELT graphitic, cordierite bearing. Moderately to strongly bleached. No mineralization and this section is showing semi- brittle deformation.

652 m- 684 m- PELT moderately to heavily bleached with moderate chloritization and heavy clay alteration. Also local areas of stockwork quartz veins.

6

CX- 44- 1: 592.5- 827.0 METERS

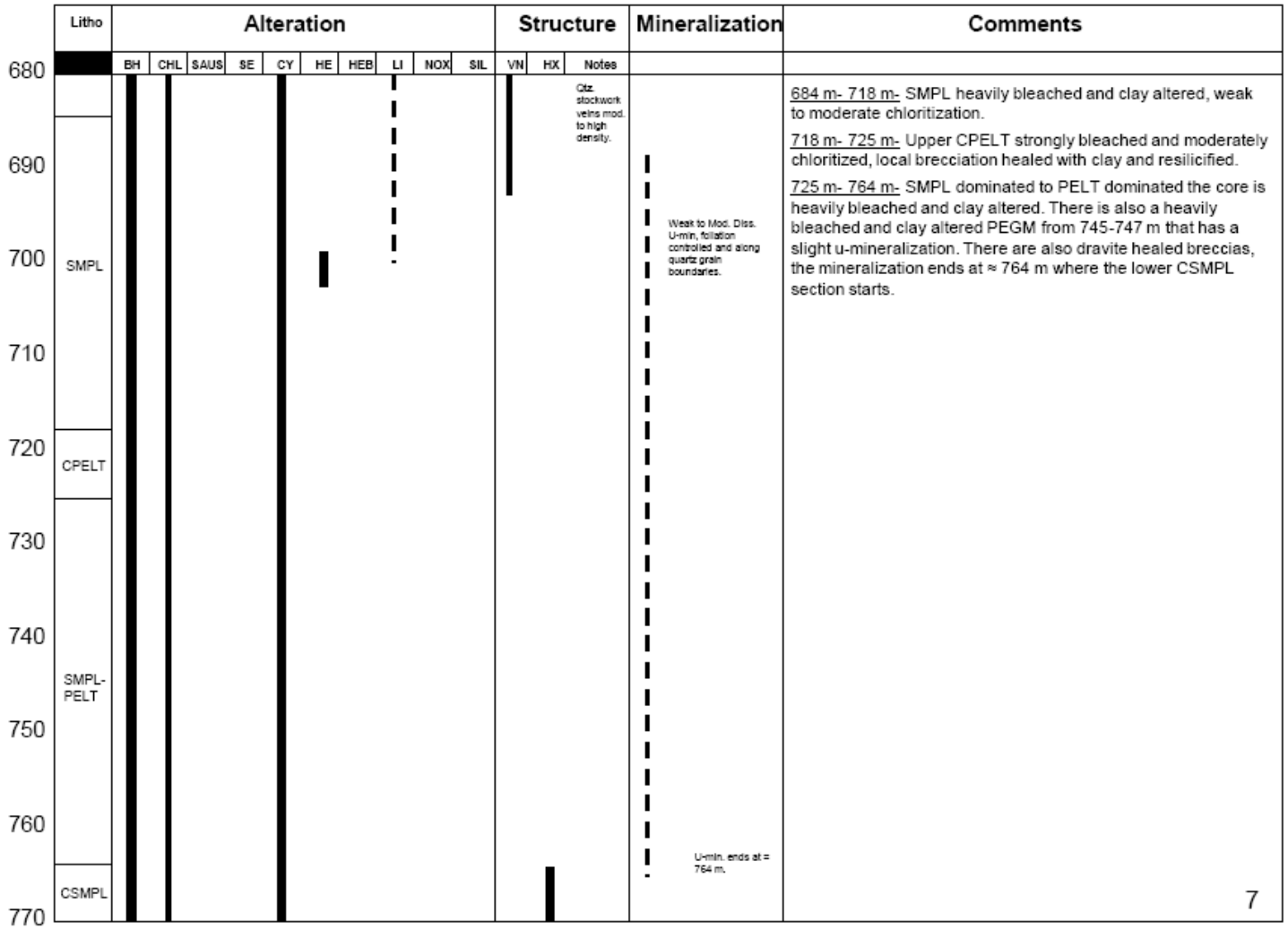

684 m- 718 m- SMPL heavily bleached and clay altered, weak to moderate chloritization.

718 m- 725 m- Upper CPELT strongly bleached and moderately chloritized, local brecciation healed with clay and resilicified.

725 m- 764 m- SMPL dominated to PELT dominated the core is heavily bleached and clay altered. There is also a heavily bleached and clay altered PEGM from 745-747 m that has a slight u-mineralization. There are also dravite healed breccias, the mineralization ends at ≈ 764 m where the lower CSMPL section starts.

7

CX- 44- 1: 592.5- 827.0 METERS

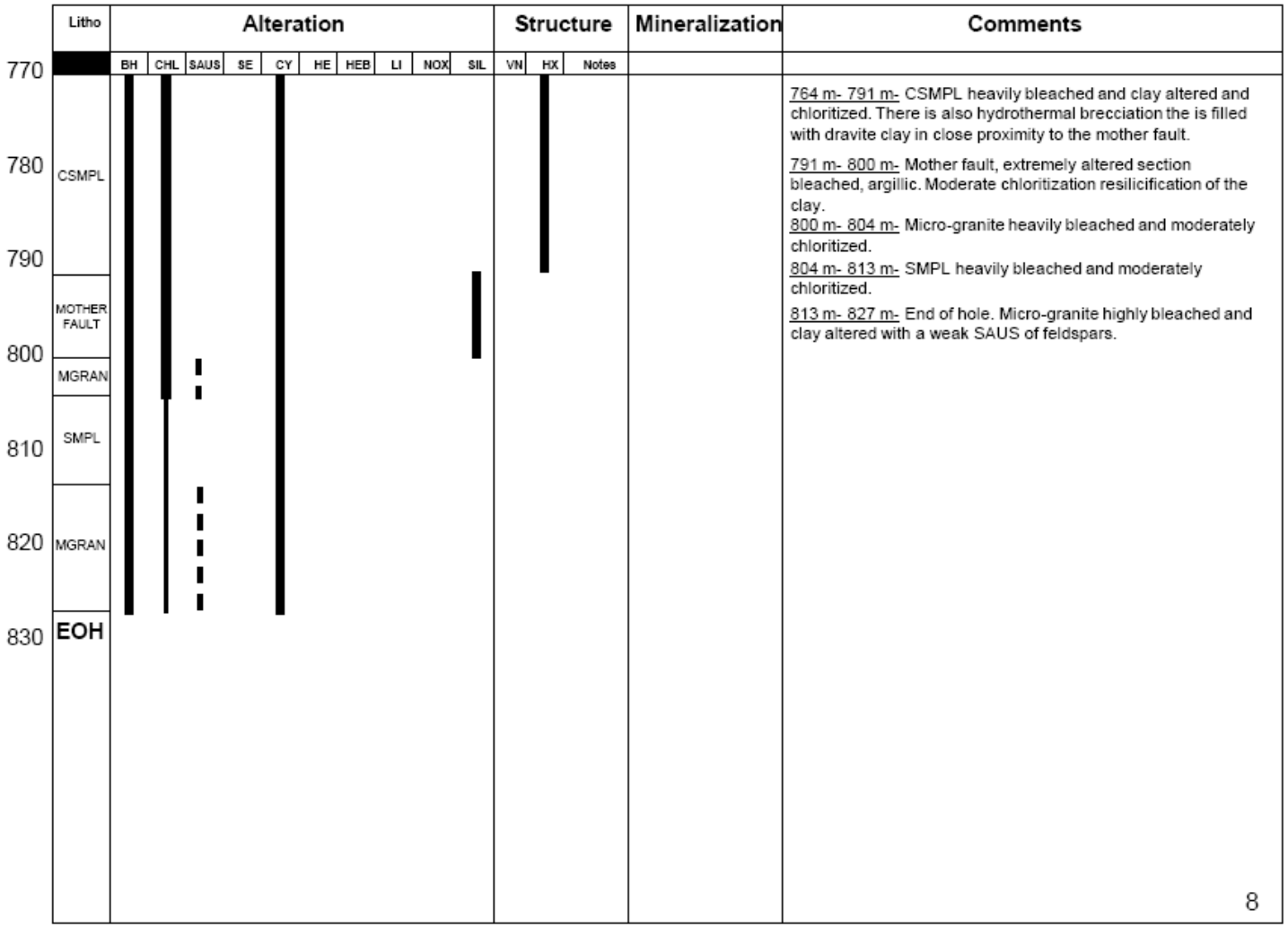

CX- 47: 561.0 - 854.0 METERS

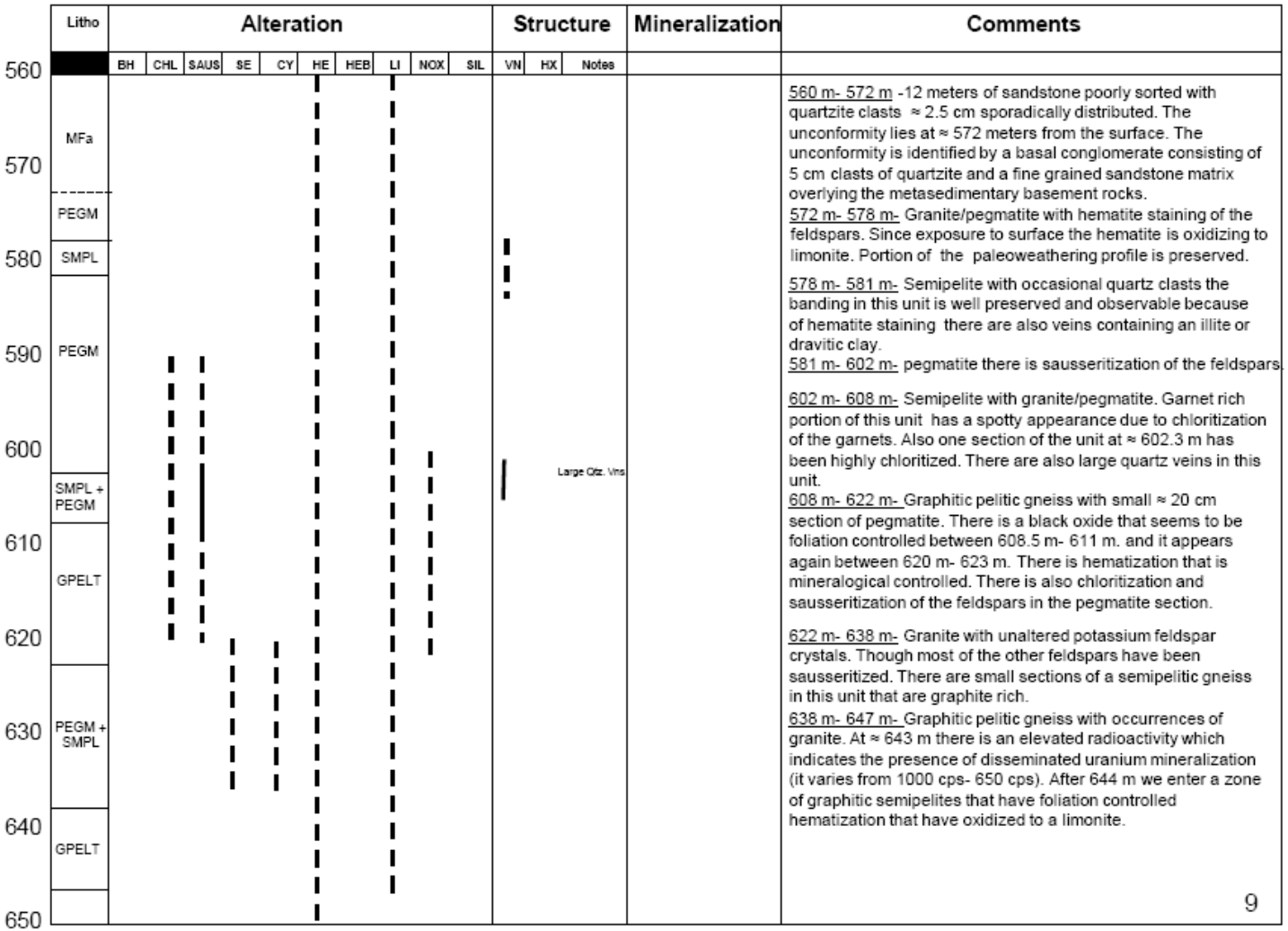

560 m- 572 m -12 meters of sandstone poorly sorted with quartzite clasts ≈ 2.5 cm sporadically distributed. The unconformity lies at ≈ 572 meters from the surface. The unconformity is identified by a basal conglomerate consisting of 5 cm clasts of quartzite and a fine grained sandstone matrix overlying the metasedimentary basement rocks.

572 m- 578 m- Granite/pegmatite with hematite staining of the feldspars. Since exposure to surface the hematite is oxidizing to limonite. Portion of the paleoweathering profile is preserved.

578 m- 581 m- Semipelite with occasional quartz clasts the banding in this unit is well preserved and observable because of hematite staining there are also veins containing an illite or dravitic clay.

581 m- 602 m- pegmatite there is sausseritization of the feldspars.

602 m- 608 m- Semipelite with granite/pegmatite. Garnet rich portion of this unit has a spotty appearance due to chloritization of the garnets. Also one section of the unit at ≈ 602.3 m has been highly chloritized. There are also large quartz veins in this unit.

608 m- 622 m- Graphitic pelitic gneiss with small ≈ 20 cm section of pegmatite. There is a black oxide that seems to be foliation controlled between 608.5 m- 611 m. and it appears again between 620 m- 623 m. There is hematization that is mineralogical controlled. There is also chloritization and sausseritization of the feldspars in the pegmatite section.

622 m- 638 m- Granite with unaltered potassium feldspar crystals. Though most of the other feldspars have been sausseritized. There are small sections of a semipelitic gneiss in this unit that are graphite rich.

638 m- 647 m- Graphitic pelitic gneiss with occurrences of granite. At ≈ 643 m there is an elevated radioactivity which indicates the presence of disseminated uranium mineralization (it varies from 1000 cps- 650 cps). After 644 m we enter a zone of graphitic semipelites that have foliation controlled hematization that have oxidized to a limonite.

9

CX- 47: 561.0 - 854.0 METERS

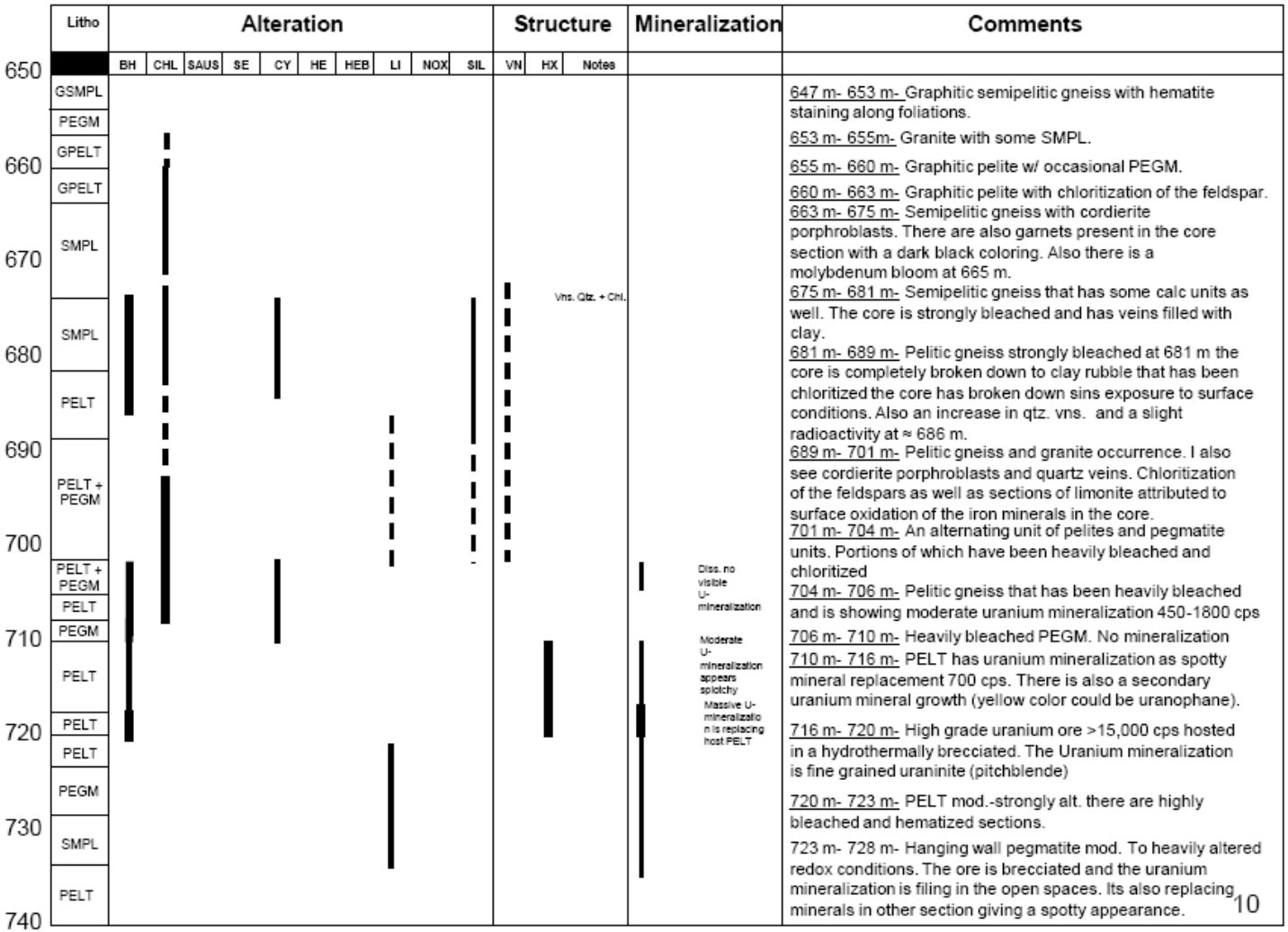

CX- 47: 561.0 - 854.0 METERS

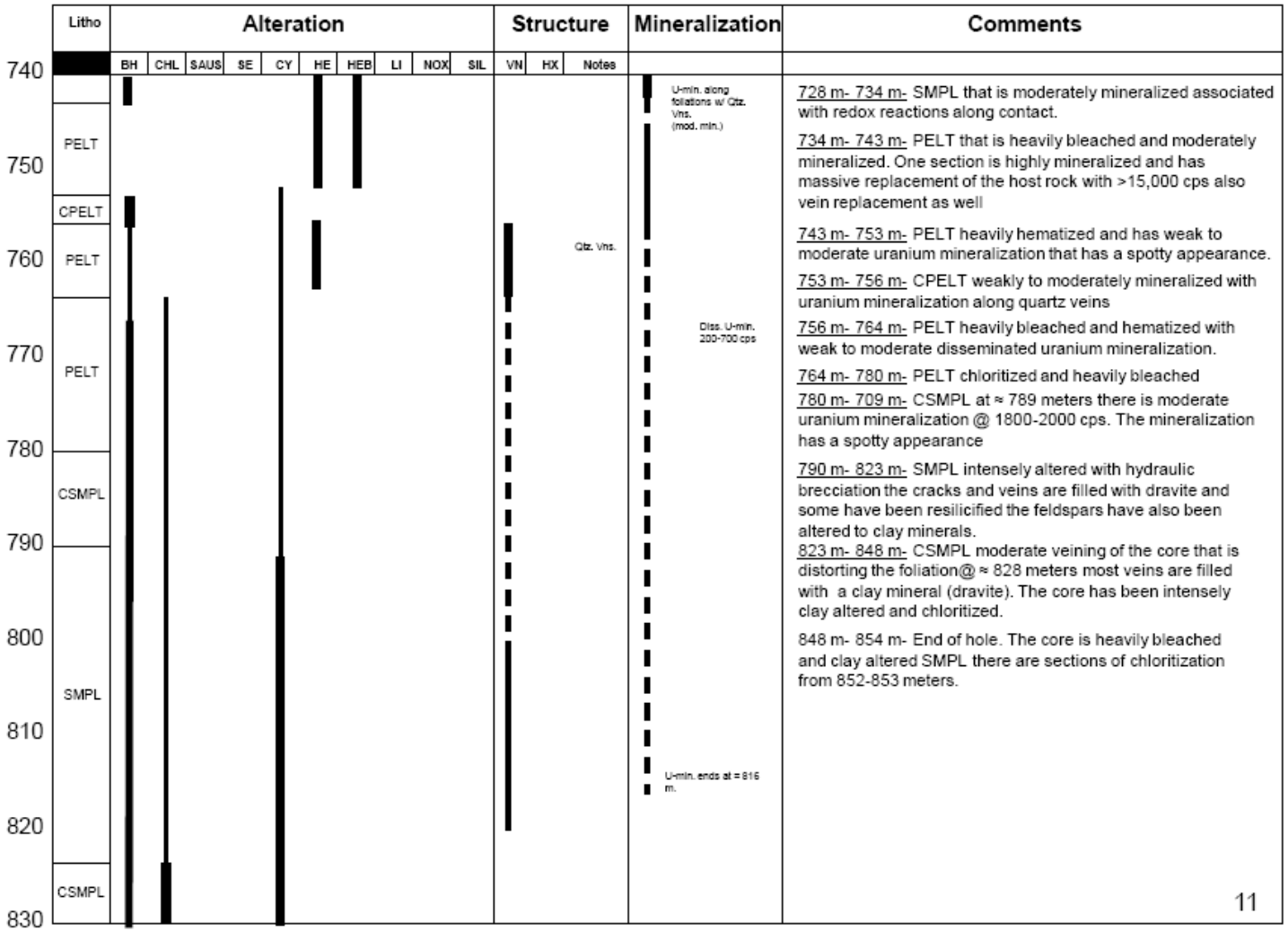

728 m- 734 m- SMPL that is moderately mineralized associated with redox reactions along contact.

734 m- 743 m- PELT that is heavily bleached and moderately mineralized. One section is highly mineralized and has massive replacement of the host rock with >15,000 cps also vein replacement as well

743 m- 753 m- PELT heavily hematized and has weak to moderate uranium mineralization that has a spotty appearance.

753 m- 756 m- CPELT weakly to moderately mineralized with uranium mineralization along quartz veins

756 m- 764 m- PELT heavily bleached and hematized with weak to moderate disseminated uranium mineralization.

764 m- 780 m- PELT chloritized and heavily bleached

780 m- 709 m- CSMPL at ≈ 789 meters there is moderate uranium mineralization @ 1800-2000 cps. The mineralization has a spotty appearance

790 m- 823 m- SMPL intensely altered with hydraulic brecciation the cracks and veins are filled with dravite and some have been resilicified the feldspars have also been altered to clay minerals.

823 m- 848 m- CSMPL moderate veining of the core that is distorting the foliation@ ≈ 828 meters most veins are filled with a clay mineral (dravite). The core has been intensely clay altered and chloritized.

848 m- 854 m- End of hole. The core is heavily bleached and clay altered SMPL there are sections of chloritization from 852-853 meters.

11

CX- 47: 561.0 - 854.0 METERS

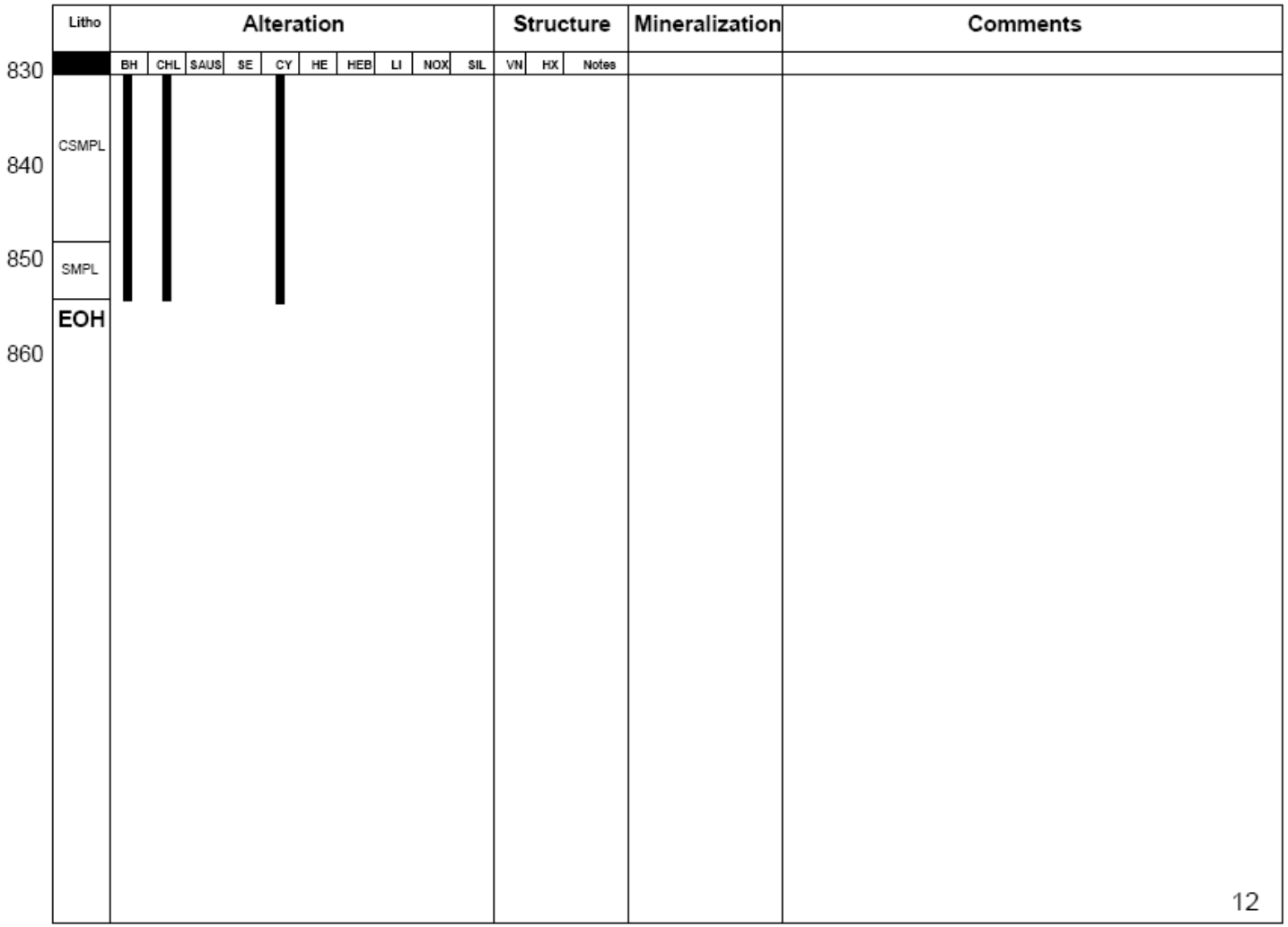

CX- 47- 1: 566.3-830.0 METERS

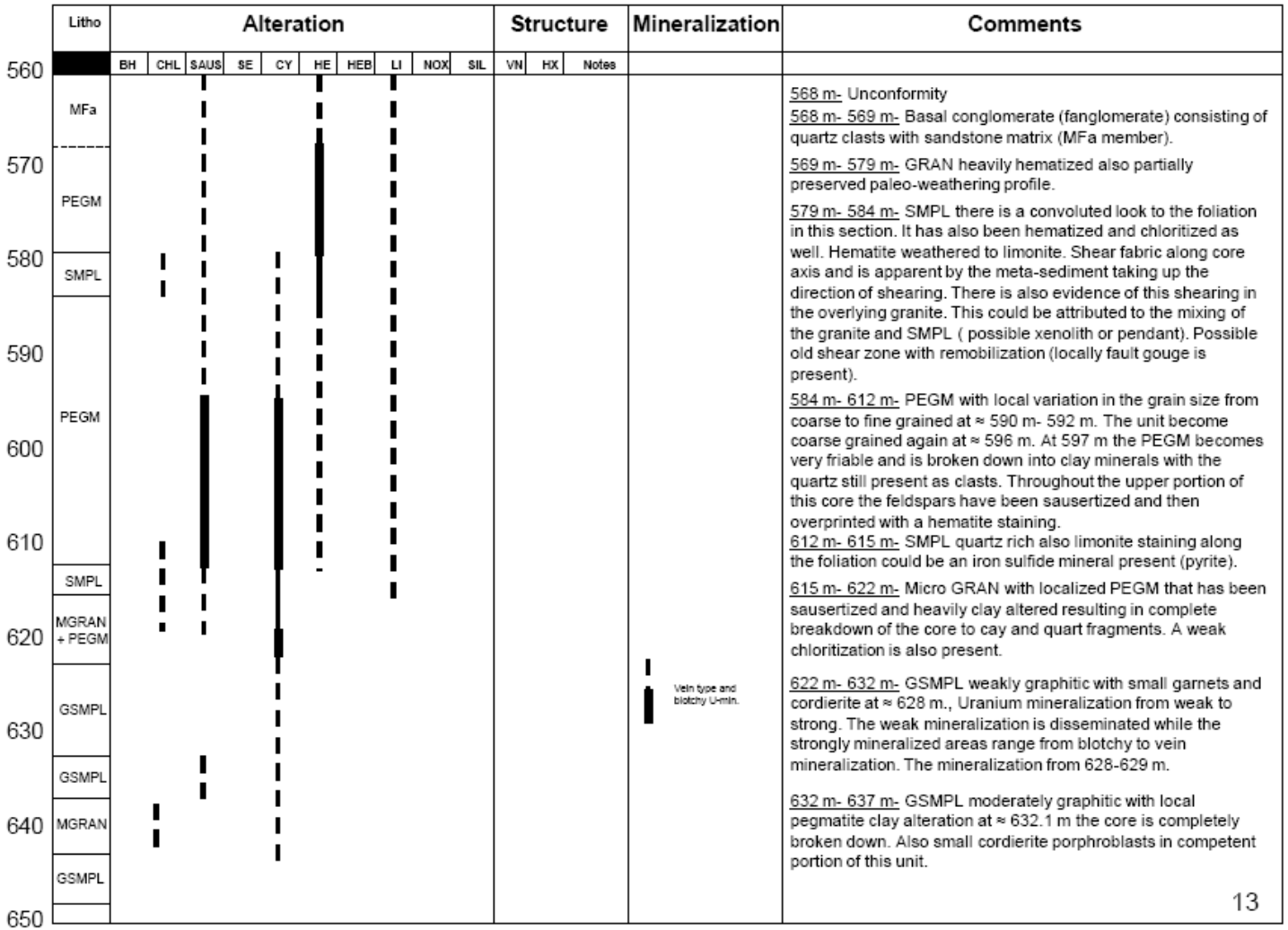

568 m- Unconformity

568 m- 569 m- Basal conglomerate (fanglomerate) consisting of quartz clasts with sandstone matrix (MFa member).

569 m- 579 m- GRAN heavily hematized also partially preserved paleo-weathering profile.

579 m- 584 m- SMPL there is a convoluted look to the foliation in this section. It has also been hematized and chloritized as well. Hematite weathered to limonite. Shear fabric along core axis and is apparent by the meta-sediment taking up the direction of shearing. There is also evidence of this shearing in the overlying granite. This could be attributed to the mixing of the granite and SMPL (possible xenolith or pendant). Possible old shear zone with remobilization (locally fault gouge is present).

584 m- 612 m- PEGM with local variation in the grain size from coarse to fine grained at ≈ 590 m- 592 m. The unit become coarse grained again at ≈ 596 m. At 597 m the PEGM becomes very friable and is broken down into clay minerals with the quartz still present as clasts. Throughout the upper portion of this core the feldspars have been sausertized and then overprinted with a hematite staining.

612 m- 615 m- SMPL quartz rich also limonite staining along the foliation could be an iron sulfide mineral present (pyrite).

615 m- 622 m- Micro GRAN with localized PEGM that has been sausertized and heavily clay altered resulting in complete breakdown of the core to cay and quart fragments. A weak chloritization is also present.

622 m- 632 m- GSMPL weakly graphitic with small garnets and cordierite at ≈ 628 m., Uranium mineralization from weak to strong. The weak mineralization is disseminated while the strongly mineralized areas range from blotchy to vein mineralization. The mineralization from 628-629 m.

632 m- 637 m- GSMPL moderately graphitic with local pegmatite clay alteration at ≈ 632.1 m the core is completely broken down. Also small cordierite porphroblasts in competent portion of this unit.

13

CX- 47- 1: 566.3-830.0 METERS

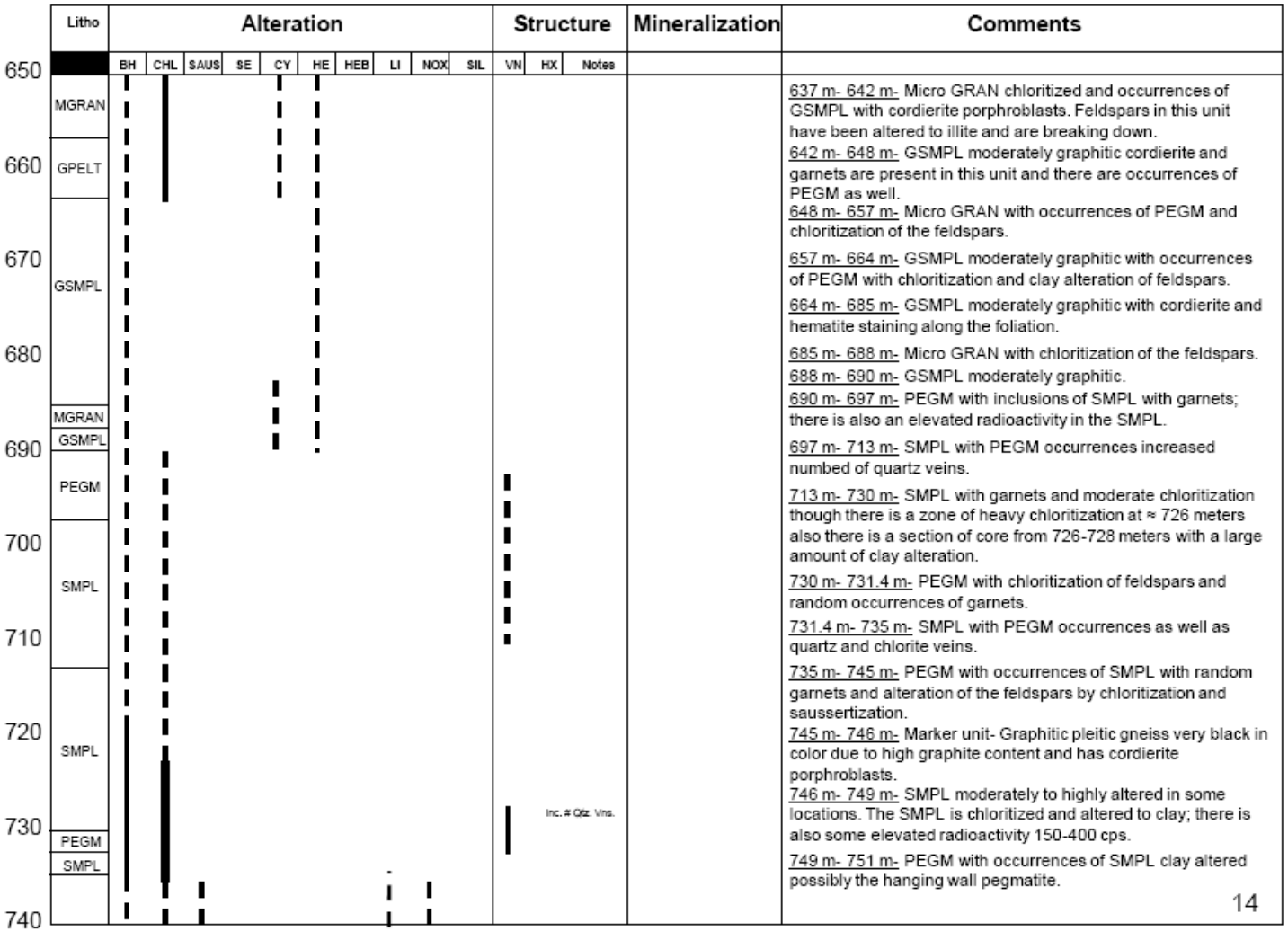

637 m- 642 m- Micro GRAN chloritized and occurrences of GSMPL with cordierite porphroblasts. Feldspars in this unit have been altered to illite and are breaking down.

642 m- 648 m- GSMPL moderately graphitic cordierite and garnets are present in this unit and there are occurrences of PEGM as well.

648 m- 657 m- Micro GRAN with occurrences of PEGM and chloritization of the feldspars.

657 m- 664 m- GSMPL moderately graphitic with occurrences of PEGM with chloritization and clay alteration of feldspars.

664 m- 685 m- GSMPL moderately graphitic with cordierite and hematite staining along the foliation.

685 m- 688 m- Micro GRAN with chloritization of the feldspars.

688 m- 690 m- GSMPL moderately graphitic.

690 m- 697 m- PEGM with inclusions of SMPL with garnets; there is also an elevated radioactivity in the SMPL.

697 m- 713 m- SMPL with PEGM occurrences increased numbed of quartz veins.

713 m- 730 m- SMPL with garnets and moderate chloritization though there is a zone of heavy chloritization at ≈ 726 meters also there is a section of core from 726-728 meters with a large amount of clay alteration.

730 m- 731.4 m- PEGM with chloritization of feldspars and random occurrences of garnets.

731.4 m- 735 m- SMPL with PEGM occurrences as well as quartz and chlorite veins.

735 m- 745 m- PEGM with occurrences of SMPL with random garnets and alteration of the feldspars by chloritization and saussertization.

745 m- 746 m- Marker unit- Graphitic pleitic gneiss very black in color due to high graphite content and has cordierite porphroblasts.

746 m- 749 m- SMPL moderately to highly altered in some locations. The SMPL is chloritized and altered to clay; there is also some elevated radioactivity 150-400 cps.

749 m- 751 m- PEGM with occurrences of SMPL clay altered possibly the hanging wall pegmatite.

14

CX- 47- 1: 566.3-830.0 METERS

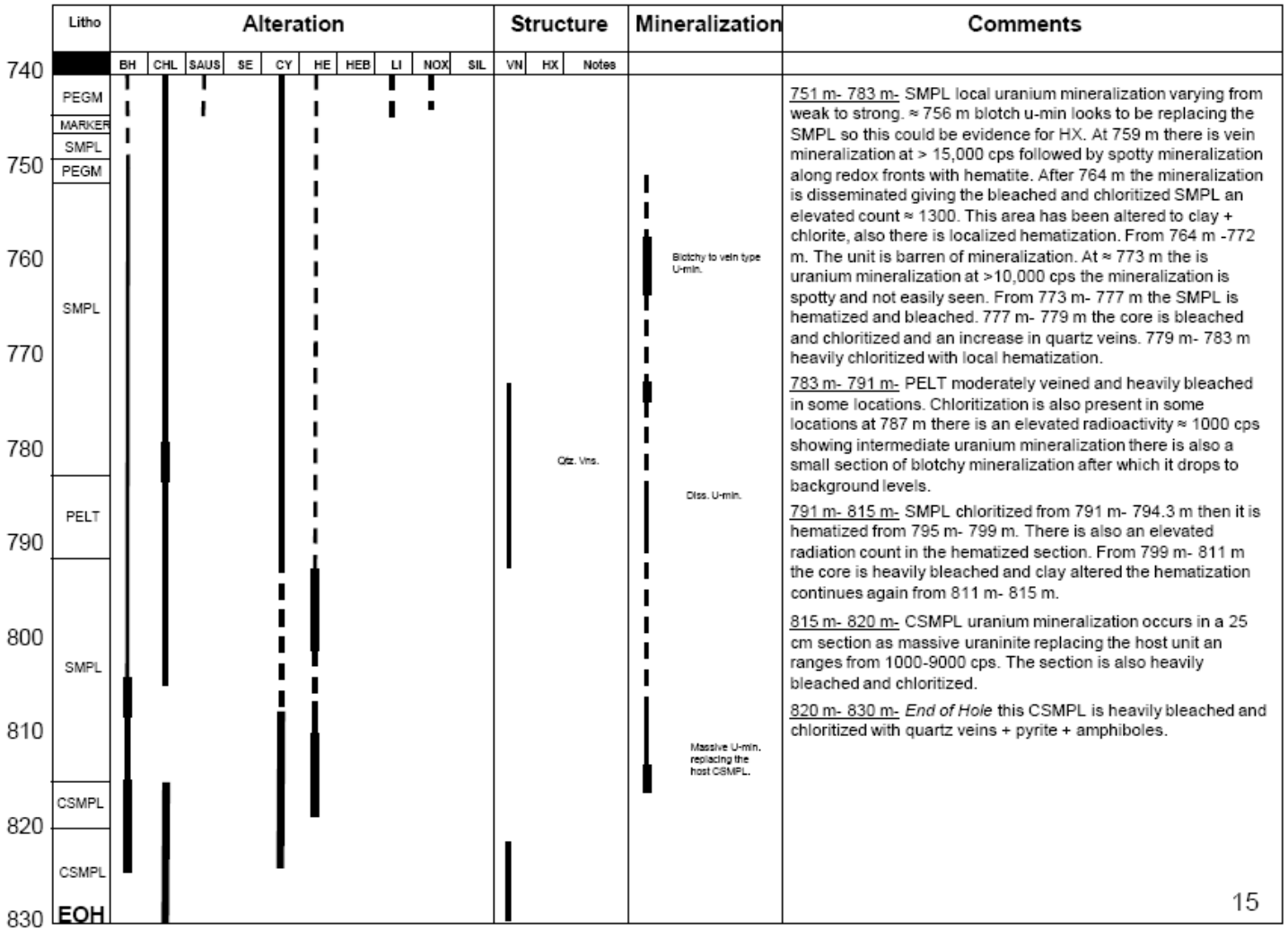

751 m- 783 m- SMPL local uranium mineralization varying from weak to strong. ≈ 756 m blotch u-min looks to be replacing the SMPL so this could be evidence for HX. At 759 m there is vein mineralization at > 15,000 cps followed by spotty mineralization along redox fronts with hematite. After 764 m the mineralization is disseminated giving the bleached and chloritized SMPL an elevated count ≈ 1300. This area has been altered to clay + chlorite, also there is localized hematization. From 764 m -772 m. The unit is barren of mineralization. At ≈ 773 m the is uranium mineralization at >10,000 cps the mineralization is spotty and not easily seen. From 773 m- 777 m the SMPL is hematized and bleached. 777 m- 779 m the core is bleached and chloritized and an increase in quartz veins. 779 m- 783 m heavily chloritized with local hematization.

783 m- 791 m- PELT moderately veined and heavily bleached in some locations. Chloritization is also present in some locations at 787 m there is an elevated radioactivity ≈ 1000 cps showing intermediate uranium mineralization there is also a small section of blotchy mineralization after which it drops to background levels.

791 m- 815 m- SMPL chloritized from 791 m- 794.3 m then it is hematized from 795 m- 799 m. There is also an elevated radiation count in the hematized section. From 799 m- 811 m the core is heavily bleached and clay altered the hematization continues again from 811 m- 815 m.

815 m- 820 m- CSMPL uranium mineralization occurs in a 25 cm section as massive uraninite replacing the host unit an ranges from 1000-9000 cps. The section is also heavily bleached and chloritized.

820 m- 830 m- *End of Hole* this CSMPL is heavily bleached and chloritized with quartz veins + pyrite + amphiboles.

15

CX- 47- 2: 582.O- 776.7 METERS

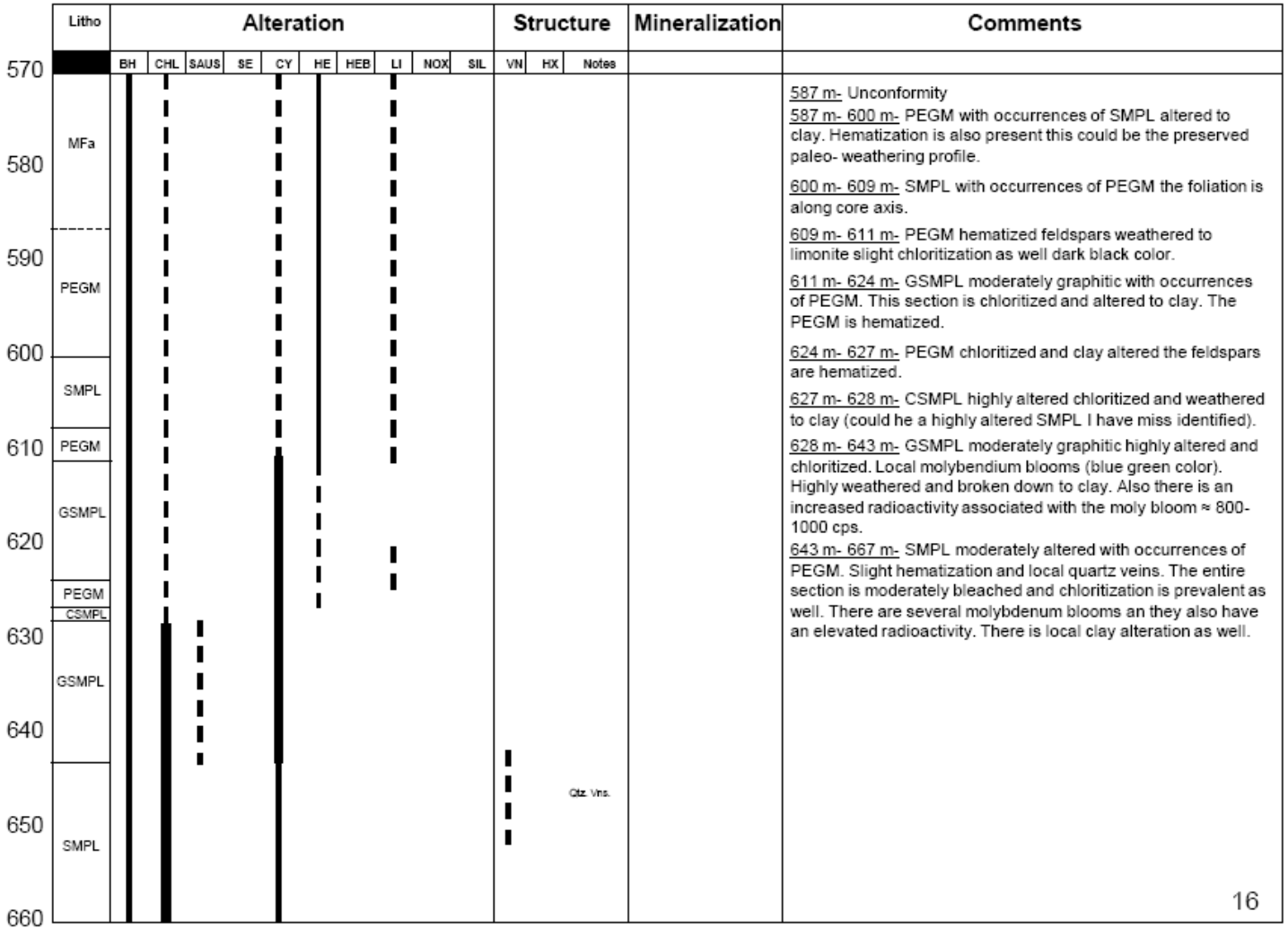

587 m- Unconformity

587 m- 600 m- PEGM with occurrences of SMPL altered to clay. Hematization is also present this could be the preserved paleo- weathering profile.

600 m- 609 m- SMPL with occurrences of PEGM the foliation is along core axis.

609 m- 611 m- PEGM hematized feldspars weathered to limonite slight chloritization as well dark black color.

611 m- 624 m- GSMPL moderately graphitic with occurrences of PEGM. This section is chloritized and altered to clay. The PEGM is hematized.

624 m- 627 m- PEGM chloritized and clay altered the feldspars are hematized.

627 m- 628 m- CSMPL highly altered chloritized and weathered to clay (could he a highly altered SMPL I have miss identified).

628 m- 643 m- GSMPL moderately graphitic highly altered and chloritized. Local molybendium blooms (blue green color). Highly weathered and broken down to clay. Also there is an increased radioactivity associated with the moly bloom ≈ 800-1000 cps.

643 m- 667 m- SMPL moderately altered with occurrences of PEGM. Slight hematization and local quartz veins. The entire section is moderately bleached and chloritization is prevalent as well. There are several molybdenum blooms an they also have an elevated radioactivity. There is local clay alteration as well.

16

CX- 47- 2: 582.O- 776.7 METERS

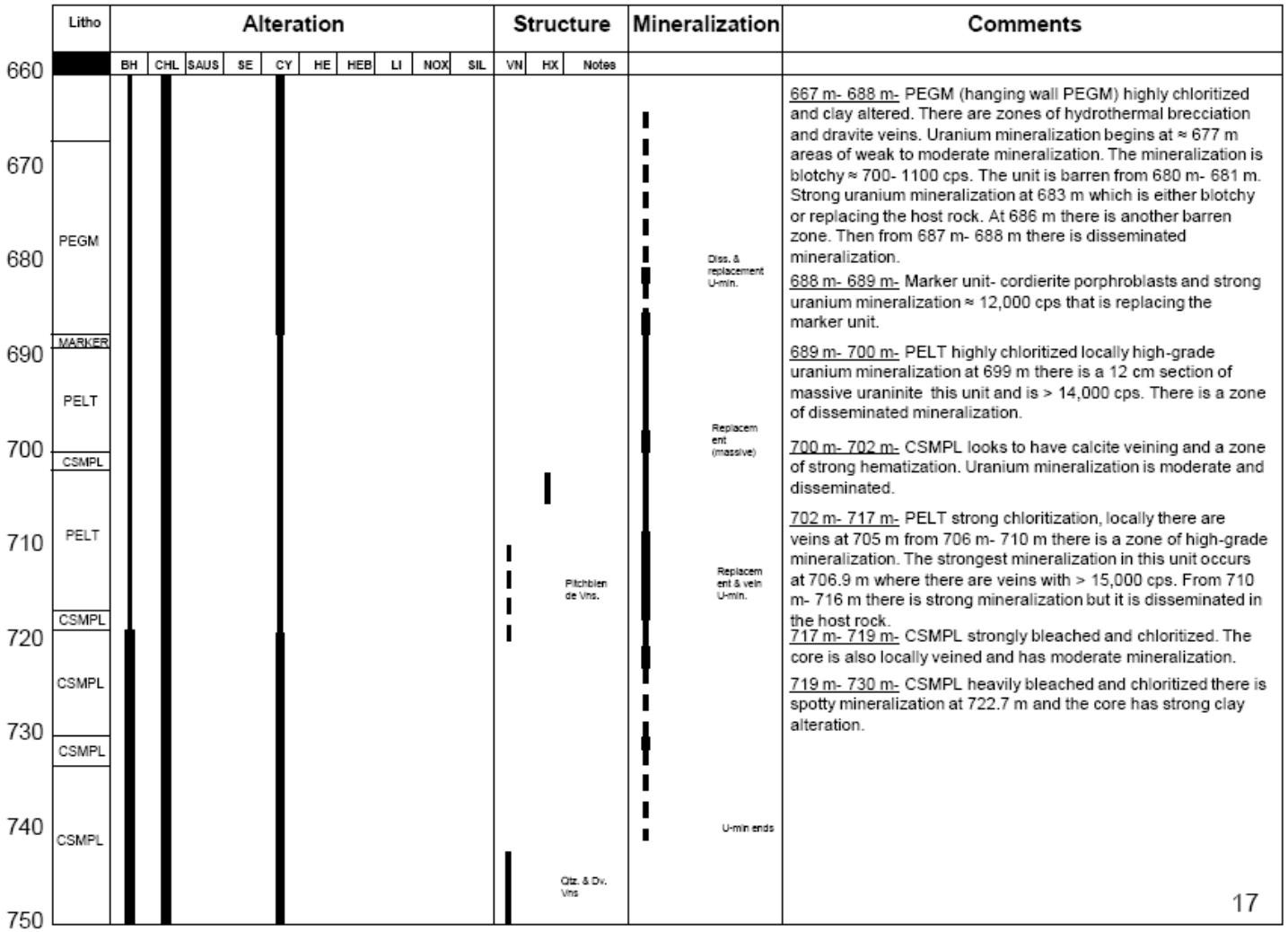

CX- 47- 2: 582.O- 776.7 METERS

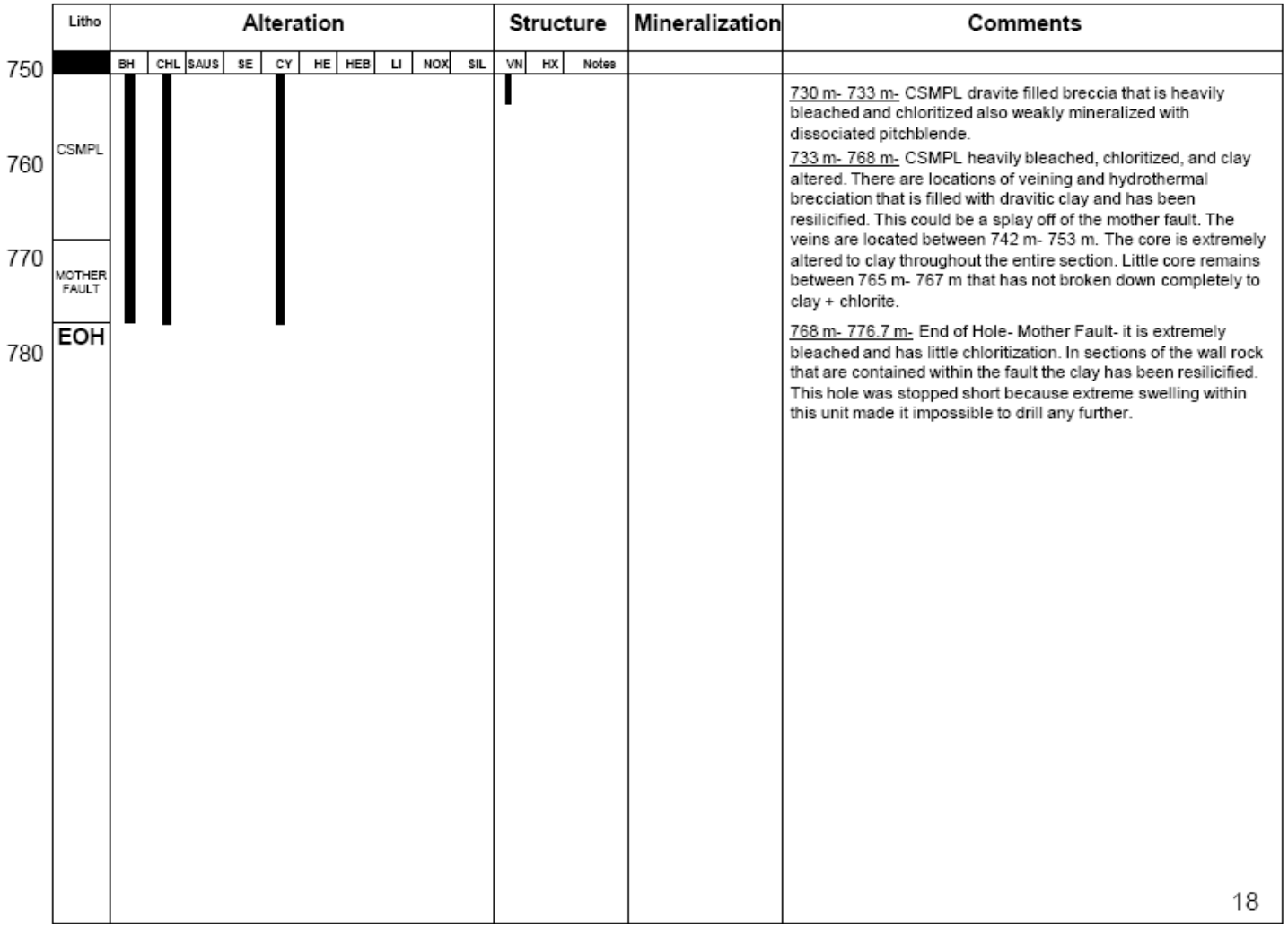

CX- 51: 558.6- 854.6 METERS

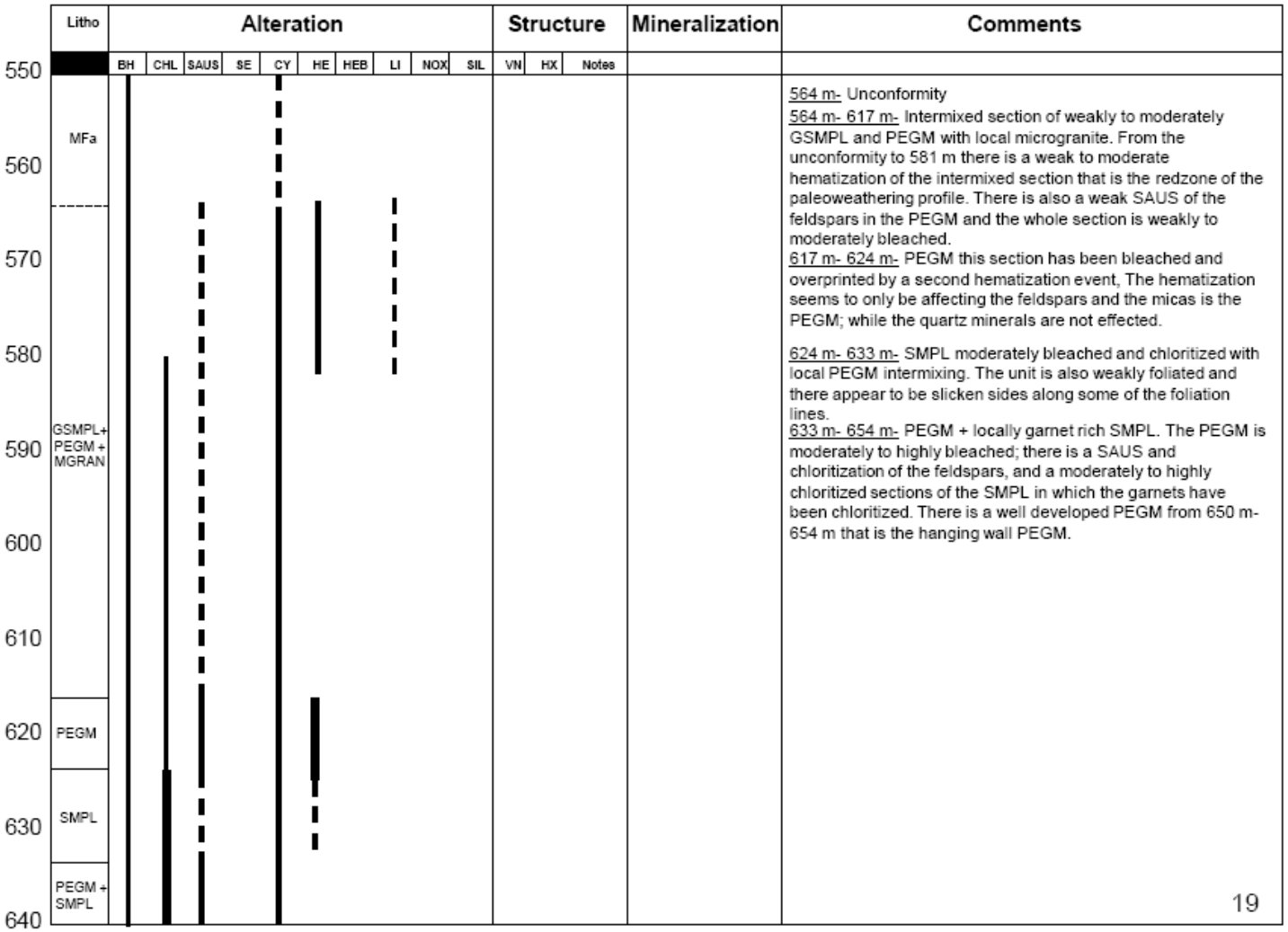

564 m- Unconformity

564 m- 617 m- Intermixed section of weakly to moderately GSMPL and PEGM with local microgranite. From the unconformity to 581 m there is a weak to moderate hematization of the intermixed section that is the redzone of the paleoweathering profile. There is also a weak SAUS of the feldspars in the PEGM and the whole section is weakly to moderately bleached.

617 m- 624 m- PEGM this section has been bleached and overprinted by a second hematization event, The hematization seems to only be affecting the feldspars and the micas is the PEGM; while the quartz minerals are not effected.

624 m- 633 m- SMPL moderately bleached and chloritized with local PEGM intermixing. The unit is also weakly foliated and there appear to be slicken sides along some of the foliation lines.

633 m- 654 m- PEGM + locally garnet rich SMPL. The PEGM is moderately to highly bleached; there is a SAUS and chloritization of the feldspars, and a moderately to highly chloritized sections of the SMPL in which the garnets have been chloritized. There is a well developed PEGM from 650 m- 654 m that is the hanging wall PEGM.

19

CX- 51: 558.6- 854.6 METERS

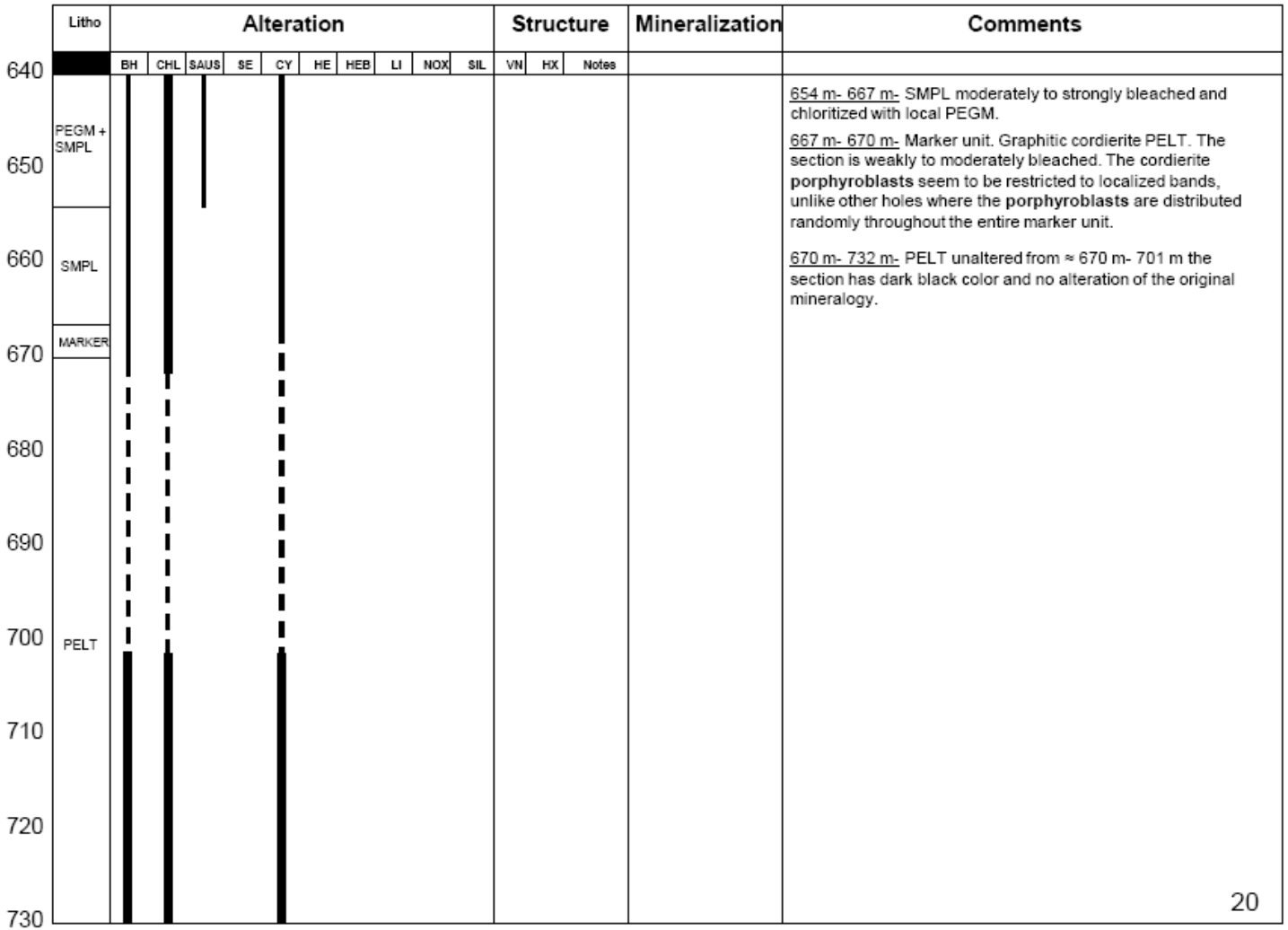

CX- 51: 558.6- 854.6 METERS

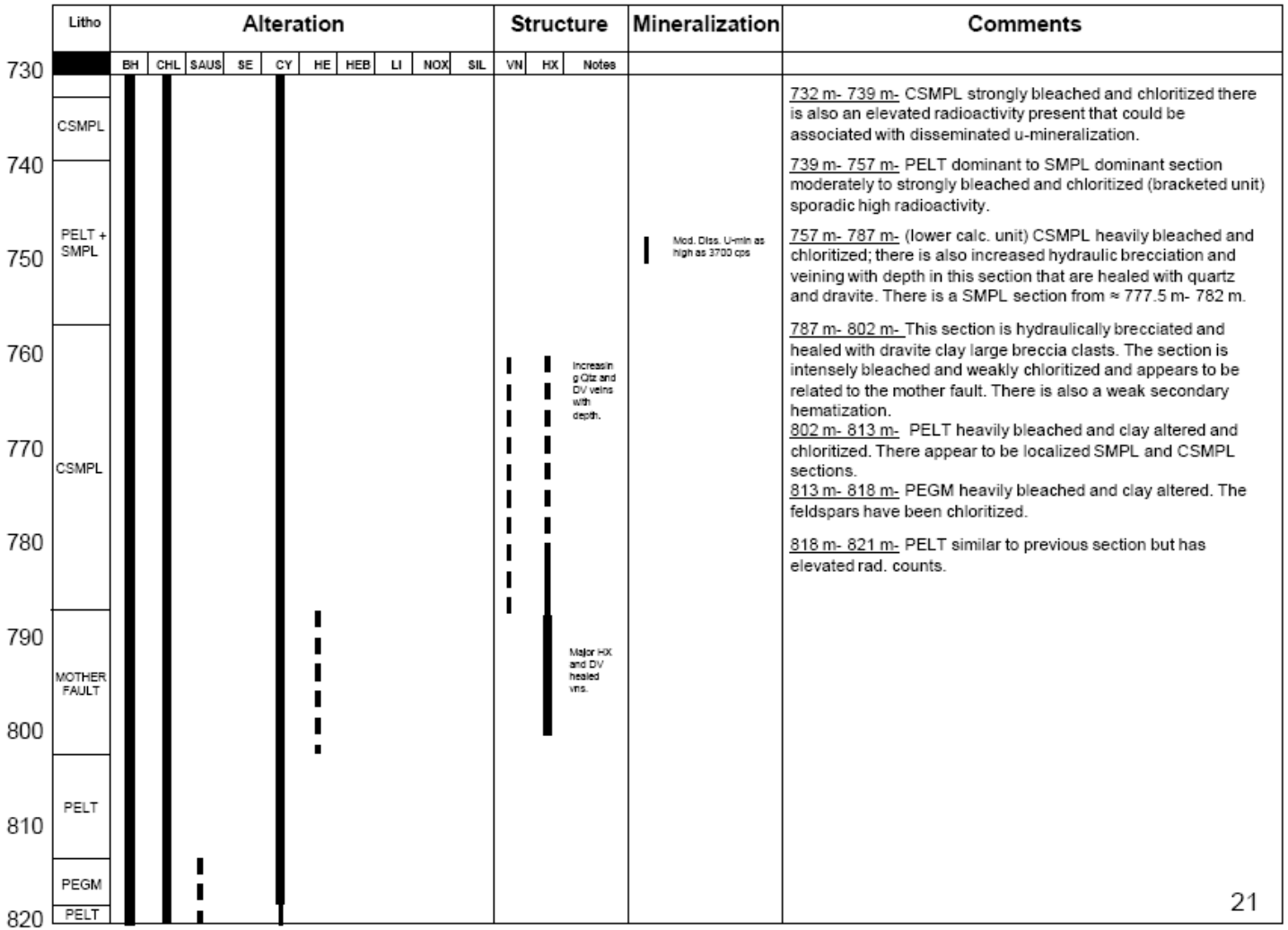

CX- 51: 558.6- 854.6 METERS

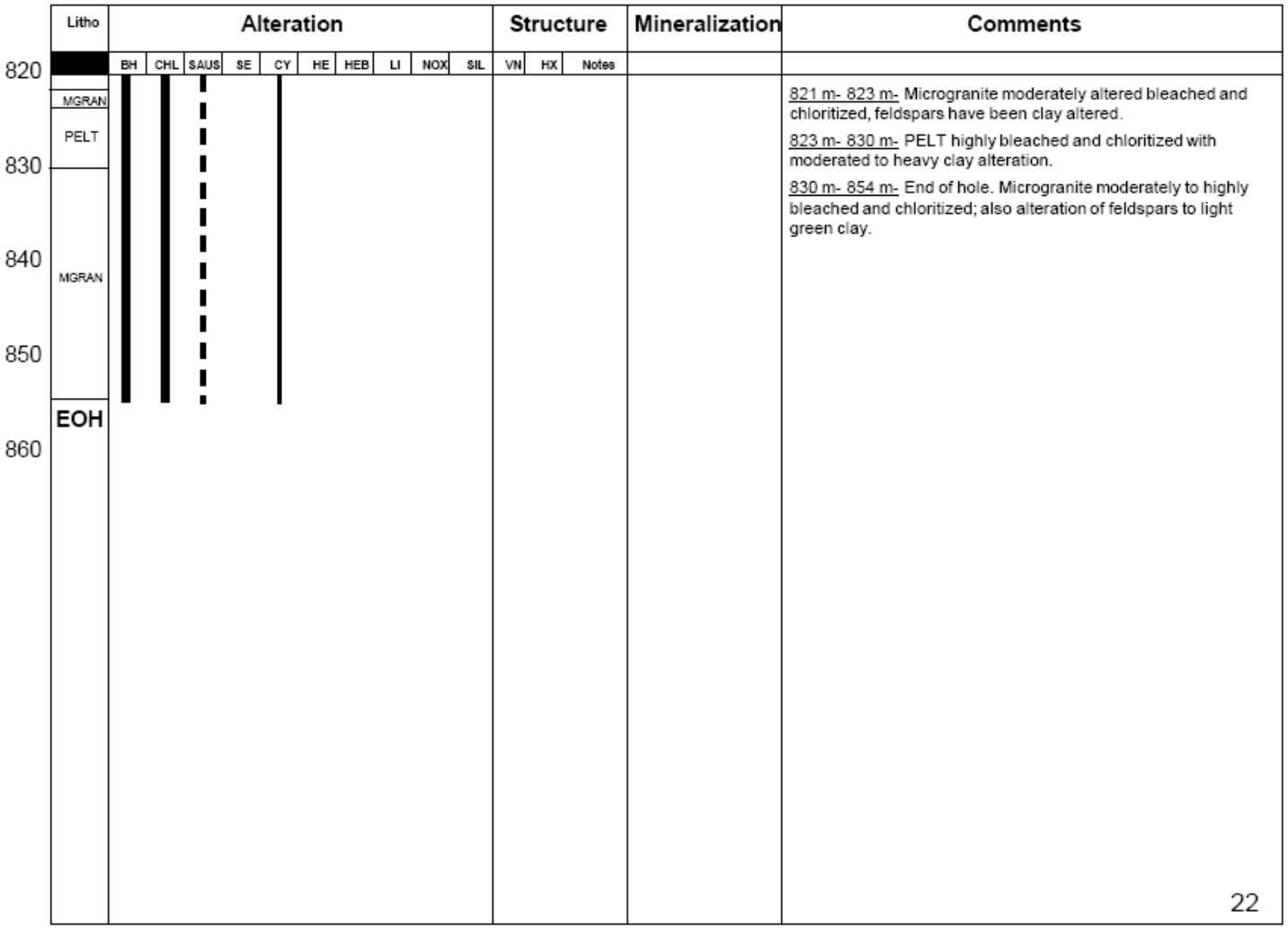

821 m- 823 m- Microgranite moderately altered bleached and chloritized, feldspars have been clay altered.

823 m- 830 m- PELT highly bleached and chloritized with moderated to heavy clay alteration.

830 m- 854 m- End of hole. Microgranite moderately to highly bleached and chloritized; also alteration of feldspars to light green clay.

22

CX- 51- 1: 563.0- 812.0 METERS

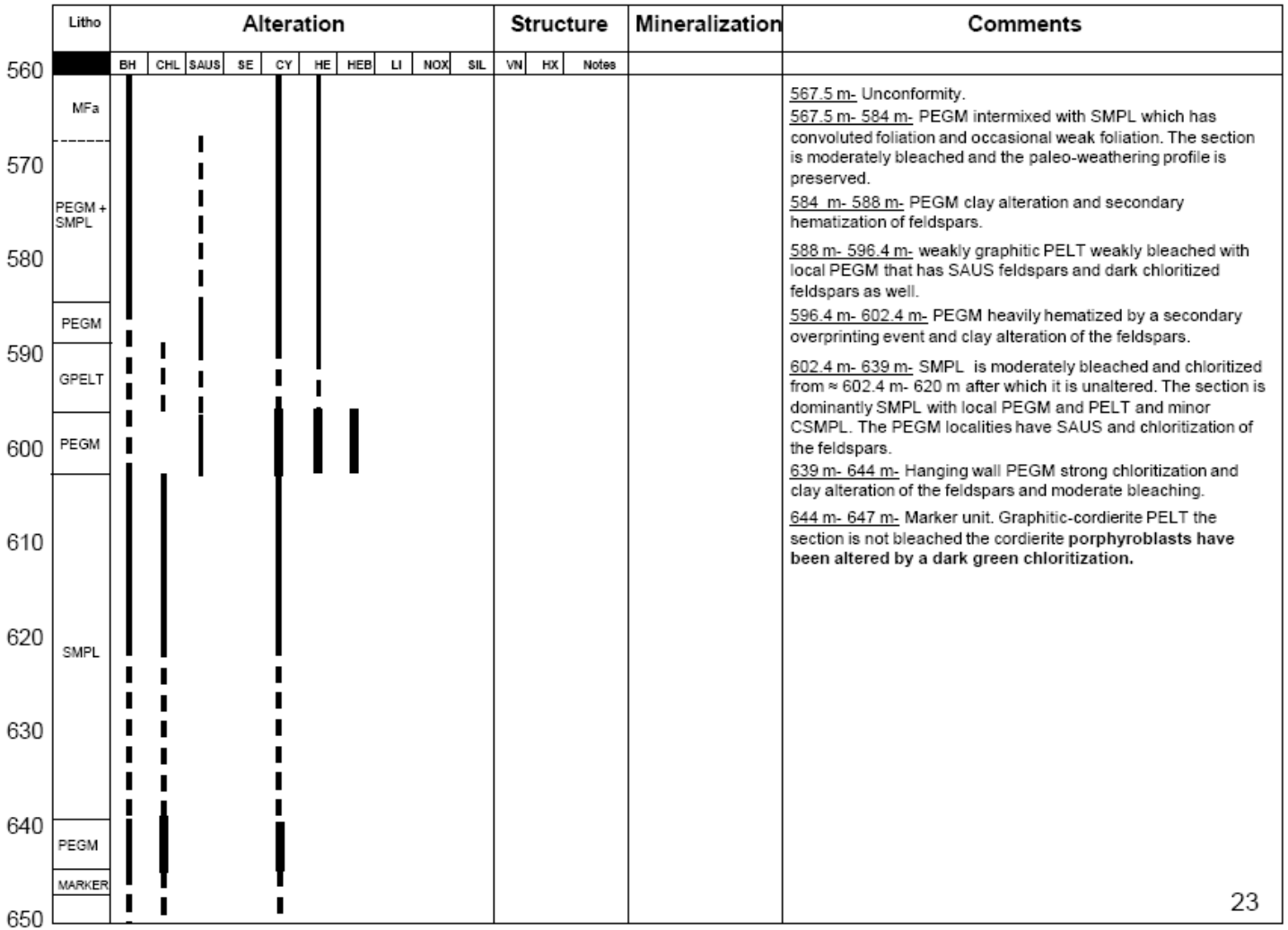

CX- 51- 1: 563.0- 812.0 METERS

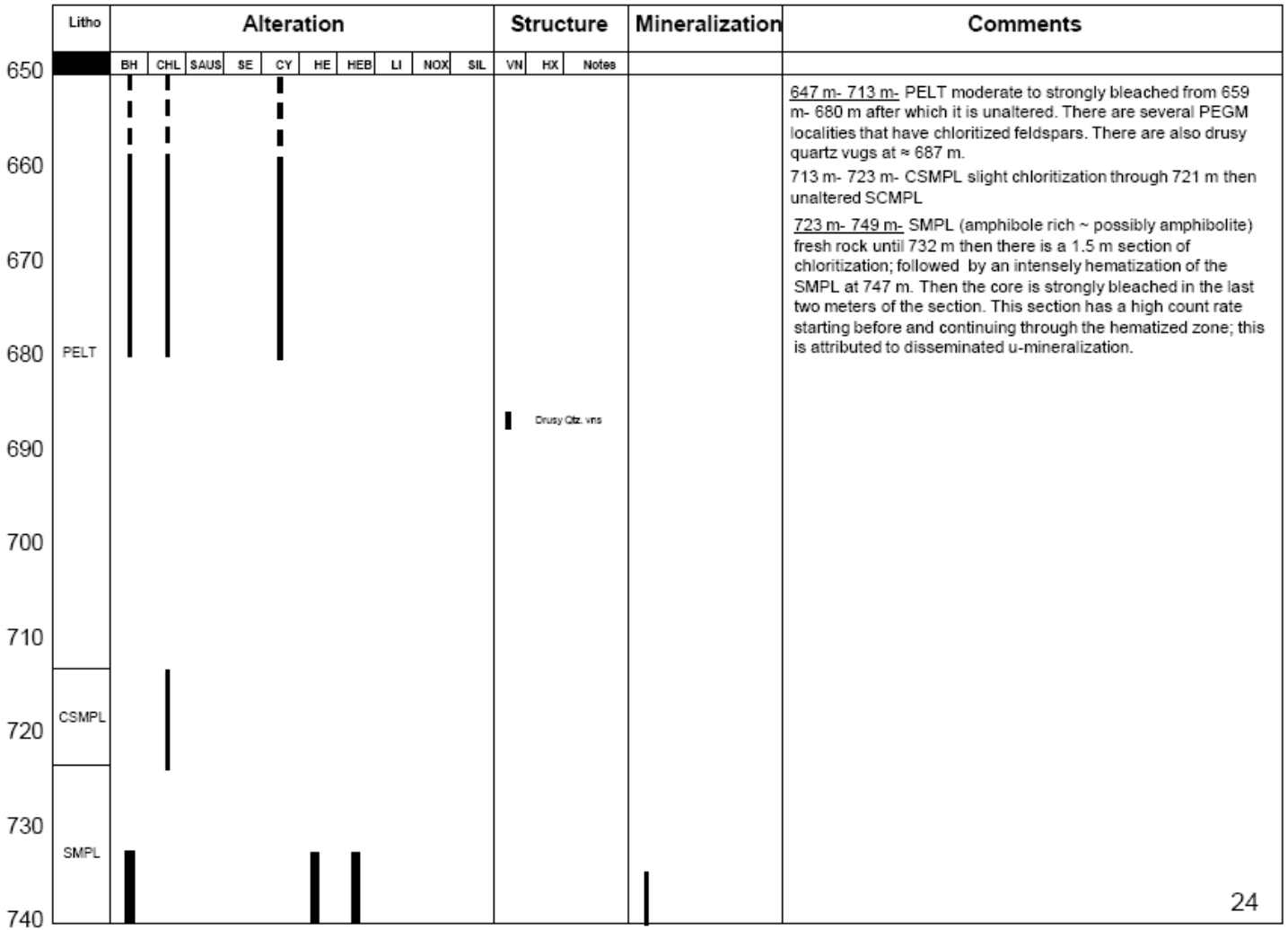

CX- 51- 1: 563.0- 812.0 METERS

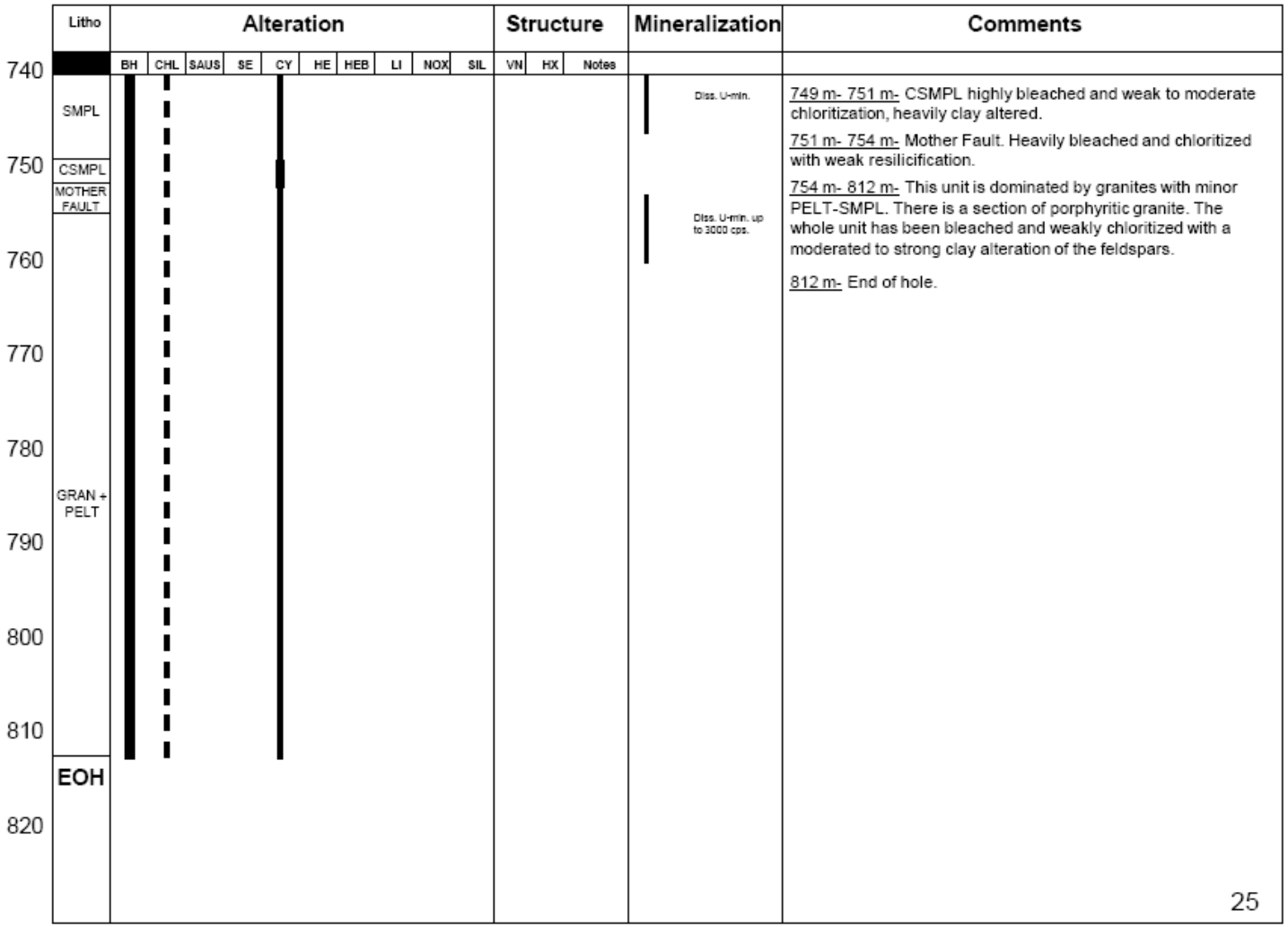

CX- 56-1: 579.5- 728.0 METERS

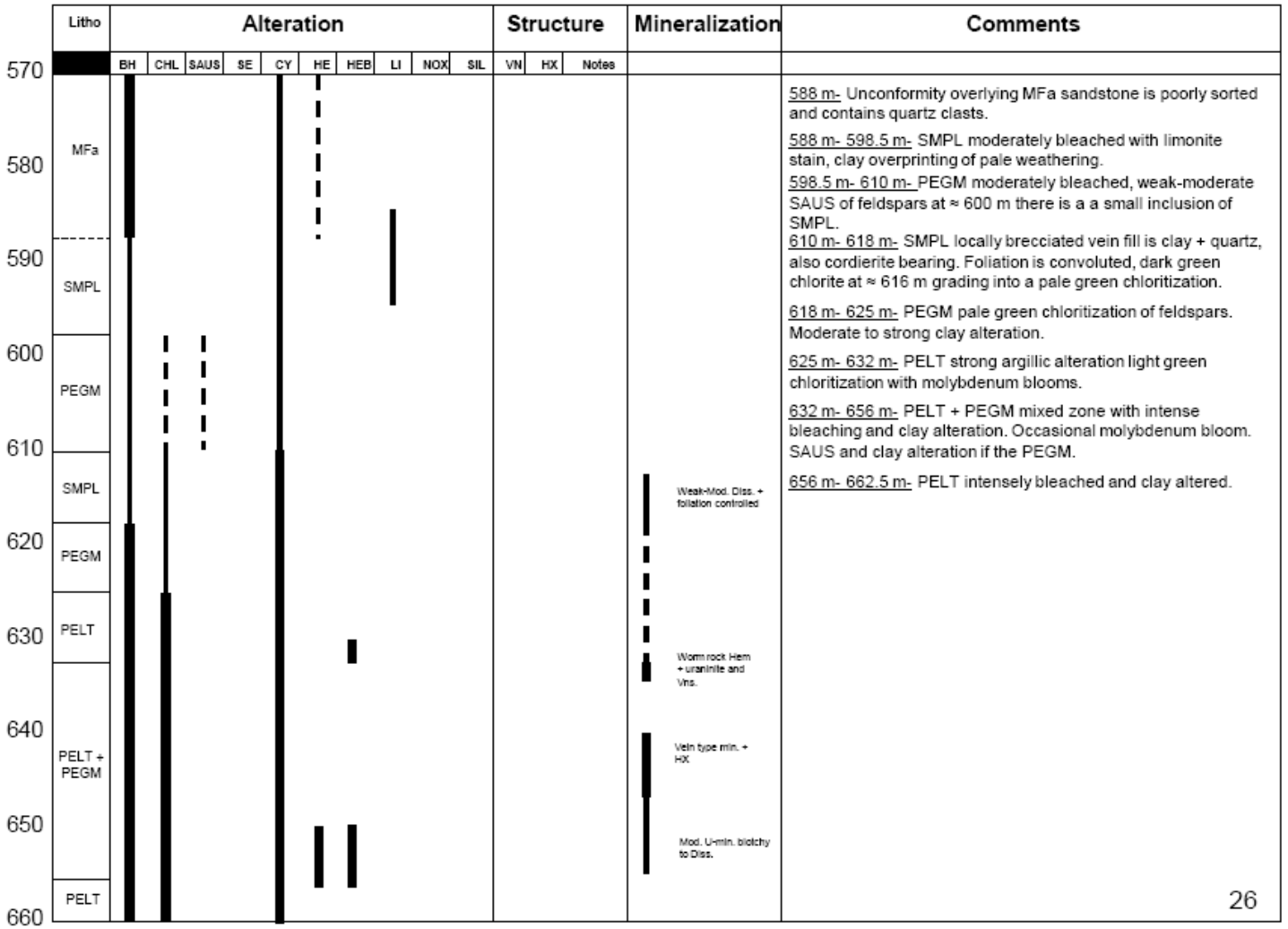

CX- 56-1: 579.5- 728.0 METERS

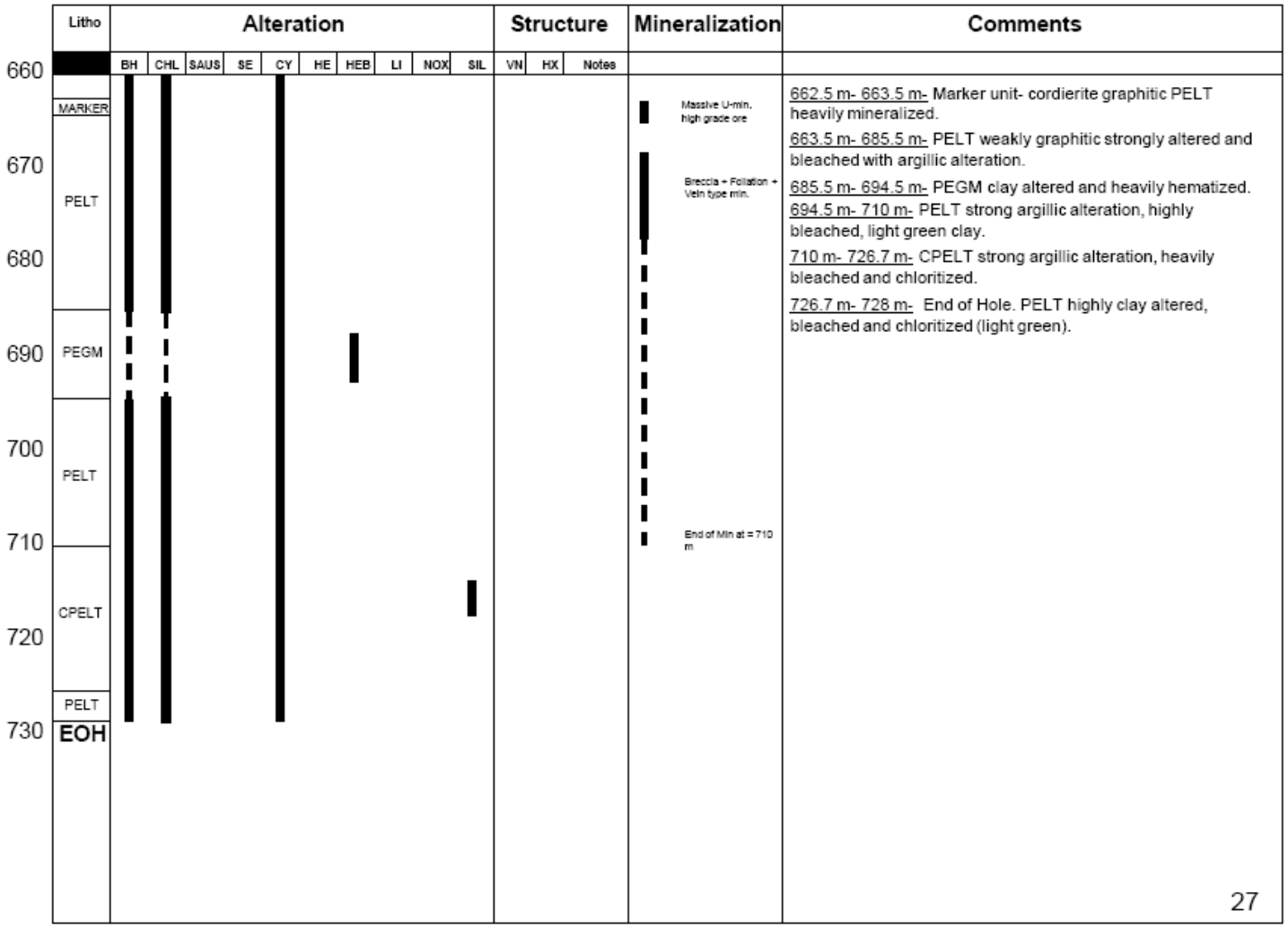

CX- 56- 4: 586.2- 734.0 METERS

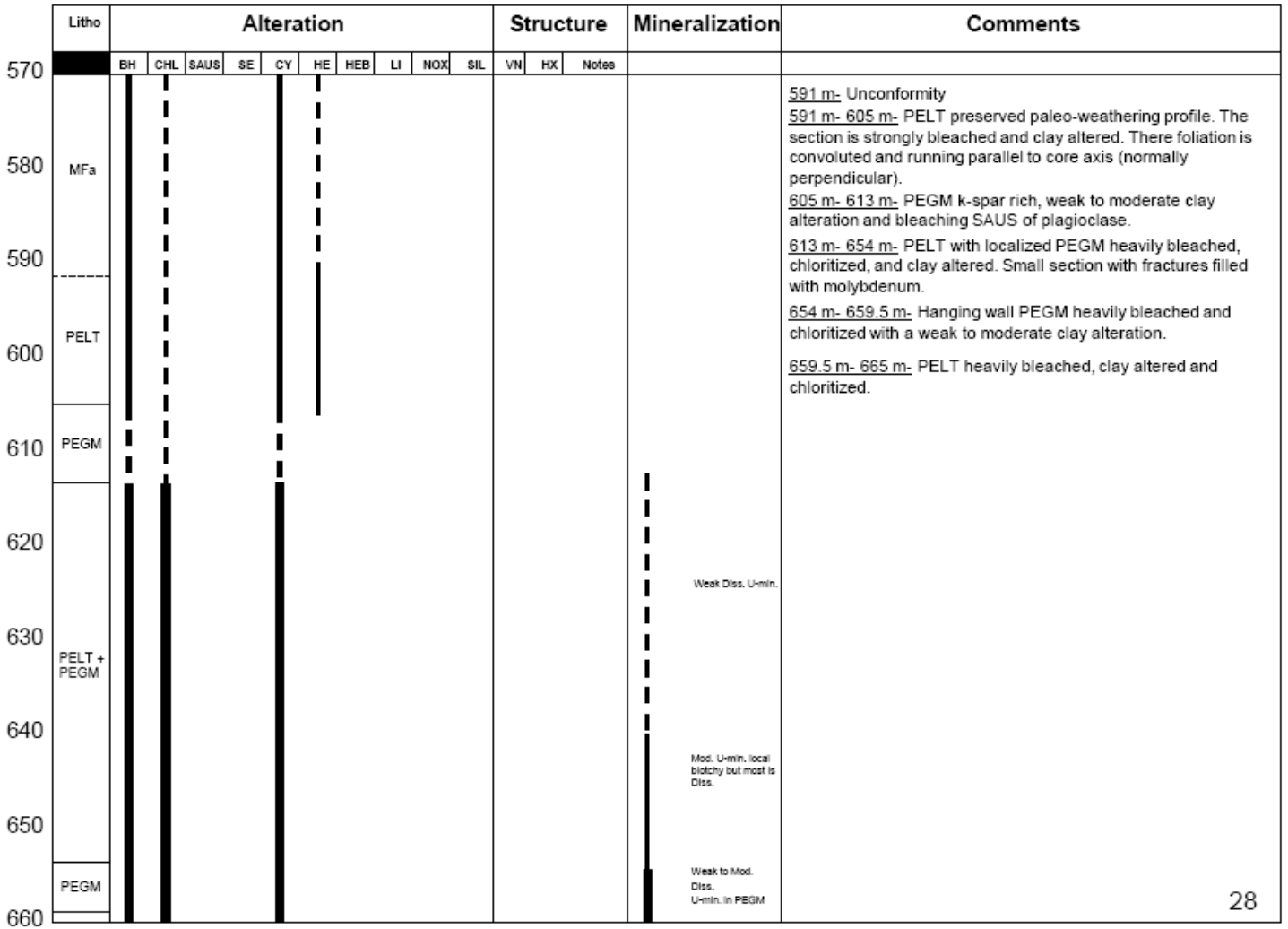

CX- 56- 4: 586.2- 734.0 METERS

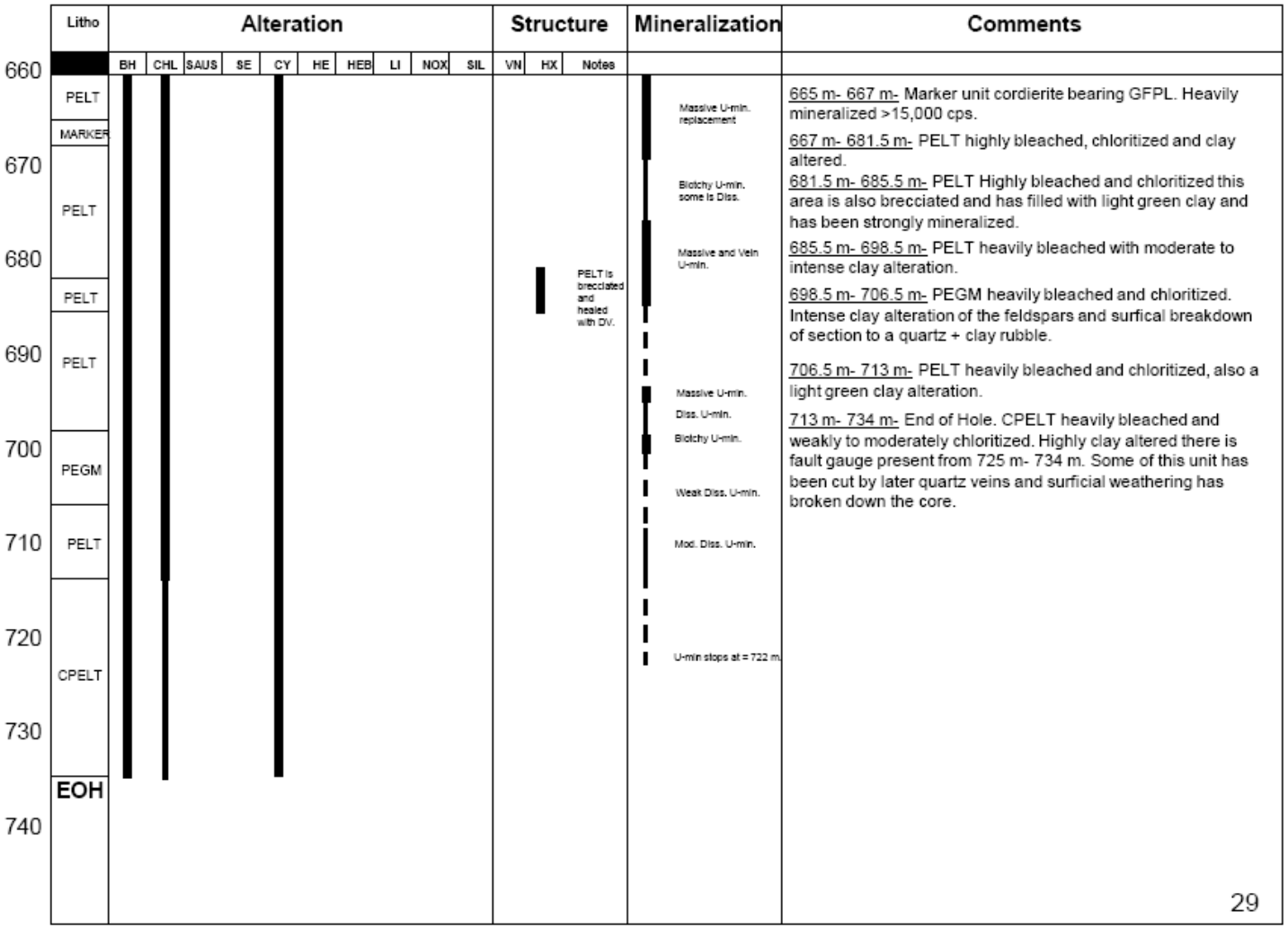

CX- 58: 541.6- 847.6 METERS

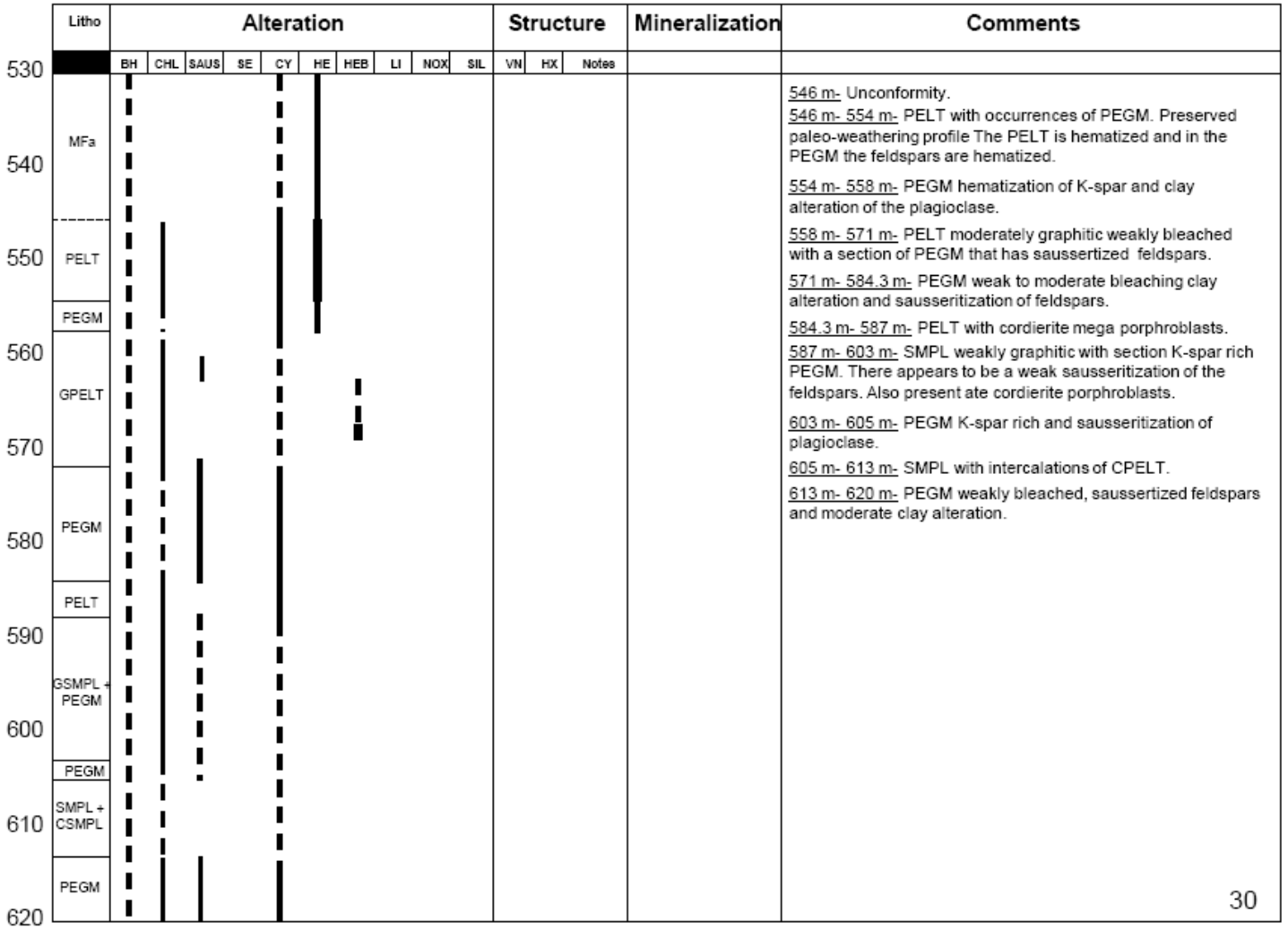

CX- 58: 541.6- 847.6 METERS

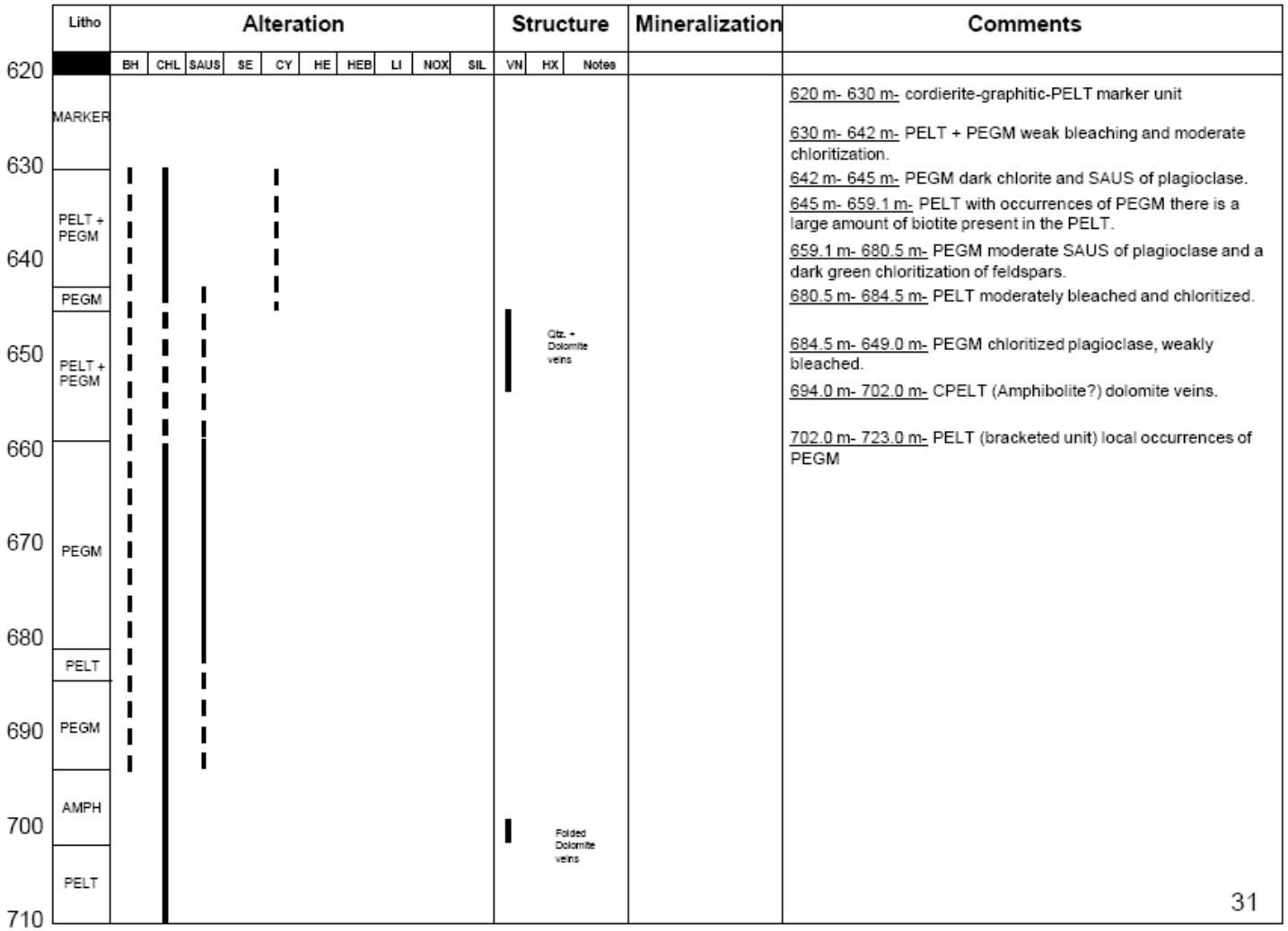

620 m- 630 m- cordierite-graphitic-PELT marker unit

630 m- 642 m- PELT + PEGM weak bleaching and moderate chloritization.

642 m- 645 m- PEGM dark chlorite and SAUS of plagioclase.

645 m- 659.1 m- PELT with occurrences of PEGM there is a large amount of biotite present in the PELT.

659.1 m- 680.5 m- PEGM moderate SAUS of plagioclase and a dark green chloritization of feldspars.

680.5 m- 684.5 m- PELT moderately bleached and chloritized.

684.5 m- 649.0 m- PEGM chloritized plagioclase, weakly bleached.

694.0 m- 702.0 m- CPELT (Amphibolite?) dolomite veins.

702.0 m- 723.0 m- PELT (bracketed unit) local occurrences of PEGM

31

CX- 58: 541.6- 847.6 METERS

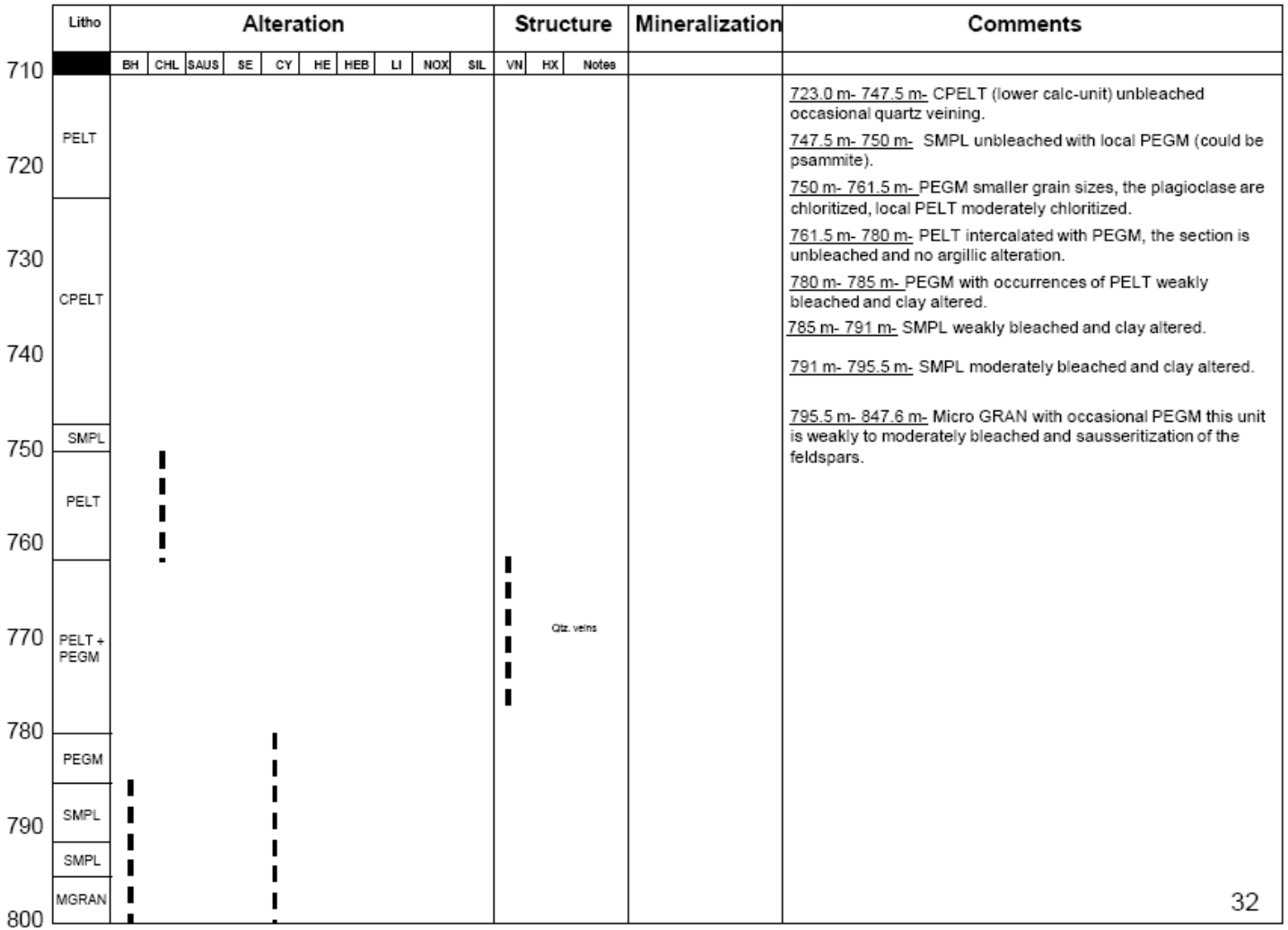

CX- 58: 541.6- 847.6 METERS